

ZTE COMMUNICATIONS

September 2012, Vol.10 No.3

SPECIAL TOPIC:

100G and Beyond: Trends in Ultrahigh-Speed Communications (Part II)



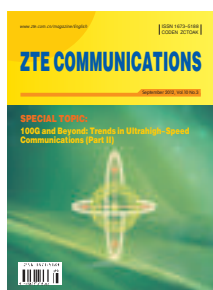
ISSN 1673-5188



09>

C CONTENTS

[Http://www.zte.com.cn/magazine/English](http://www.zte.com.cn/magazine/English)
Email: magazine@zte.com.cn



ZTE Communications Editorial Board

Chairman:

Houlin Zhao

International Telecommunication Union (ITU)

Vice Chairmen:

Lirong Shi

ZTE Corporation (China)

Cheng-Zhong Xu

Wayne State University (USA)

Members (in Alphabetical Order)

Cheng-Zhong Xu

Wayne State University (USA)

Houlin Zhao

International Telecommunication Union (ITU)

Huifang Sun

Mitsubishi Electric Research Laboratories (USA)

Ke-Li Wu

The Chinese University of Hong Kong (China)

Lirong Shi

ZTE Corporation (China)

Shiduan Cheng

Beijing University of Posts and Telecommunications (China)

Wen Gao

Peking University (China)

Wenjun (Kevin) Zeng

University of Missouri (USA)

Zhenge (George) Sun

ZTE Corporation (China)

Zhengkun Mi

Nanjing University of Posts and Telecommunications (China)

Special Topic

100G and Beyond: Trends in Ultrahigh-Speed Communications (Part II)

01 Guest Editorial

by Gee-Kung Chang and Jianjun Yu

02 FSK Modulation Scheme for High-Speed Optical Transmission

by Nan Chi, Wuliang Fang, Yufeng Shao, Junwen Zhang, and Li Tao

12 Computationally Efficient Nonlinearity Compensation for Coherent Fiber-Optic Systems

by kai Zhu and Guifang Li

16 Flipped-Exponential Nyquist Pulse Technique to Optimize PAPR in Optical Direct-Detection OFDM Systems

by Jiangnan Xiao, Zizheng Cao, Fan Li, Jin Tang, and Lin Chen

22 100 Gbit/s Nyquist-WDM PDM 16-QAM Transmission over 1200 km SMF-28 with Ultrahigh Spectrum Efficiency

by Zeng Dong

28 Field Transmission of 100G and Beyond: Multiple Baud Rates and Mixed Line Rates Using Nyquist-WDM Technology

by Zhensheng Jia, Jianjun Yu, Hung-Chang Chien, Ze Dong, and Di Huo

Research Papers

39 Open Augmented Reality Standards: Current Activities in Standards–Development Organizations

by Christine Perey

47 Mobile Cloud for Personalized Any–Media Services

by Bhumi Khasnabish

55 Multiple–Constraint–Aware RWA Algorithms based on a Comprehensive Evaluation Model:

Use in Wavelength–Switched Optical Networks

by Hui Yang, Yongli Zhao, Shanguo Huang, Dajiang Wang, Xuping Cao, and Xuefeng Lin

Roundup

21 ZTE Partners with KPN Group Belgium to Deploy Packet–Switched Core Network

27 ZTE Wins Contract to Provide LTE Wireless Ufi Set to UNE

55 Introduction to ZTE Communications

62 New Members of ZTE Communications Editorial Board

ZTE COMMUNICATIONS

Vol. 10 No.3 (Issue 35)

Quarterly

First Issue Published in 2003

Supervised by:

Anhui Science and Technology Department

Sponsored by:

ZTE Corporation and Anhui Science and Technology Information Research Institute

Staff Members:

Editor–in–chief: Xie Daxiong

Associate Editor–in–chief: Zhao Jinming
Executive Associate

Editor–in–chief: Huang Xinming

Editor in Charge: Zhu Li

Editors: Paul Sleswick, Xu Ye, Yang Qinyi,
Lu Dan

Producer: Yu Gang

Circulation Executive: Wang Pingping

Assistant: Wang Kun

Editorial Correspondence:

Add: 12/F Kaixuan Building,
329 Jinzhai Road,
HeFei 230061, P. R. China

Tel: +86–551–5533356

Fax: +86–551–5850139

Email: magazine@zte.com.cn

Published and Circulated (Home and Abroad) by:

Editorial Office of
ZTE COMMUNICATIONS

Printed by:

Hefei Zhongjian Color Printing Company

Publication Date:

September 25, 2012

Publication Licenses:

ISSN 1673–5188

CN 34–1294/TN

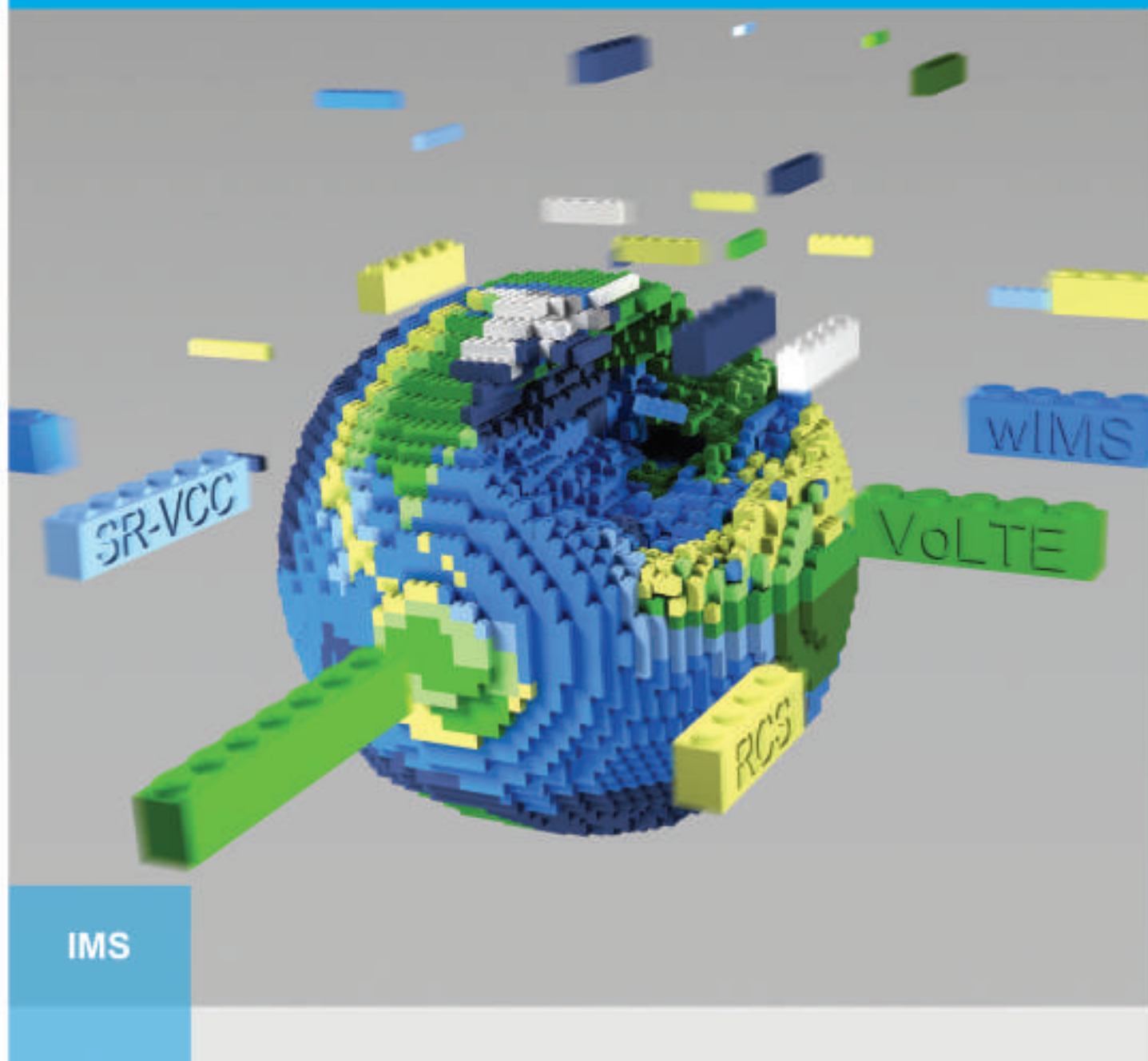
Advertising License:

皖合工商广字 0058 号

Annual Subscription Rate:

USD\$50

Responsibility for content rests
on authors of signed articles and
not on the editorial board of
ZTE COMMUNICATIONS or its sponsors.
All rights reserved.



Here's a single platform that simplifies a world of network services.

As a telecoms operator you've probably sought and deployed cutting edge services in your growing network. But it's just as likely that these services are separate, governed by independent systems. And it's not easy to manage multiple systems—voice, multimedia, WEB—when they're all starkly different.

At ZTE, we've got a solution: IMS. It's a single, flawless platform that integrates all

your services and gives you total centralized control via an all IP environment. Featuring full compatibility with existing technologies, business service capabilities and optimized logistics, it's a system that puts all your services in one platform. Which makes them much simpler, easier, and low cost to manage.

Begin integrating your network services at www.zte.com.cn.

ZTE中兴

A1



ZXR10 T8000

**We've packed
the power of ten
routers into one.**

In this 3G-4G era, operators face a deluge of users who all demand high speed access. How many? Try 160 million, all at once, just as world's highest-switching-capacity router has to handle.

At ZTE, we've gone one better. We've developed a cluster core router—the ZXR10 T8000—that can handle and instantly re-assign capacity up to 200Tbps, with no data loss, in a single unit.

With advanced high-speed core routing forwarding up to 100G, high-capacity packet switching, and flawless traffic management that uses 5-level QoS mechanisms, it's the industry's most versatile bandwidth switcher. Oh, and it saves energy too.

www.zte.com.cn

ZTE中兴

100G and Beyond: Trends in Ultrahigh-Speed Communications (Part II)

Gee-Kung Chang



Jianjun Yu



This is the second part of a special issue on “100G and Beyond: Trends in Ultrahigh-speed Communications.” The first part of this special issue contained nine papers written by service providers, telecommunications equipment manufacturers, and top universities and research institutes. This special issue includes comprehensive reviews as well as original technical contributions covering the rapid advances and broad scope of ultrahigh-speed technologies in optical fiber communications. All papers in this issue have been invited. After peer review, five papers were selected to be published. We hope this issue serves as a timely and high-quality networking forum for scientists and engineers.

The first paper, “FSK Modulation Scheme for High-Speed Optical Transmission,” by Nan Chi et al. from Fudan University, describes the generation, detection, and performance of frequency-shift keying (FSK) for high-speed optical transmission and label switching.

The second paper, “Computationally Efficient Nonlinearity Compensation for Coherent Fiber-Optic System,” by Li et al. from the University of Central Florida, describes how split-step digital backward propagation (DBP) can be combined with coherent detection to compensate for fiber nonlinear impairments.

The third paper, “Flipped-Exponential Nyquist Pulse Technique to Optimize the PAPR in Optical Direct Detection OFDM System,” by Xiao et al. from Hunan University, describes the use of advanced coding to reduce peak-to-average power ratio of the OFDM signal and extend the transmission distance.

The fourth paper, “100Gb/s Nyquist-WDM PDM-16QAM Transmission over 1200-km SMF-28 with Ultrahigh Spectrum Efficiency,” by Dong et al. from ZTE USA, describes the use of pre- and post-equalization to improve transmission system performance and realize ultrahigh spectrum efficiency.

The fifth paper, “Field Transmission of 100G and Beyond: Multiple Baud Rates and Mixed Line Rates Using Nyquist-WDM Technology,” by Jia et al. from ZTE USA, describes a field trial experiment of mixed 100G, 400G, and 1 Tbit/s signal transmission. Joint experiments between ZTE and Deutsche Telecom (DT) have been conducted on long-haul transmission of 100G and beyond over standard

single-mode fiber (SSMF) and inline EDFA-only amplification.

We would like to thank all authors for their valuable contributions and all the reviewers for their timely and constructive feedback on all submitted papers. We hope that the contents of this issue are informative and useful for all readers.

Biographies

Gee-Kung Chang received his PhD degree in physics from the University of California, Riverside. He worked for 23 years at Telcordia Technologies (formerly Bell Systems-Bell Labs, and then Bellcore), where he held research and management positions, including director and chief scientist of optical internet research, director of optical networking systems and testbed, and director of optical system integration and network interoperability. Prior to joining Georgia Institute of Technology, he was vice president and chief technology strategist at OpNext Inc., an offshoot of Hitachi Telecom. Dr. Chang is currently the Byers endowed chair professor of optical networking at the School of Electrical and Computer Engineering, Georgia Institute of Technology. He is an eminent scholar of the Georgia Research Alliance. He is also co-director of the 100G Optical Networking Center at Georgia Tech. He holds 56 U.S. patents and has co-authored more than 360 peer-reviewed journal and conference papers. He was made a Telcordia Fellow in 1999 for pioneering work in the optical networking project, MONET, and NGI. He was made a fellow of the Photonic Society of Chinese-Americans in 2000. He is a fellow of the IEEE Photonics Society and a fellow of the Optical Society of America, recognized for his contributions to DWDM optical networking and label switching technologies. He has served at many IEEE LEOS and OSA conferences. He has been the lead guest editor for three special issues of the Journal of Lightwave Technology, which is sponsored by IEEE LEOS and OSA.

Jianjun Yu received his PhD degree in electrical engineering from Beijing University of Posts and Telecommunications in 1999. From June 1999 to January 2001, he was an assistant research professor at the Research Center COM, Technical University of Denmark. From February 2001 to December 2002, he was a member of the technical staff at Lucent Technologies and Agere Systems, Murray Hill, NJ. He joined the Georgia Institute of Technology in January 2003 as a research faculty member and director of the Optical Network Laboratory. From November 2005 to February 2010, he was a senior member of technical staff at NEC Laboratories America, Princeton, NJ. Currently, he works for ZTE Corporation as the chief scientist on high-speed optical transmission and director of optics labs in North America. He is also a chair professor at Fudan University and adjunct professor and PhD supervisor at the Georgia Institute of Technology, Beijing University of Posts and Telecommunications, and Hunan University. He has authored more than 100 papers for prestigious journals and conferences. Dr. Yu holds 8 U.S. patents with 30 others pending. He is a fellow of the Optical Society of America. He is editor-in-chief of Recent Patents on Engineering and an associate editor for the Journal of Lightwave Technology and Journal of Optical Communications and Networking. Dr. Yu was a technical committee member at IEEE LEOS from 2005 to 2007 and a technical committee member of OFC from 2009 to 2011.

FSK Modulation Scheme for High-Speed Optical Transmission

Nan Chi, Wuliang Fang, Yufeng Shao, Junwen Zhang, and Li Tao

(State Key Lab of ASIC & System, and Department of Communication Science and Engineering, Fudan University, Shanghai 200433, China)

Abstract

In this paper, we describe the generation, detection, and performance of frequency-shift keying (FSK) for high-speed optical transmission and label switching. A non-return-to-zero (NRZ) FSK signal is generated by using two continuous-wave (CW) lasers, one Mach-Zehnder modulator (MZM), and one Mach-Zehnder delay interferometer (MZDI). An RZ-FSK signal is generated by cascading a dual-arm MZM, which is driven by a sinusoidal voltage at half the bit rate. Demodulation can be achieved on 1 bit rate through one MZDI or an array waveguide grating (AWG) demultiplexer with balanced detection. We perform numerical simulation on two types of frequency modulation schemes using MZM or PM, and we determine the effect of frequency tone spacing (FTS) on the generated FSK signal. In the proposed scheme, a novel frequency modulation format has transmission advantages compared with traditional modulation formats such as RZ and differential phase-shift keying (DPSK), under varying dispersion management. The performance of an RZ-FSK signal in a 4×40 Gb/s WDM transmission system is discussed. We experiment on transparent wavelength conversion based on four-wave mixing (FWM) in a semiconductor optical amplifier (SOA) and in a highly nonlinear dispersion shifted fiber (HNDSF) for a 40 Gb/s RZ-FSK signal. The feasibility of all-optical signal processing of a high-speed RZ-FSK signal is confirmed. We also determine the receiver power penalty for the RZ-FSK signal after a 100 km standard single-mode fiber (SMF) transmission link with matching dispersion compensating fiber (DCF), under the post-compensation management scheme. Because the frequency modulation format is orthogonal to intensity modulation and vector modulation (polarization shift keying), it can be used in the context of the combined modulation format to decrease the data rate or enhance the symbol rate. It can also be used in orthogonal label-switching as the modulation format for the payload or the label. As an example, we propose a simple orthogonal optical label switching technique based on 40 Gb/s FSK payload and 2.5 Gb/s intensity modulated (IM) label.

Keywords

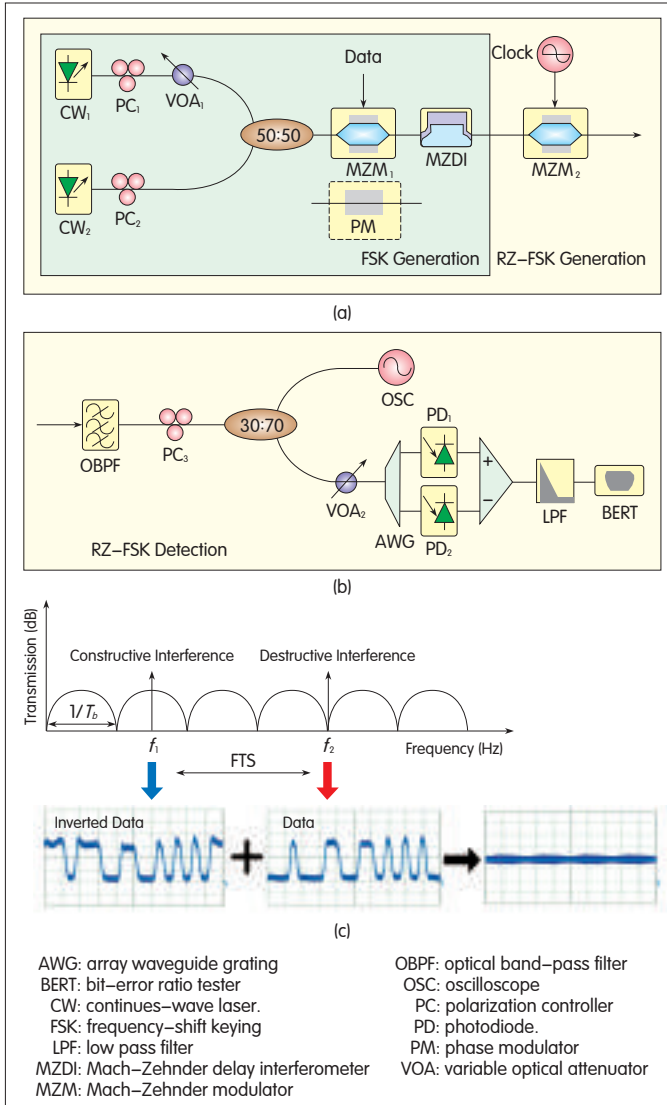
optical communication; return-to-zero frequency shift keying; Mach-Zehnder modulator; Mach-Zehnder delay interferometer; chromatic dispersion; wavelength conversion; label switching

1 Introduction

Advanced modulation formats increase the tolerance of optical signals to chromatic dispersion and fiber nonlinearity, and they lessen the need for greater bandwidth in electrical circuits [1]–[7]. In many modulation formats, frequency-shift keying (FSK) enables differential detection. Simulations have shown that FSK has a comparable optical-to-signal noise ratio (OSNR) sensitivity to differential phase-shift keying (DPSK) in a 10 Gb/s transmission system [6]. Orthogonal modulation of amplitude-shift keying (ASK) and FSK has recently attracted much attention for its high-spectral efficiency [7]–[11]. One example is the combination of ASK and FSK, FSK can be used for payload or label modulation in the orthogonal optical label-switching schemes [12]–[15]. FSK is a potential

solution for future high-speed transmission systems and optical packet switching networks. An FSK signal can be generated by directly modulating electric current in a laser light source. This idea, however, is limited by the relatively low frequency modulation response of the laser and has a detrimental effect of parasitic intensity modulation. In [15], a scheme is proposed to generate high-speed FSK signals at 40 Gb/s. This scheme uses an LiNbO₃ external FSK modulator with a complicated design. We previously proposed using FSK signals in 40 Gb/s applications and showed the power penalty after 50 km SMF transmission is 0.8 dB. We speculated on a novel scheme for generating and detecting return-to-zero FSK (RZ-FSK) signals for 40 Gb/s transmission.

In this paper, we detail the scheme for generating RZ-FSK signals that have a bit rate of 40 Gb/s or higher. In section 2, the RZ-FSK transmitter and receiver configuration is



▲ Figure 1. Principle of RZ-FSK generation and detection and the generated FSK signal by experiment. (a) Configuration of our proposed transmitter, (b) configuration of the used receiver, (c) measured FSK waveforms of the two tones.

described, and the principles of RZ-FSK generation and detection are given.

In section 3, we use simulations to compare FSK, DPSK, and RZ-FSK at 40 Gb/s for 12 spans of 80 km SMF. RZ-FSK is more tolerant to nonlinearity and chromatic dispersion than the other modulation formats. We also analyze an RZ-FSK signal in a 4 × 40 Gb/s WDM transmission system. In section 4, we experiment with a 40 Gb/s RZ-FSK signal over 100 km SMF with full dispersion compensation. We compare transparent wavelength conversion based on four-wave mixing (FWM) in a semiconductor optical amplifier (SOA) with transparent wavelength conversion based on FWM in a highly nonlinear dispersion-shifted fiber (HNDSF). The feasibility of all-optical signal processing of a 40 Gb/s RZ-FSK signal is validated. In section 5, we discuss the use of the RZ-FSK

generation method in a high-speed label switching system. Section 6 concludes the paper.

2 RZ-FSK Transmitter and Receiver

Fig. 1(a) shows the schematic of the RZ-FSK transmitter, and Fig. 1(b) shows the schematic of the RZ-FSK receiver. A low-speed RZ-FSK signal can be produced by directly modulating distributed feedback (DFB) lasers. The lasers are driven by a bias current far above threshold, and a relatively small modulation current is added. To generate an FSK signal at 40 Gb/s and above, two continuous-wave (CW) lasers with carefully selected center frequency are combined by a 3 dB coupler and fed into the Mach-Zehnder modulator (MZM1) or phase modulator (PM). The combined input is modulated by NRZ data and then demodulated to intensity modulation by a Mach-Zehnder delay interferometer (MZDI). The MZDI is imbalanced by the introduction of a one-bit time-delay line. The wavelengths of the two beams are carefully selected so that one beam is at the maximum transmission of the MZDI (constructive interference) and the other is at the minimum transmission of the MZDI (destructive interference). Thus, the

frequency tone spacing (FTS) is $\frac{(N+1)/2}{T_b}$ Hz, where

$N = 1, 2, 3, \dots, n$ and T_b is a bit period. The center frequencies of the two beams are f_1 and f_2 . The optical field exiting a phase modulator for f_1 is given by

$$E_1(t) = E_0 \cdot \exp \left(j \frac{2\pi f_1 T_b + \Phi_1 + \Phi_2}{2} \right) \cdot \cos \left(\frac{2\pi f_1 T_b + \Phi}{2} \right) \quad (1)$$

and the optical field exiting the phase modulator for f_2 is given by

$$E_2(t) = E_0 \cdot \exp \left(j \frac{2\pi f_2 T_b + \Phi_1 + \Phi_2}{2} \right) \cdot \cos \left(\frac{2\pi f_2 T_b + \Phi}{2} \right) \quad (2)$$

where Φ_1 and Φ_2 are the phases of the neighboring bits, and the data information is reflected in the phase difference Φ . The f_1 center frequency is given by

$$f_1 = m / T_b \quad (m = 0, 1, 2, 3, \dots, M) \quad (3)$$

and the f_2 center frequency is given by

$$f_2 = f_1 + \frac{2n+1}{2T_b} \quad (n = 0, 1, 2, 3, \dots, N) \quad (4)$$

However, in a real transmitter, the rise and fall time of the input signal needs to be taken into consideration. If $1/f_1 = T_b/m$ ($m = 0, 1, 2, 3, \dots, M$), then T_b/M must be greater than the rise time of the input-signal pulse width. If T_b/m is too small, the phase information generated by the MZM1 or PM could not be transferred to the intensity signal in the MZDI. Even if the phase information is accurately transferred to the amplitude information, the difference between the generated amplitude information for binary data 1 and 0 is small. The rise and fall time of the input signal should not exceed T_b/m . With this prerequisite, the maximum value of m can be calculated. The bandwidth of the transmitted signal is a function of the carrier's rise and fall times, and it should be determined

whether the generated FSK signal is normal. In our model, an electrical rectangular NRZ pre-shaped input data (data) pulse with symbol period T_b is filtered by a linear time-invariant filter with a normalized Gaussian shaped impulse response:

$$h(t) = \frac{2}{\sqrt{\pi} T_e} e^{-(2t/T_e)^2} \quad (5)$$

where T_e denotes a $1/e$ pulse duration. The output pulse $y(t)$ is given as convolution of $h(t)$ with the rectangular input time function:

$$y(t) = \frac{1}{2} \left(\operatorname{erfc} \frac{2(t-T)}{T_e} - \operatorname{erfc} \frac{2t}{T_e} \right) \quad (6)$$

The 10% to 90% amplitude values of $y(t)$ are the rise time, and the 90% to 10% amplitude values of $y(t)$ are the fall times. In the module, the rise time in the module is denoted Δt and is equal to the fall time. If the pulse duration T_b is compared with the filter time over a long period of time, T_e , then $\Delta t \approx 3T_e/4$. For $T_b = 3T_e/2$, the approximation error is less than 10%. In the frequency domain, the filter is also Gaussian shaped. The $1/e$ bandwidth, Δf_e , is given by

$$\Delta f_e = 4/\pi T_e \quad (7)$$

so that when $\Delta t \leq T/2$, the $1/e$ bandwidth is

$$\Delta f_e \leq 3/\pi \Delta t \quad (8)$$

Therefore, $-\Delta t$ should not exceed T_b/M , and this can be expressed as

$$\Delta f_e \leq 3M/\pi T_b \quad (9)$$

At the transmitter, the maximum $1/e$ bandwidth is

$$\Delta f_{e,\max} \approx 3M/\pi T_b \quad (10)$$

When f_2 is greater than f_1 , the maximum $1/e$ bandwidth only depends on f_1 . Also, assuming the edge of the generated FSK signal is not sharp, f_1 can meet the bandwidth limit of the transmitter; however, f_2 is too large, and $1/f_2$ is less than the rise and fall time of the input-signal pulse width. In this case, (4) can be written as

$$f_2 = \frac{1}{T_b} (m+n+1/2) \quad (11)$$

$$\text{Next, we let } L = m+n \ (l = 0, 1, 2, 3, \dots, L) \quad (12)$$

where L is integer wave number of f_2 . Assuming the edge of the generated FSK signal is not sharp, in the Mach-Zehnder delay interferometer (MZDI), L should be below a certain number, and the $T_b(L+1/2)$ can be introduced to ensure the phase-to-intensity transform is perfect. Similar to the previous derivation, (11) can be modified to give the maximum $1/e$ bandwidth of the proposed transmitter:

$$\Delta f_e \leq \frac{3}{\pi T_b} (L+1/2) \quad \Delta f_{e,\max} \leq \left(\frac{3}{\pi T_b} \right) (L+1/2) \quad (13)$$

From (3) and (4), the FTS of the generated FSK signal is

$$\text{FTS} = \frac{2n+1}{2T_b} \quad (n=0, 1, 2, 3, \dots, N) \quad (14)$$

The two couplers in the MZDI both have a coupling ratio of 50:50, and the output at a constructive port of the MZDI is given by

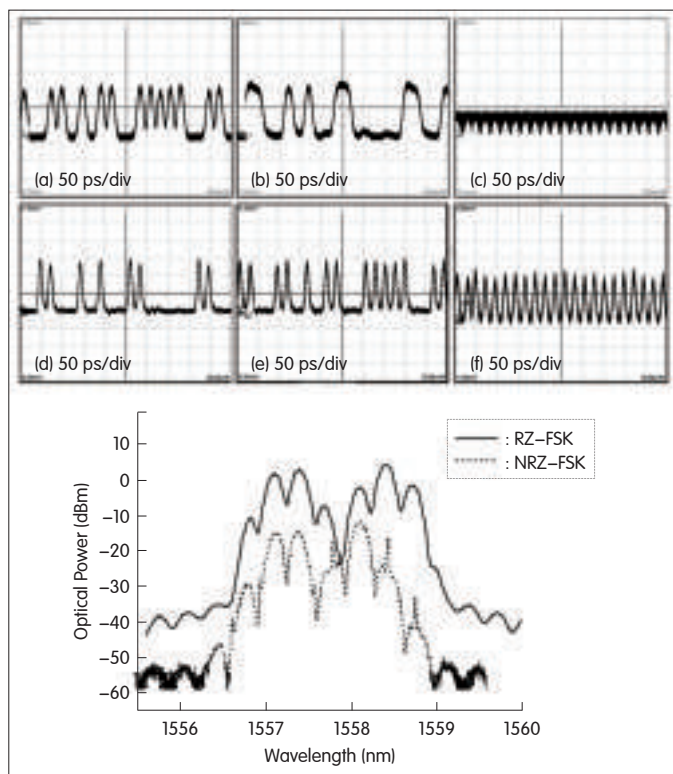
$$P_o = P_i \left\{ -\frac{1}{2} \cos \left[(2\pi f_1 + 2\pi f_2) \text{FTS} + \Delta\phi \frac{\pi}{2} \right] + \frac{1}{2} \right\} \quad (15)$$

where P_i is the input optical power, P_o is the output optical power, and $\Delta\phi$ is the phase difference between the two arms of the MZDI. According to (15), if the central frequency of the laser locates such a position that f_1 is exactly at the maximum transmission point of the MZDI and f_2 is at the minimum transmission point, two logically inverted data streams are created at each MZDI output (Fig. 1c). In this way, an optical FSK signal is generated at the output of an MZDI. An FSK signal with an optical pulse at every bit slot is generated. The constructive wavelength carries duobinary (DB) modulation, whereas the destructive wavelength carries alternate-mark inversion (AMI) [2]. Hence, the FSK signal can be regarded as the combination of two intensity modulated (IM) signals with non-information-bearing phase modulation.

In practice, the frequency modulation format with RZ shape is widely used in long-haul optical communications because of its superior performance. The RZ pulse carver can be implemented cascading an MZM₂ after the MZDI. In our scheme, the MZM₂ is driven by a sinusoidal voltage at half the bit rate. As a result, the generated FSK signal passes through the MZM₂ to generate an RZ-FSK signal. Fig. 1(b) shows the configuration of the RZ-FSK receiver. The optical bandpass filter (OBPF) creates more than 25 dB suppression ratio between the two FSK tones. An array waveguide grating (AWG) demultiplexer is used to separate the two FSK tones and demodulate the FSK into IM. The data obtained in one output is identical to the original data; but in the other output, the detected data is logically inverted. Hence, these two outputs can be detected by a differential receiver. A lowpass filter is positioned after the differential electrical amplifier to remove the high-frequency pulses induced by the beating of the two modes. Fig. 2(a) to (f) shows the measured waveforms for an FSK and RZ-FSK signal. The clear waveforms show that the proposed FSK and RZ-FSK generation schemes are feasible. In Fig. 2(g), an asymmetrical FSK component and an RZ-FSK component can be observed for conventional spectra. These are generated using the proposed scheme; the FSK signal is obtained by demodulating two DPSK signals. According to the position of the two RZ-FSK tones shown in Fig. 2(g), the low-frequency RZ-FSK component carries the spectrum of the RZ-DB modulation format, and the high-frequency spectrum represents the spectrum of the RZ-AMI modulation format. The degree of overlapping of these two spectral components increases as tone spacing decreases.

3 Numerical Simulation and Results

Here, the tolerance of RZ-FSK to some transmission impairments is evaluated using numerical simulations and commercial software. We compare currently used modulation



▲ Figure 2. The measured waveforms for (a) non-return-to zero (NRZ) FSK tone 1, (b) NRZ-FSK tone 2, (c) NRZ-FSK, (d) RZ-FSK tone 1, (e) RZ-FSK tone 2, (f) RZ-FSK, and (g) optical spectra curves for NRZ-FSK signal and RZ-FSK signal.

formats such as RZ and DPSK. Fig. 1(a), shows two CW lasers with carefully selected center frequencies are used as the transmitter's source. Center frequencies of 193 THz and 193.1 THz are selected for the two light beams. One beam is at the maximum transmission (constructive interference) of the MZDI, and the other is at the minimum transmission (destructive interference) of the MZDI. At the transmitter, the data stream from the 40 Gb/s pattern generator with $2^{23}-1$ NRZ binary sequence, is pre-coded and drives a PM. The phase shift in the PM is π . The flowing one-bit-delay MZDI is used to demodulate the two DPSK signals into two IM signals. Assuming that the coupling ratios of the two couplers of the MZDI are both 50:50, a high-speed FSK signal can be regarded as a combination of two logically inverted IM signals with phase modulation in none information bearing way. One MZM driven by a sinusoidal voltage at half the bit rate is used for RZ carving. Fig. 1(a) shows the schematic modulation of a 40 Gb/s RZ-FSK signal clock. At the receiver, an OBPF and AWG demultiplexer are used as the frequency discriminator to demodulate the received FSK signal (or RZ-FSK signal) into an IM signal for direct detection.

3.1 Comparison of Two Frequency Modulation Schemes Using MZM and PM

The phase can be changed by PM or MZM. A PM keeps the optical intensity constant and modulates the phase

subject to its bandwidth limit. However, a PM causes significant chirp on the signal. A PM introduces imperfect phase modulation in the data transition region, which causes additional power penalty.

For this reason, an MZM is usually used for phase modulation. An MZM produces instantaneous phase jumps at the expense of some residual IM. Although the difference between the PM and MZM is not critical when the center frequencies of the two beams are properly aligned, impairments from timing misalignment can be caused by this difference. When timing is misaligned, the data transition region of another beam center frequency is located in the mid-point of the data time slot of the FSK signal. Therefore, by using MZM, data-related dips inevitably lead to inter-symbol interference (ISI) to the FSK signal. For the PM, if the bandwidth of the OBPF is sufficiently large so that the signal keeps its constant intensity after filtering, ISI can be avoided. However, in strong optical filtering systems, or for sharp-edged input data pulses, dips may also be introduced after filtering. Therefore, MZM and PM schemes should be compared.

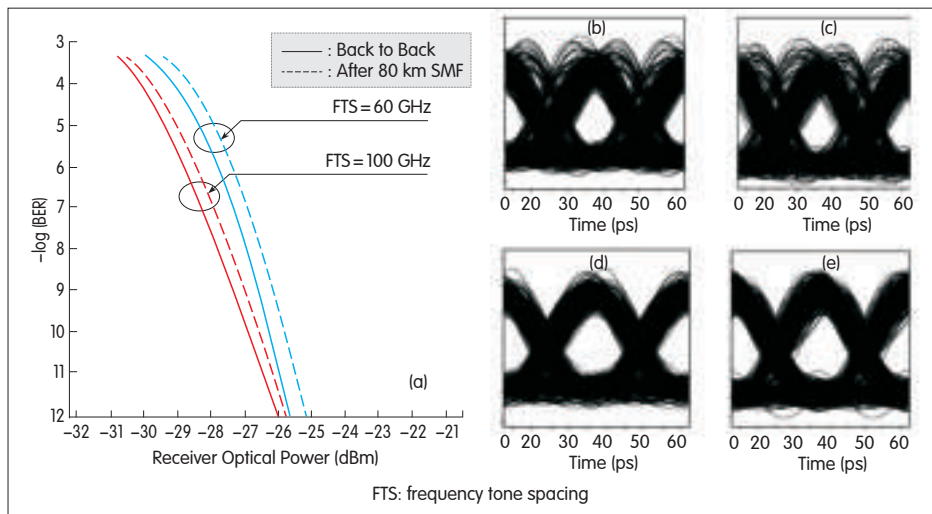
We run Monte-Carlo numerical simulations to investigate frequency modulation between PM + MZDI and MZM + MZDI. By substituting the PM with an MZM, receiver sensitivity can be improved by approximately 0.51 dB. This improvement is due to the fact that the upward overshoots can be partly pre-compensated for by the downward intensity dips of MZM modulation. Hence, MZM + MZDI is more suitable than PM + MZDI for frequency modulation in terms of receiver sensitivity. MZM + MZDI has higher receiver sensitivity than PM + MZDI.

3.2 Effect of a Different FTS

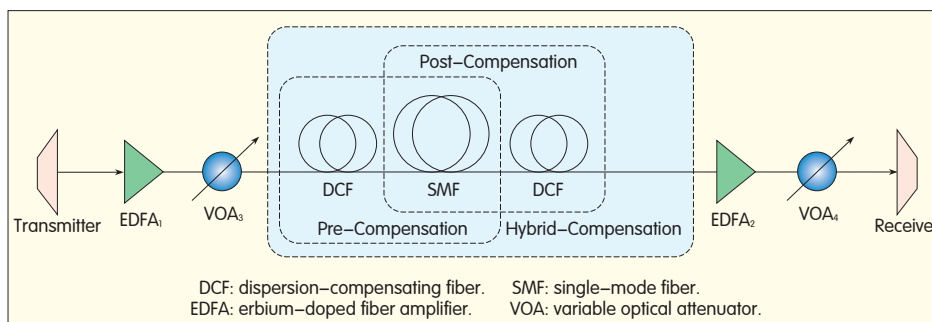
In the optical FSK generating technique, the FTS should be well-preserved to ensure one beam is at the maximum transmission of the MZDI and the other is at the minimum. This is especially important to the center frequencies of the two beams. Using a different FTS to generate an FSK signal changes the transmission performance. The FTS is given by (14). Fig. 3(a) shows the bit-error ratio (BER) the two FSK signals. The power penalty after transmission for a 40 Gb/s FSK with 60 GHz FTS is 0.58 dB, and the power penalty after transmission for a 40 Gb/s FSK with 100 GHz FTS is 0.46 dB. The bandwidth of the discrimination filter is set to 60 GHz and 100 GHz for the two FSK signals. Fig. 3(b) to (e) shows the eye diagrams at $\text{BER} = 10^{-9}$ for the two FSK signals in back-to-back and after 80 km transmission link. Clear and open eyes show convincingly the feasibility of the generated FSK scheme. Pulse timing jitter increases as spectral overlapping increases between the two FSK components. Hence, the FSK signal with 100 GHz FTS is superior in terms of power penalty, and sampling and deciding are easier in the receiver.

3.3 Comparison of Transmission Properties of FSK, DPSK, and RZ

In Fig. 4, one erbium-doped fiber amplifier (EDFA) is placed at the beginning of each span to compensate for



▲ Figure 3. (a) BER curves for back-to-back FSK (with 60 GHz FTS, 100 GHz FTS) and after 100 km SMF link, (b) eye diagram of demodulated FSK with 60 GHz FTS for back-to-back and (c) after 80 km SMF, (d) eye diagram of demodulated RZ-FSK with 100 GHz FTS for (d) back-to-back and (e) after 80 km SMF.



▲ Figure 4. Transmission link with three different schemes to compensate the fiber dispersion.

signal attenuation in the SMF and DCF and is followed by a variable optical attenuator (VOA) to adjust the span launch power. For long-distance transmission, dispersion compensation is always compensated for in each amplifier span. Each fiber span consists of 80 km SMF with dispersion-matching DCF. The optical fiber parameters for long-distance transmission are shown in Table 1.

System performance under different dispersion compensation schemes can be determined through simulation. A 1 dB tolerance range of the compensation ratio is between 98% to 102%, corresponding to a residual dispersion of 26 ps/nm, which is almost half the dispersion tolerance of RZ and DPSK. In this simulation, the DPSK signal is produced by a PM, and the RZ signal is generated by push-pull RZ modulation followed by NRZ modulation. Because of the relatively large signal bandwidth, dispersion should be carefully managed in the transmission of the FSK signal.

Fig. 5 shows how the dispersion compensation scheme and span input power affect system performance over 11 spans of 80 km transmission link. Multispan transmission over 880 km SMF is achieved for FSK. If the receiver sensitivity is defined

as the received optical power at BER of 10^{-9} , and given the same sensitivity penalty, DPSK has the maximum reach, and RZ has the minimum reach. For FSK and DPSK, post-compensation results in better performance than pre-compensation. However, for RZ, pre-compensation is preferred. Fig. 5 shows the tolerance to nonlinearity where the sensitivity penalty is calculated from the input power of each span. At low power, performance is degraded by amplified spontaneous emission (ASE) noise from the amplifiers. If the power is increased, self-phase modulation and dispersion degrades the signal. Between the two extremes, the optimal input power range is approximately 5 dBm to 8 dBm for FSK. The generated FSK signal has high tolerance to fiber input power for long distance transmission with post-compensation.

3.4 Performance of FSK with Different Dispersion Compensation Schemes

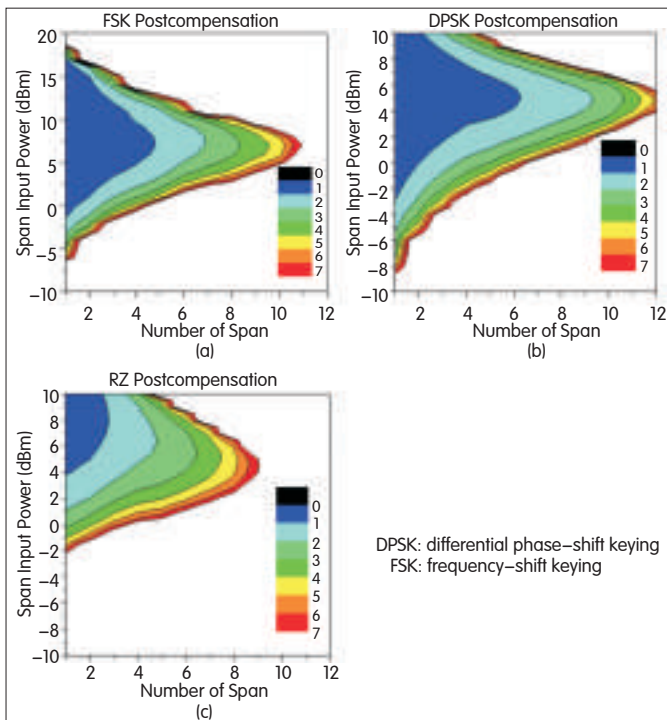
In this section, we show how dispersion compensation schemes affect performance of the FSK transmission system. At present, there are several techniques, including dispersion compensating fiber (DCF) and fiber bragg grating (FBG), that can be used to compensate for accumulated dispersion in the fiber. In

the following, we describe pre-compensation, post-compensation, and hybrid compensation for compensate for fiber dispersion. We use an ideal DCF for the dispersion compensation schemes. The DCF is placed at different points in each transmission span.

Fig. 4 shows the pre-compensation, post-compensation, and hybrid-compensation configurations. In each scheme, we use two EDFAs before and after the fiber link to compensate for and adjust the input power. In pre-compensation, the DCF is placed before the SMF. In post-compensation, the DCF is placed after the SMF. In hybrid compensation, the DCF is placed first, followed by the SMF and DCF. In these three schemes, the transmission span

▼ Table 1. Optical fiber parameters

Fiber Parameters	SMF	DCF
Dispersion D (ps/nm/km)	16	-90
Fiber Loss (dB/km)	0.2	0.6
Nonlinear Coefficient γ (W-km) ⁻¹	2.6	4
Dispersion Slope dD/d λ (ps/nm ² /km)	0.08	-0.21



▲ Figure 5. Receiver sensitivity penalty as a function of the span input power and the number of spans for (a) FSK with post-compensation scheme, (b) DPSK with post-compensation scheme and (c) 33% RZ with pre-compensation scheme.

length is 80 km. Fig. 6(a) to (c) shows the sensitivity of the receiver to the FSK signal for the three compensation schemes. Receiver sensitivity depends on SMF length and input power. The optimum span input power in each of the schemes is approximately 10 dBm. Post-compensation has the best tolerance to residual dispersion, and receiver sensitivity is below 1 dB. When the sensitivity power exceeds -20 dBm, post-compensation can tolerate about 60 ps/nm residual dispersion more than the other schemes. The optimized compensation ratio in the three schemes is less than 100%, and the dispersion compensation ratio degrades if the input power in each span is increased. Moreover, post-compensation has considerable tolerance to the power level. Post-compensation has very low receiver penalty and up to 25 dB tolerance of input power. Thus, transmission performance of post-compensation in transmitting an FSK signal is better than that of pre-compensation or hybrid compensation.

In the simulation, we found that dispersion tolerance in the post-compensation scheme is 95 ps/nm, and is the highest of all the compensation schemes. The optimized dispersion compensation ratio in each scheme is less than 100%. Full compensation or overcompensation causes pulse broadening, and transmission performance is degraded. In the different schemes, dispersion tolerance is at the maximum when the input power is 10 dBm. When the input power is relatively small, the power penalty is higher. On the contrary, when the input power is high, fiber nonlinearity causes power

loss. Post-compensation has the lowest power penalty; that is, when the input power is constant, post-compensation has the largest eye-opening. In practice, FSK signals should be transmitting in a long distance optical transmission link using post-compensation.

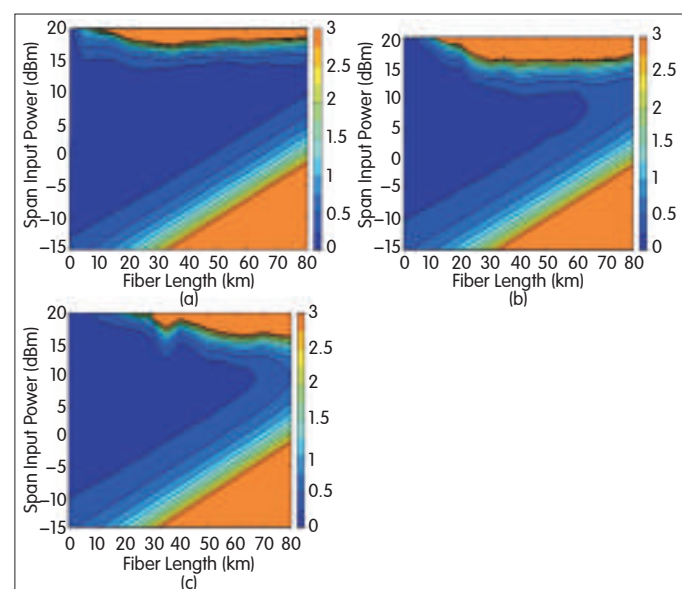
3.5 Performance of RZ-FSK with Different Dispersion Compensation Schemes

Fig. 1 shows the transmitter that generates the RZ-FSK signal can be divided into transmitter unit, fiber link unit, and receiver unit. In the simulation, the signal bit rate is fixed at 40 Gb/s, and the FTS of RZ-FSK is 100 GHz. For each compensation scheme, the transmission span consists of 80 km of SMF.

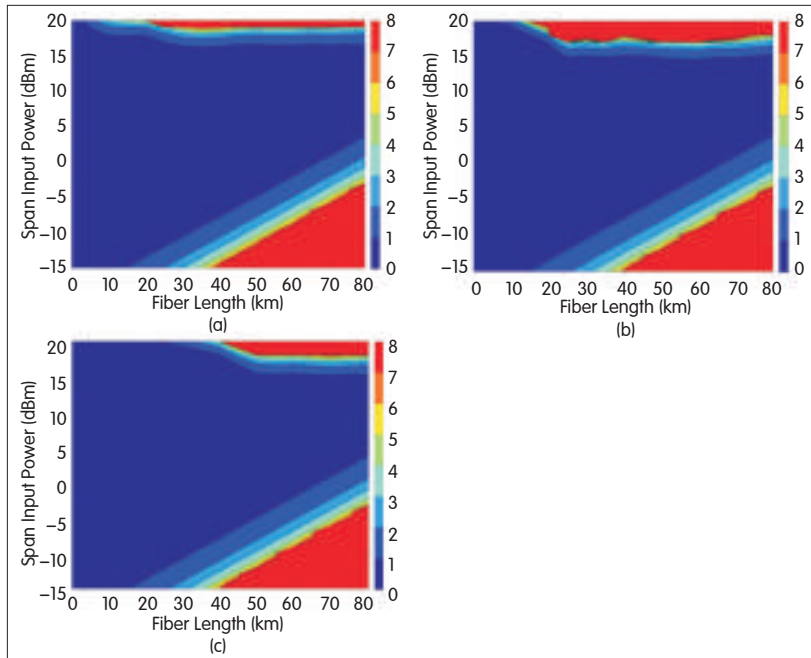
Fig. 7 shows how fiber input power affects receiver sensitivity in the three schemes. The optimized fiber input power in the three schemes ranges from 5 dBm to 15 dBm. Each of the schemes has a low receiver penalty and considerable resilience to fiber input power. Furthermore, post-compensation performs the best for transmitting RZ-FSK signals.

In Fig. 6 and Fig. 7, transmission performance of FSK and RZ-FSK formats is compared. In the three schemes, transmission using the RZ-FSK format is preferable for an FSK format with NRZ shape. First, the receiver power penalty using the RZ-FSK format is lower than that using the FSK format. Second, the RZ-FSK has high tolerance of input power level.

Finally, the RZ-FSK modulation format also has the good dispersion tolerance. We compare FSK and RZ-FSK formats to find the optimum frequency modulation format for high-bit-rate optical transmission systems. Receiver sensitivity is higher for RZ-DPSK than for RZ-FSK. However, for RZ-DPSK and RZ-FSK, pre-compensation provides



▲ Figure 6. Contour plot of receiver sensitivity for the FSK signal as a function of Input power and fiber length for (a) post-compensation, (b) pre-compensation and (c) hybrid compensation.



▲ Figure 7. Contour plot of receiver sensitivity for the RZ-FSK signal as a function of input power and fiber length for (a) post-compensation, (b) pre-compensation and (c) hybrid-compensation.

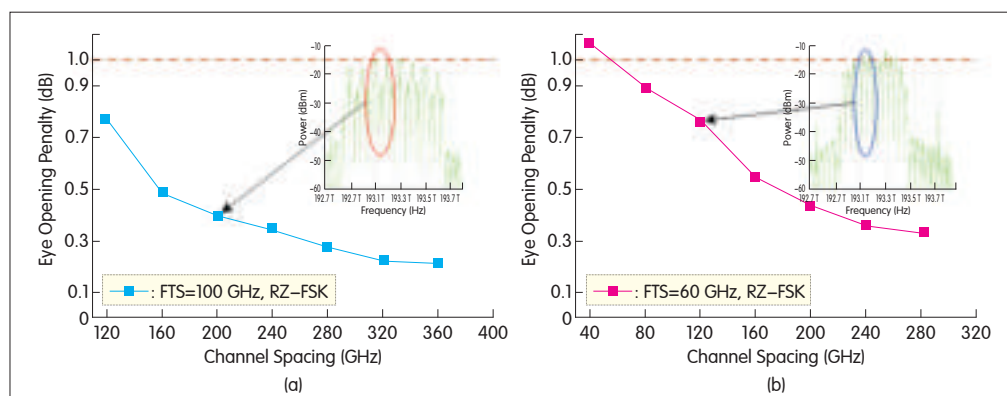
lower receiver sensitivity than post-compensation. Hybrid compensation provides the highest receiver sensitivity for RZ-DPSK or RZ-FSK signal transmission. Post-compensation provides higher receiver sensitivity than pre-compensation, which is similar to hybrid compensation and is easily to implement practice. Therefore, dispersion post-compensation is chosen for our experiment on RZ-FSK signal transmission.

3.6 Performance of RZ-FSK Signal in a 4 × 40 Gb/s WDM Transmission System

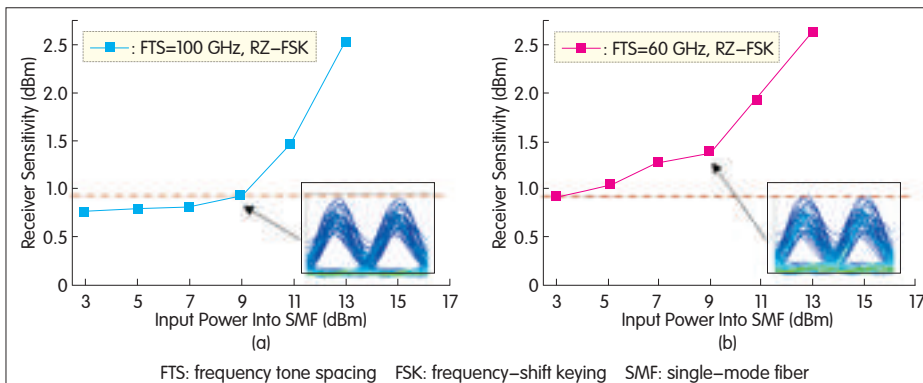
Wavelength division multiplexing (WDM) transmission at 40 Gb/s/channel is a hot topic in high-speed optical transmission. The main aim of such transmission is to achieve high spectral efficiency and overcome limitations to transmission distance cause by fiber nonlinearity and chromatic dispersion. In this section, we analyze RZ-FSK signals with different FTSs. We determine advantages and disadvantages in terms of spectral efficiency, tolerance against fiber nonlinearity, and chromatic dispersion in a 4 × 40 Gb/s WDM transmission system. We show linear cross penalty as a function of channel spacing for both signal formats in a four-channel WDM configuration. We use flat-top AWGs for wavelength multiplexing

and de-multiplexing (Fig. 8). The optical bandwidth of the AWGs is set to three quarters of the channel spacing. The PRBS pattern length is $2^{23}-1$. The PRBS patterns in the neighboring optical channels are offset by 25% of the total pattern length for de-correlation. Fig. 8(a) (insert) shows the WDM optical spectrum for an RZ-FSK signal with 100 GHz FTS, and Fig. 8(b) (insert) shows the WDM optical spectrum of an RZ-FSK signal with 60 GHz FTS. Both signals have double FTS channel spacing. Fig. 8(a) and (b) shows the crosstalk penalties at the center channel (the second channel) as a function of channel spacing. As the channel spacing is reduced, the linear crosstalk penalty gradually increases. For the same channel spacing, the eye-opening penalty (EOP) for the RZ-FSK signal with 100 GHz FTS is lower than that of the RZ-FSKZ signal with 60 GHz FTS. Kerr nonlinearity and chromatic dispersion of the fiber are significant issues of deterioration in WDM systems and cause EOP. The ITU G.692 proposal has three channel spacings for WDM application: 50 GHz, 100 GHz, and 200 GHz. Spectral efficiency in the RZ-FSK format (if it is intended for WDM transmission) has a limitation.

The channel spacing must be greater than or equal to the FTS; otherwise, crosstalk occurs between channels. To avoid linear crosstalk as much as possible, the WDM source in our configuration includes four DFB lasers with a frequency spacing of 200 GHz. The centre frequencies of the generated RZ-FSK signals are 193, 193.2, 193.4, and 193.6 THz, which conforms to the ITU-standard. In a 4 × 40 Gb/s WDM transmission system, two RZ-FSK signals (both with 100 GHz or 60 GHz FTS) are transmitted and received over 4 × 80 km spans of SMF followed by DCF. Fig. 9 (a) and (b) shows receiver sensitivity as a function of input power. RZ-FSK modulation with 100 GHz FTS is more tolerant of Kerr nonlinear distortion than RZ-FSK modulation with 60 GHz FTS. RZ-FSK with 60 GHz FTS has more compact optical spectra than RZ-FSK with 100 GHz, but RZ-FSK with 100 GHz is more suitable for WDM transmission systems



▲ Figure 8. Measured eye opening penalty versus channel spacing for RZ-FSK with (a) 100 GHz FTS, (b) 60 GHz FTS in 4 × 40 Gb/s WDM transmission system.



▲ Figure 9. Measured receiver sensitivities versus different input powers into SMF-28 for RZ-FSK with (a) 100 GHz FTS, (b) 60 GHz FTS in 4 × 40 Gb/s WDM transmission system.

because its transmission performance is better.

4 Experiment Setup and Results

Fig. 10 shows the experiment setup. The signal sources include one external cavity laser (ECL) at 1557.64 nm and a tunable laser at 1558.46 nm with 100 GHz FTS. In this experiment, we launch an RZ-FSK signal with 100 GHz FTS, because it has better transmission performance than an RZ-FSK signal with 60 GHz FTS. Two beams can be generated by an MZM driven by 50 GHz clock. The data at 40 Gb/s (PRBS $2^{23}-1$, ITU-T G.709 FEC) is generated by an SHF BPG44E BT pattern generator and added to the MZM₁. The phase-modulated signal is then demodulated by the MZDI with 25 ps delay, and this creates a 40 Gb/s FSK signal. MZM₂ is driven by 20 GHz clock and is used to generate the RZ-FSK signal. The output power of the two lasers has to be fine tuned so that the optical pulse of the RZ-FSK transmitter is relatively constant. The transmission span consists of 100 km of SMF with a matching length of DCF for post-compensation. We choose post-compensation in the experiment because the simulations show that receiver performance in post-compensation is good, and post-compensation is easily implemented in practice. The SMF dispersion at 1550 nm is 16.9 ps/nm/km, and the DCF dispersion at 1550 nm is -100 ps/nm/km. In each span, the SMF input power is 6 dBm, and the DCF input power is 0 dBm.

Optical wavelength conversion (OWC) technology is important in large-capacity optical networks because it can reduce the probability of blocking, and it allows interconnected links and distributed network management. To the convert

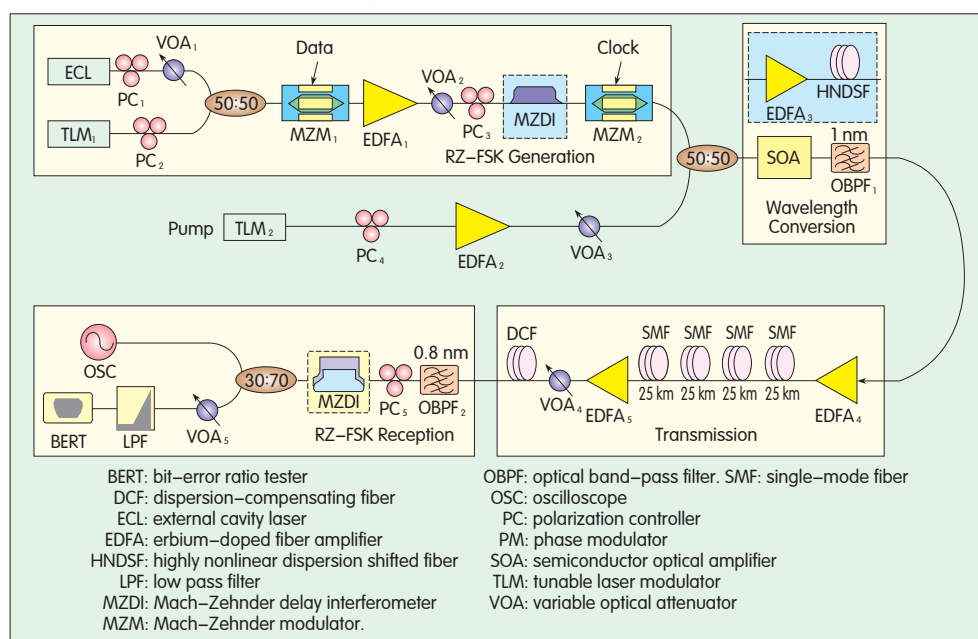
wavelength of a high-speed RZ-FSK signal, an interferometer based on cross-phase modulation (XPM) in the SOA cannot be used; instead, a transparent wavelength conversion scheme must be used to preserve the frequency information. By using FWM in fibers, it is possible to implement a modulation-transparent wavelength converter. Recent FWM wavelength conversion experiments also show that using HNDSF can result in large spectral and dynamic ranges.

Therefore, wavelength conversion using SOA or HNDSF is an ideal way of transparently converting wavelength

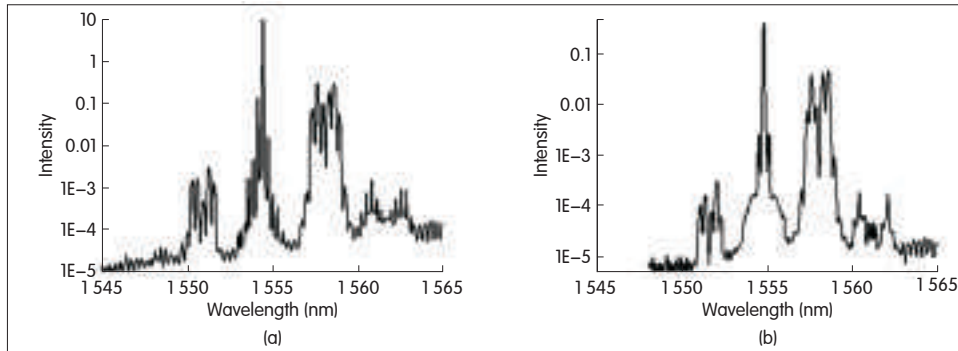
conversion of an RZ-FSK signal.

The pump source is an ECL at 1554.8 nm. The RZ-FSK signal is amplified and combined with the pump after polarization alignment. FWM occurs in the 300 m long HNDSF with a nonlinear coefficient $\gamma = 10 \text{ W}^{-1}\text{km}^{-1}$. The zero dispersion wavelength of the HNDSF is 1556 nm, and the dispersion slope is 0.022 ps/nm²/km. The SOA is 500 μm long with a 200 mA driving current. An OBPF₁ with 1 nm bandwidth is used to filter out the converted signal.

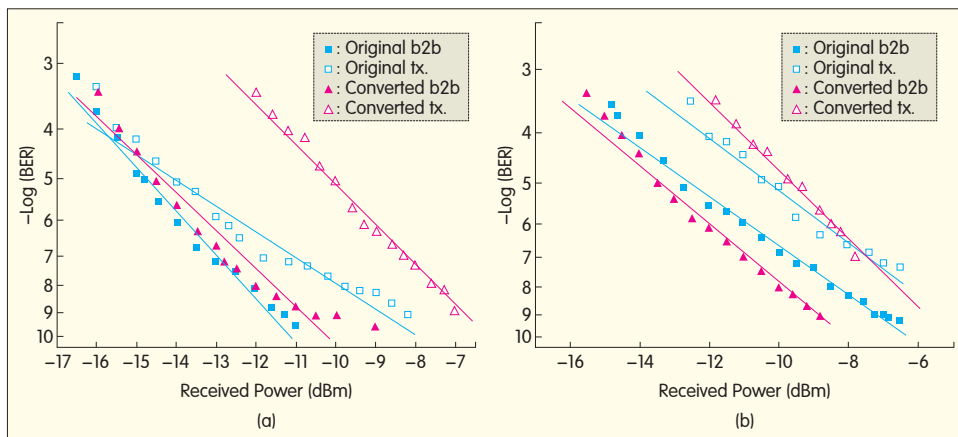
Fig. 11 shows the optical spectra at the output of the HNDSF and the SOA. FWM conversion efficiency of to -19 dB can be achieved in SOA, and conversion efficiency of up to -21 dB can be achieved in HNDSF. Fig. 12 shows the BER of the RZ-FSK signal for back-to-back and wavelength conversion. Because the FWM in fibers can be exploited to achieve all-optical reshaping, the ER of the converted FSK signal is enhanced. This is confirmed in our experiment. 2R regeneration is observed in HNDSF. The sensitivity to the



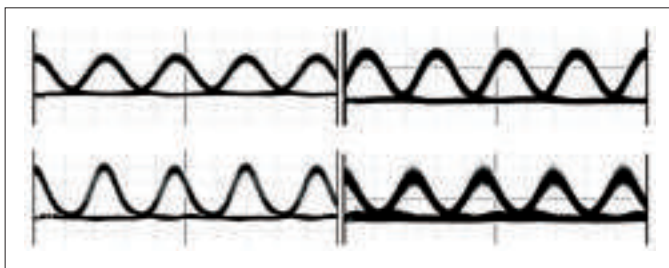
▲ Figure 10. Experiment setup.



▲ Figure 11. Measured FWM output from (a) the SOA and (b) the HNDSF.



▲ Figure 12. Measured BER curves for (a) SOA and (b) HNDSF.



▲ Figure 13. Measured eye diagrams (10 ps/div) for (a) original RZ-FSK, (b) converted by SOA, (c) converted by HNDSF, (d) converted and transmitted.

converted RZ-FSK signal is improved by 1.8 dB and results in less than 2 dB penalty after 100 km transmission. Fig. 13 shows the eye diagrams. The converted RZ-FSK signal in HNDSF has a narrower pulse width and higher ER, which indicates 2R regeneration.

At the receiver, frequency discrimination for RZ-FSK demodulation is achieved by an OBPF2 with 0.8 nm bandwidth filter, which provides more than 25 dB suppression ratio between the two FSK tones. This demodulated signal is detected by a SHF 47100A V/E converter and BER is measured by SHF EA44 error analyzer.

We also measured BER in RZ-FSK transmission. Fig. 14(a) shows the measured BER curves before and after the

transmission link, where error-free transmission in RZ-FSK and FSK occurs. The power penalty for FSK at $\text{BER} = 10^{-9}$ is about 5.0 dB. The transmission penalties for tone one and tone two of RZ-FSK are both less than 5 dB. Fig. 14(b) to (e) shows eye-diagrams of FSK and RZ-FSK for back-to-back, and after transmission through a 100 km SMF transmission link with matching DCF. Because FSK is orthogonal to intensity modulation and vector modulation (polarization shift keying), it can be used in the context of the combined modulation format to decrease the data rate or enhance the symbol rate. It can also be utilized in the orthogonal labeling as the modulation format for the payload or the label.

5 Conclusion

In this paper, we have proposed a new optical modulation transmitter that transmits RZ-FSK signals by using two CW lasers, an MZM, an MZDI, and another MZM driven by a sinusoidal voltage at half the bit rate. The demodulation can be simply

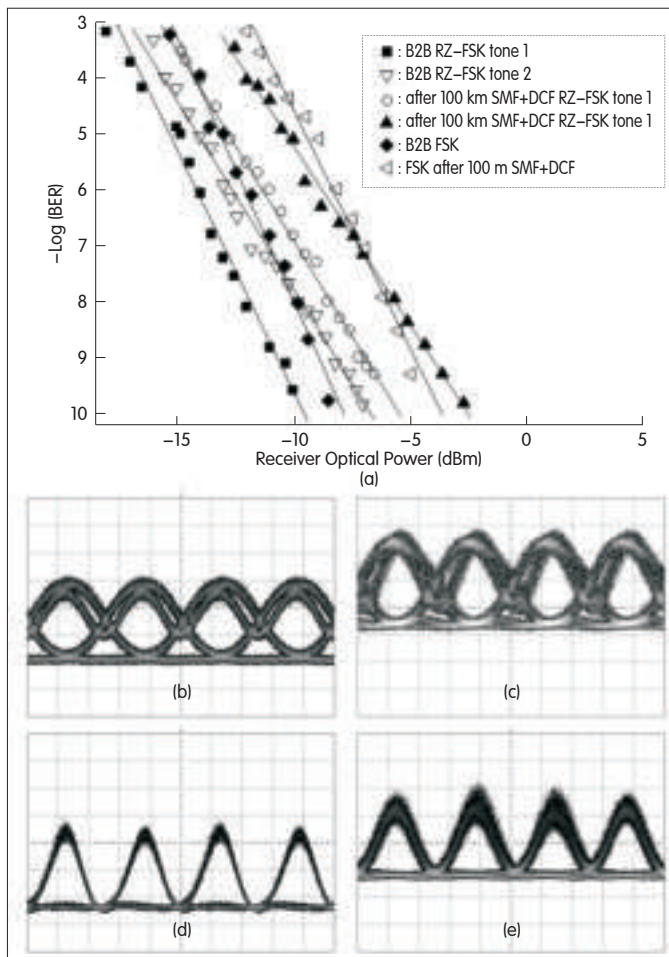
achieved on one bit rate through one MZDI or an AWG demultiplexer with balanced detection. Using numerical simulation, MZM and PM was analyzed and the effect of different FTSs on the generated FSK signal were determined. The advantage of the proposed frequency modulation scheme is that the FTS of the generated signal is tunable by changing the center frequencies of two used lasers. For high speed transmission, it is useful to adjust the FTS and achieve higher receiver sensitivity. Moreover, this proposed scheme is simple and potentially inexpensive. We also experiment with transparent wavelength conversion based on FWM in a SOA and in a HNDSF for a 40 Gb/s RZ-FSK signal. We have analyzed 40 Gb/s RZ-FSK signal transmission over 100 km SMF link with matching DCF. The results of our experiment suggest that RZ-FSK modulation could be a promising candidate for future high-speed transmission system and optical label-switching networks.

Acknowledgments

This work was supported by the National High Technology Research and Development Program (973) of China (Grant No. 2010CB328300), and National Natural Science Foundation of China (No. 61107064, No. 61177071, No. 600837004, No. 60777010), Doctoral Fund of Ministry of Education, Open Fund of State Key Lab of ASIC & System (No. 11MS009), Pujiang Fund and Shuguang fund.

FSK Modulation Scheme for High-Speed Optical Transmission

Nan Chi, Wuliang Fang, Yufeng Shao, Junwen Zhang, and Li Tao



▲ Figure 14. Measured BER curves for back-to-back RZ-FSK and after 100km SMF + DCF link(a), the eye diagram of demodulated FSK (10 ps/div) for (b) back-to-back (c) after 100 km SMF + DCF link, the eye diagram of demodulated RZ-FSK for (d) back-to-back and (e) after 100 km SMF + DCF link.

References

- [1] P. J. Winzer, R. J. Essiambre, "Advanced Optical Modulation Formats," *Proc. ECOC 2003*, Rimini, Italy, Invited paper Th2.6.1, pp. 1002–1003, 2003.
- [2] J. Yu, X. Zhou, "Multilevel Modulations and Digital Coherent Detection," *Optics Fiber Technology*, vol. 15, pp. 197–208, 2009.
- [3] J. Yu, X. Zhou, M. F. Huang, Y. Shao, D. Qian, T. Wang, M. Cvijetic, P. Magill, L. Nelson, M. Birk, S. Ten, H. B. Matthew, S. K. Mishra, "17 Tb/s (161 × 114 Gb/s) PolMux-RZ-8PSK Transmission over 662 km of Ultra-Low Loss Fiber using Cband EDFA Amplification and Digital Coherent Detection," *ECOC 2008*, PDP Th.3. E.2, 2008.
- [4] A. Gnauck, P. Winzer, "Optical Phase-Shift-Keyed Transmission," *IEEE J. Lightwave Technol.*, vol. 23, no. 1, pp. 115–130, 2005.
- [5] Y. Han, G. F. Li, "Theoretical Sensitivity of Direct-Detection Multilevel Modulation Formats for High Spectral Efficiency Optical Communications," *IEEE Journal of Selected Topics in Quantum Electronics*, vol. 12, no. 4, pp. 115–130, 2006.
- [6] Yufeng Shao, Shuangchun Wen, Lin Chen, Ying Li, and Huiwen Xu, "A Staggered Differential Phase-Shift Keying Modulation Format for 100Gb/s Applications," *Optics Express*, vol. 16, no. 7, pp. 12937–12942, 2008.
- [7] Klekamp, W. Idler, and R. Dischler, "Comparison of FSK by Directly Modulated DFB Laser with DPSK, NRZ, and RZ Modulation Formats at 10 Gb/s," in *Proc. ECOC '03*, Paper We4.P.118, Rimini, Italy, 2003.
- [8] N. Chi, J. Zhang, P. V. Holm-Nielsen, L. Xu, I. T. Monroy, C. Peucheret, K. Yvind, L. J. Christiansen, and P. Jeppesen, "Experimental demonstration of cascaded transmission and all-optical label swapping of orthogonal IM/FSK labelled signal," *Electron. Lett.*, vol. 39, no. 8, pp. 676–678, 2003.
- [9] J. Zhang, N. Chi, P. V. Holm-Nielsen, C. Peucheret, and P. Jeppesen,

- "Performance of Manchester-Coded Payload in An Optical FSK Labeling Scheme," *IEEE Photonics Technol. Lett.*, vol. 15, no. 8, pp. 1174–1176, 2003.
- [10] T. Kawanishi, K. Higuma, T. Fujita, J. Ichikawa, T. Sakamoto, S. Shinada, and M. Izutsu, "High-Speed Optical FSK Modulator for Optical Packet Labeling," *IEEE J. Lightwave Technol.*, vol. 23, no. 1, pp. 87–94, 2005.
- [11] Y. Yu, G. Mulvihill, S. O'Duill, and R. O'Dowd, "Performance Implications of Wide-Band Lasers for FSK Modulation Labeling Scheme," *IEEE Photon. Technol. Lett.*, vol. 16, no. 1, pp. 39–41, 2004.
- [12] E. N. Lallas, N. Skarmoutsos, and D. Syvridis, "Coherent Encoding of Optical FSK Header for All Optical Label Swapping Systems," *IEEE J. Lightwave Technol.*, vol. 23, no. 3, pp. 1199–1209, 2005.
- [13] N. Chi, J. Zhang, P. V. Holm-Nielsen, L. Xu, I. T. Monroy, C. Peucheret, K. Yvind, L. J. Christiansen, and P. Jeppesen, "Experimental Demonstration of Cascaded Transmission and All-Optical Label Swapping of Orthogonal IM/FSK Labelled Signal," *Electron. Lett.*, vol. 39, no. 8, pp. 676–678, 2003.
- [14] J. Zhang, N. Chi, P. V. Holm-Nielsen, C. Peucheret, and P. Jeppesen, "Performance of Manchester-Coded Payload in An Optical FSK Labeling Scheme," *IEEE Photon. Technol. Lett.*, vol. 15, no. 8, pp. 1174–1176, 2003.
- [15] T. Kawanishi, T. Sakamoto, T. Miyazaki, and M. Izutsu, "High-Speed Optical DQPSK and FSK Modulation Using Integrated Mach-Zehnder Interferometers," *Optics Express*, vol. 14, no. 10, pp. 4469–4478, 2006.

Manuscript received: November 30, 2011

Biographies

Nan Chi (nanchi@fudan.edu.cn) received her BS and PhD degrees in electrical engineering from Beijing University of Posts and Telecommunications in 1996 and 2001. From July 2001 to December 2004, she worked as assistant professor at the Research Center COM, Technical University of Denmark, Lyngby. From January 2005 to April 2006, she was a research associate at the University of Bristol, UK. In June 2006, she joined the Wuhan National Laboratory for Optoelectronics, Huazhong University of Science and Technology. There, she worked as a full professor. She joined the School of Information Science and Engineering, Fudan University, in June 2008. She is the author or co-author of more than 150 papers and the co-holder of two US patents. She has given seven invited talks in international conferences and workshops. She was chair of the optical switching and routing technologies workshop at the Asia-Pacific Optical Conference 2007, and she was the local committee chair of ACP 2010. She has received a New Century Excellent Talent Award from the Education Ministry of China in 2006 and the Shuguang Scholarship in 2009. Her research interests include optical packet/burst switching, all-optical processing, and advanced modulation formats.

Wuliang Fang (fangwuliang2005@163.com) received his BS degree in optical information and technology from Huazhong University of Science and Technology, Wuhan, China, in 2009. Since 2009, he has been studying for his master's degree in the Department of Communication Science and Engineering, Fudan University. His research interests include multimode fiber theories, spatial multiplexing, coherent optical communication, and signal processing.

Yufeng Shao (shaoyufeng@fudan.edu.cn) received his BS and ME degrees from Chongqing University of Post and Communications, China, in 2000 and 2005. He received his PhD degree from Hunan University, China, in 2009. He is currently a postdoctoral researcher and lecturer at the State Key Lab of ASIC & Systems, and also at the Department of Communication Science and Engineering, Fudan University, Shanghai. From April 2011 to August 2011, he was a research associate at Hong Kong Polytechnic University. His research interests include new modulation format techniques, all-optical signal processing, optical label switching, and optical OFDM technology. He has authored or coauthored more than 80 publications in international journals and at conferences. He holds one Chinese patent and has five Chinese patents pending.

Junwen Zhang (hustzjw@gmail.com) received his BS degree in optical information and technology from Huazhong University of Science and Technology, Wuhan, China, in 2009. Since 2009, he has been studying for his PhD degree in the Department of Communication Science and Engineering, Fudan University. His research interests include high-speed optical transmission, coherent optical communication, and signal processing.

Li Tao (taoli522930@gmail.com) received his BS degree in optical information and technology from Huazhong University of Science and Technology, Wuhan, China, in 2010. Since 2010, he has been studying for his PhD degree in the Department of Communication Science and Engineering, Fudan University. His research interests include high-speed optical transmission, coherent optical communication, OFDM, and signal processing.

Computationally Efficient Nonlinearity Compensation for Coherent Fiber–Optic Systems

Likai Zhu and Guifang Li

(CREOL, The College of Optics and Photonics, University of Central Florida, 4000 Central Florida Boulevard, Orlando, Florida 32816, USA)

Abstract

Split-step digital backward propagation (DBP) can be combined with coherent detection to compensate for fiber nonlinear impairments. A large number of DBP steps is usually needed for a long-haul fiber system, and this creates a heavy computational load. In a trade-off between complexity and performance, interchannel nonlinearity can be disregarded in order to simplify the DBP algorithm. The number of steps can also be reduced at the expense of performance. In periodic dispersion-managed long-haul transmission systems, optical waveform distortion is dominated by chromatic dispersion. As a result, the nonlinearity of the optical signal repeats in every dispersion period. Because of this periodic behavior, DBP of many fiber spans can be folded into one span. Using this distance-folded DBP method, the required computation for a transoceanic transmission system with full inline dispersion compensation can be reduced by up to two orders of magnitude with negligible penalty. The folded DBP method can be modified to compensate for nonlinearity in fiber links with non-zero residual dispersion per span.

Keywords

coherent fiber communication; nonlinearity compensation; folded digital backward propagation

1 Introduction

Coherent detection is emerging as the most attractive candidate for next-generation fiber communication systems. A coherent detector is highly sensitive and can detect all the information about the optical field, including amplitude, phase, and polarization. This enables linear and nonlinear impairments to be compensated for using digital signal processing (DSP).

Chromatic dispersion is usually a dominant factor that distorts the optical waveform as it propagates along the fiber. In most fiber links, chromatic dispersion is optically compensated for by cascading two or more kinds of fiber with inverse dispersion parameters. New inverse dispersion fibers compensate for both dispersion and dispersion slope while minimizing the total polarization mode dispersion (PMD). This results in wideband dispersion flatness [1]. With coherent detection, chromatic dispersion and PMD can also be compensated for using DSP [2].

Nonlinear impairments, including self-phase modulation (SPM), cross-phase modulation (XPM) and four-wave mixing

(FWM), increase with launching power. A trade-off between high optical signal-to-noise ratio (OSNR) and low nonlinear impairments results in a power level that allows optimal performance in a fiber link. As linear impairment compensation technology matures, nonlinear effects become the factor that limits the capacity and transmission distance of long-haul fiber communication systems [3].

Optical propagation in fiber is governed by the nonlinear Schrödinger equation (NLSE), which has no analytical solution. Thus, split-step digital backward propagation (DBP) is necessary to compensate for the joint effects of dispersion and nonlinearity. For the split-step method to be accurate, the step size has to be small enough for the linear and nonlinear effects to be decoupled in each step; however, this results in heavy computational load [4], [5].

2 Simplified DBP Methods

In [6], DSP for wavelength-division multiplexing (WDM) transmission was performed by solving the NLSE for the total optical field in the fiber. With phase-locked local oscillators, the relative phases between the WDM channels are preserved

so that the total optical field can be reconstructed before DBP. The SPM, XPM, and FWM can be compensated for using the total-field NLSE; however, the large total optical bandwidth results in a small dispersion-limiting step size and high sampling rate [7].

DBP can also be performed by disregarding the FWM and solving the coupled NLSE. Compared to solving the total-field NLSE, solving the coupled NLSE requires a smaller step number and lower sampling rate [8], [9]. In addition, phase-locking between the local oscillators is not necessary. In the coupled NLSE algorithm, the step number can be further reduced by factorizing the dispersive interchannel walk-off effects [10].

Moreover, compared to interchannel nonlinearity compensation, intrachannel nonlinearity compensation usually requires a smaller number of steps because the step size is not limited by the interchannel walk-off effect. In [11] and [12], Fujitsu gave the results of one-step-per-span DBP for intrachannel nonlinearity compensation of dual polarization quadrature phase-shift keying (DP-QPSK) transmission.

As a one-step-per-link approach, lumped-phase de-rotation is proportional to the received single-channel optical intensity and can be used for SPM compensation [13], or it is proportional to the multichannel optical intensity and can be used for XPM compensation [14]. The lumped-phase de-rotation method is based on the assumption that the intensity waveform remains unchanged throughout the fiber propagation.

In the split-step DBP, the step size has to be small enough so that the linear dispersion and nonlinear effects being compensated for are accurately described. Because the optical intensity along the fiber varies, step sizes can be variable to minimize the number of steps [5]. The DBP algorithm can be simplified by neglecting FWM or XPM; however, for a fiber link in which chromatic dispersion causes significant pulse reshaping and interchannel walk-off, multiple steps per span are usually needed, especially for interchannel nonlinearity compensation. Reducing complexity by simply increasing the step size reduces performance.

In addition to these DBP methods, other DSP methods combined with coherent detection have been proposed for nonlinearity compensation. In [15], adaptive filtering in carrier phase recovery (AFCPR) was proposed to suppress nonlinear phase noise. However, information about the neighboring channels, which is necessary for complete XPM compensation, is not used in the AFCPR algorithm. In [16], a pilot-based XPM compensation method for a coherent optical (CO-OFDM) system is proposed. This method may not be applicable to systems with other modulation formats.

3 Distance-Folded DBP

In [17], we took advantage of the periodic behavior of an optical signal in a periodic dispersion-managed fiber-optic system to propose a computationally efficient distance-folded DBP method for nonlinearity compensation. With periodic dispersion management, the linear and

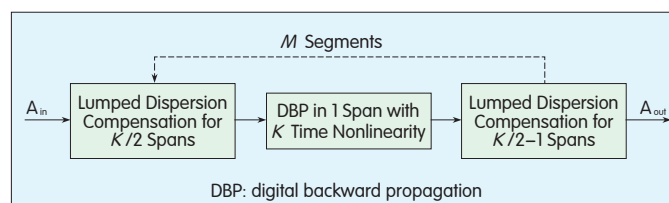
nonlinear behavior of the signal repeats itself in every dispersion period, and the DBP of many fiber spans can be folded into one span.

For long-haul fiber-optic transmission, an optimum power is derived from the trade-off between high OSNR and low nonlinear effects. The nonlinear phase shift at the optimum power level is on the order of one radian [18]. Therefore, for transoceanic fiber transmission systems, which consist of more than 100 amplified spans, the nonlinear effects in each span are weak. As a result, chromatic dispersion is the dominant factor that determines the optical waveform evolution within each span.

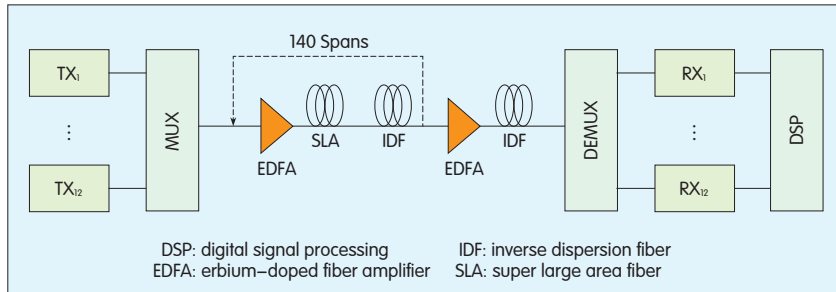
Assuming weak nonlinearity and periodic dispersion management, the optical field after K spans of propagation is equivalent to the optical field after propagation in one fiber span where the nonlinearity is K times that of the original fiber. This equivalence suggests that the DBP for K spans can be folded into a single span with K times the nonlinearity. Assuming the step size for the split-step implementation of DBP is unchanged, the computational load for the folded DBP can be saved by a folding factor of K .

The assumption that the nonlinear behavior is repeated in every span is not exactly valid because fiber nonlinearity also changes the waveform, and dispersion is not perfectly periodic if the residual dispersion per span (RDPS) is non-zero or if the dispersion slope is not compensated for. These effects accumulate and, as a result, waveform evolutions are not identical between two spans that are far away from each other. In order for nonlinearity compensation to be accurate, the entire long-haul transmission system can be divided into segments of multiple dispersion-managed spans, and distance-folded DBP can be performed within each segment. For a fiber link with $M \times K$ spans, the distance-folded DBP is as in Fig. 1.

To demonstrate the effectiveness of the distance-folded DBP, we simulate a WDM system with QPSK modulation at 56 Gbit/s using VPI Transmission Maker. The simulation setup is shown in Fig. 2. Twelve channels of non-return-to-zero (NRZ) QPSK signal are transmitted with 50 GHz channel spacing. The linewidth of the lasers is 100 KHz. The dispersion-managed fiber link consists of 140 spans of 50 km of the OFS UltraWave SLA/IDF Ocean Fiber combination. The erbium-doped fiber amplifier (EDFA) noise is 4.5 dB. The loss, dispersion, relative dispersion slope, and effective area of the SLA fiber are 0.188 dB/km, 19.5 ps/nm/km, 0.003/nm, and 106 μm^2 . The corresponding parameters for the IDF fiber are 0.23 dB/km, -44 ps/nm/km, 0.003/nm, and 31 μm^2 . A



▲ Figure 1. Folded DBP for a periodic dispersion-managed fiber link with $M \times K$ spans.



▲ Figure 2. Dispersion managed WDM system.

piece of fiber at the receiver was used to compensate for the accumulated residual dispersion.

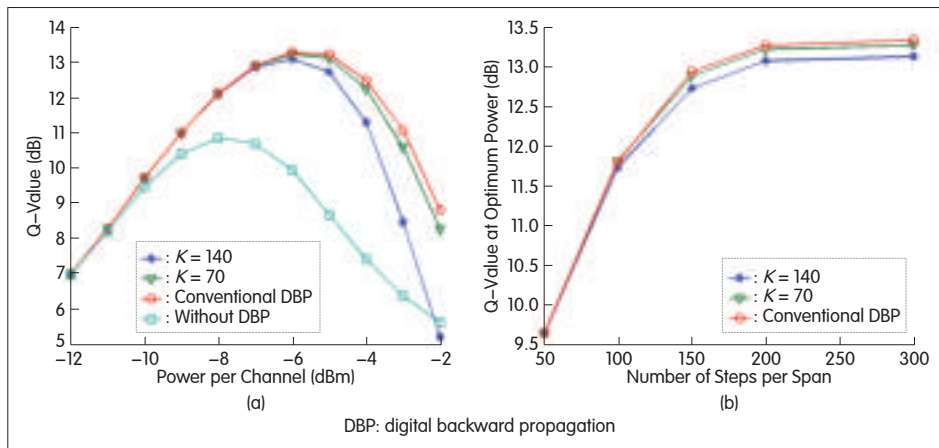
The DBP in Fig. 1 was performed in Matlab. Without loss of generality, we solved the coupled NLSE with the non-iterative asymmetric split-step Fourier method (SSFM). In long-haul WDM fiber links, the step size is usually limited by dispersion [4]. Therefore, for both SLA fiber and IDF fiber, we used the same number of steps in each span so that the dispersion in each step was approximately the same. After matched

filtering, phase estimation, and clock recovery, the Q-value averages of the WDM channels were estimated.

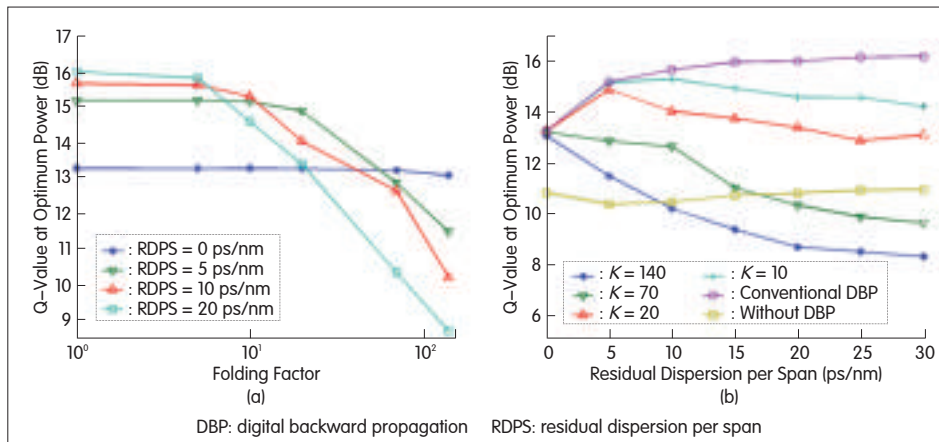
We first simulated the transmission with RDPS = 0. The Q-value as a function of the launching power is shown in Fig. 3(a). Without nonlinearity compensation, the maximum Q-value was 10.8 dB. With conventional DBP in all spans, the Q-value increased to 13.3 dB as a result of nonlinearity compensation. With folded DBP that has a folding factor of 140 ($M = 1$, $K = 140$), the maximum Q-value was 13.1 dB.

The 0.2 dB Q-value penalty was due to the accumulated nonlinear waveform distortion, which reduced the accuracy of nonlinearity compensation. There was almost no penalty when the folding factor was 70 ($M = 2$, $K = 70$). Fig. 3(b) shows the Q-value as a function of step number per span. The folded DBP method does not require an increased step number per span.

The nonlinear impairments in a dispersion-managed fiber link can be suppressed with inline residual dispersion



▲ Figure 3. (a) Q-value vs. launching power per channel and (b) Q-value at optimum power vs. step number per span with RDPS = 0 ps/nm.



▲ Figure 4. (a) Q-value vs. folding factor K and (b) Q-value vs. RDPS.

[19]–[21]. However, the non-zero RDPS can induce a penalty in the folded DBP. Fig. 4(a) shows Q-value obtained at the optimum power level as a function of the folding factor K . With an RDPS of 5 ps/nm (20 ps/nm), the maximum Q-value can be approached using a folding factor of 20 (5). Fig. 4(b) shows Q-value as functions of RDPS. With conventional DBP in all spans, the Q-value increases with RDPS and approaches the maximum value when RDPS is greater than 10 ps/nm. When folded DBP is used, the Q-value penalty increases with RDPS.

4 Discussion

In this paper, we have presented a distance-folded DBP method for periodic-dispersion-managed fiber systems. Distance-folded DBP minimizes performance penalty for a fiber link with full inline dispersion compensation. However, most of the deployed fiber links have non-zero RDPS in order to avoid resonant nonlinearity. For such fiber links, the computational load required to approach the maximum Q-value increases with the RDPS.

To solve this problem, we have recently used a dispersion-folded DBP method instead of a distance-folded DBP method. In

long-haul fiber transmission, the optical waveform and, consequently, the nonlinear behavior of the optical signal repeat at locations of identical accumulative dispersion. Hence, the DBP steps can be folded according to the accumulated dispersion. The effectiveness of dispersion-folded DBP for fiber links with large RDPS has been demonstrated numerically and experimentally.

References

- [1] Kazunori Mukasa, Katsunori Imamura, Iwao Shimotakahara, Takeshi Yagi, and Kunio Kokura, "Dispersion compensating fiber used as a transmission fiber: inverse/reverse dispersion fiber," in *J. Opt. Fiber. Commun.*, vol. 3, no. 5, pp. 292–339, 2006.
- [2] C.R.S. Fludger, T. Duthel, D. van den Borne, C. Schullien, E.-D. Schmidt, T. Wuth, J. Geyer, E. De Man, Khoe Giok-Djan, and H. de Waardt, "Coherent equalization and POLMUX-RZ-DQPSK for robust 100-GE transmission," in *J. Lightwave Technol.*, vol. 26, no. 1, pp. 64–72, Jan. 2008.
- [3] Alexei Pilipetski, "Nonlinearity management and compensation in transmission systems," in *Proc. OFC/NFOEC 2010*, San Diego, CA, paper OTuL5.
- [4] O.V. Sinkin, R. Holzlohner, J. Zweck, C.R. Menyuk, "Optimization of the split-step Fourier method in modeling optical-fiber communications systems," in *J. Lightw. Technol.*, vol. 21, no. 1, pp. 61–68, Jan. 2003.
- [5] Q. Zhang and M. I. Hayee, "Symmetrized split-step Fourier scheme to control global simulation accuracy in fiber-optic communication systems," in *J. Lightw. Technol.*, vol. 26, no. 2, pp. 302–316, Jan. 2008.
- [6] X. Li, X. Chen, G. Goldfarb, E. Mateo, I. Kim, F. Yaman, and G. Li, "Electronic post-compensation of WDM transmission impairments using coherent detection and digital signal processing," in *Opt. Express*, vol. 16, no. 2, pp. 880–888, Jan. 2008.
- [7] L. Zhu, X. Li, E. F. Mateo, and G. Li, "Complementary FIR filter pair for distributed impairment compensation of WDM fiber transmission," in *IEEE Photon. Technol. Lett.*, vol. 21, no. 5, pp. 292–294, Mar. 2009.
- [8] Eduardo Mateo, Likai Zhu, and Guifang Li, "Impact of XPM and FWM on the digital implementation of impairment compensation for WDM transmission using backward propagation," in *Opt. Express*, vol. 16, no. 20, pp. 16124–16137, Sep. 2008.
- [9] Likai Zhu, Fatih Yaman, and Guifang Li, "Experimental demonstration of XPM compensation for WDM fibre transmission," in *Electronics Lett.*, vol. 46, no. 16, pp. 1140–1141, Aug. 2010.
- [10] Eduardo F. Mateo, Fatih Yaman, and Guifang Li, "Efficient compensation of inter-channel nonlinear effects via digital backward propagation in WDM optical transmission," in *Opt. Express*, vol. 18, no. 14, pp. 15144–15154, Jul. 2010.
- [11] S. Oda, T. Tanimura, T. Hoshida, C. Ohshima, H. Nakashima, Z. Tao, and J. C. Rasmussen, "112 Gb/s DP-QPSK transmission using a novel nonlinear compensator in digital coherent receiver," in *Proc. Opt. Fiber Conf. (OFC'09)*, San Diego, CA, Paper OThR6.
- [12] L. Li, Z. Tao, L. Liu, W. Yan, S. Oda, T. Hoshida, and J. C. Rasmussen, "Nonlinear Polarization Crosstalk Canceller for Dual-Polarization Digital Coherent Receivers," in *Proc. Opt. Fiber Conf. (OFC'10)*, San Diego, CA, Paper OWE3.
- [13] K.-P. Ho and J. M. Kahn, "Electronic compensation technique to mitigate nonlinear phase noise," in *J. Lightw. Technol.*, vol. 22, no. 3, pp. 779–783, Mar. 2004.
- [14] L. B. Du and A. J. Lowery, "Practical XPM compensation method for coherent optical OFDM systems," in *IEEE Photon. Technol. Lett.*, vol. 22, no. 5, pp. 320–322, Mar. 2010.
- [15] L. Li, Z. Tao, L. Liu, W. Yan, S. Oda, T. Hoshida, and J. C. Rasmussen, "XPM tolerant adaptive carrier phase recovery for coherent receiver based on phase noise statistics monitoring," in *Proc. European Conf. Opt. Commun. (ECOC'09)*, Vienna, Austria, Paper P3.16.
- [16] L. B. Du and A. J. Lowery, "Pilot-based cross-phase modulation compensation for coherent optical orthogonal frequency division multiplexing long-haul optical communications systems," in *Optics Lett.*, vol. 36, no. 9, pp. 1647–1649, 2011.
- [17] L. Zhu and G. Li, "Folded digital backward propagation for dispersion-managed fiber-optic transmission," in *Opt. Express*, vol. 19, no. 7, pp. 5953–5959, 2011.
- [18] J. P. Gordon and L. F. Mollenauer, "Phase noise in photonic communications systems using linear amplifiers," in *Optics Lett.*, vol. 15, no. 23, pp. 1351–1353, 1990.
- [19] K. Nakkeeran, A. B. Moubissi, P. Tchofo Dinda, "Analytical design of dispersion-managed fiber system with map strength 1.65," in *Physics Lett. A*, vol. 308, no. 5–6, pp. 417–425, Mar. 2003.
- [20] V.A.J.M. Sleiffer, D. van den Borne, M.S. Alfiad, S.L. Jansen, H. de Waardt, "Dispersion management in long-haul 111-Gb/s POLMUX-RZ-DQPSK transmission systems," in *Proc. LEOS Annual Conf. 2009*, Belek-Antalya, Turkey, pp. 569–570.
- [21] B. C. Kurtzke, "Suppression of fiber nonlinearities by appropriate dispersion management," in *IEEE Photon. Technol. Lett.*, vol. 5, no. 10, pp. 1250–1252, Oct. 1993.

Manuscript received: December 1, 2011

B iographies

Likai Zhu (likai.zhu@oclaro.com) received his BSc and MSc degrees in electrical engineering from Tianjin University, China, in 2003 and 2006. He worked with Dr. Guifang Li in the Optical Fiber Communications Group of CREOL, University of Central Florida, and received his PhD degree in optics. Currently, he is working in research and development of optical fiber communication systems at Oclaro Inc. Dr. Zhu is the author or coauthor of 14 journal papers, eight conference proceedings, and four patents.

Guifang Li (li@creol.ucf.edu) is professor of optics, electrical & computer engineering and physics at the University of Central Florida. In 1991, he received his PhD degree in electrical engineering from the University of Wisconsin, Madison. His research interests include optical communications and networking, RF photonics, and all-optical signal processing. He is the recipient of the NSF CAREER award, the Office of Naval Research Young Investigator award, and the UCF Research Incentive Award 2006. He is a fellow of SPIE and the Optical Society of America and was an associate editor for Optical Networks. He is currently the deputy editor of Optics Express and an associate editor of IEEE Photonics Technology Letters.

He was the principal investigator of the NSF Instrumentation and Laboratory Improvement Program entitled "A National Model for Photonics Proficiency in Undergraduate Electrical Engineering" and the NSF Combined Research and Curriculum Development Program in Optical Communications and Networking. Dr. Li was also the director of the National Science Foundation Integrative Graduate Education and Research Traineeship (IGERT) in Optical Communications and Networking. He received the UCF Teaching Incentive Program (TIP) Award in 2004.

AD Index

**A1–A3, and Back Cover:
ZTE Corporation**



Flipped-Exponential Nyquist Pulse Technique to Optimize PAPR in Optical Direct-Detection OFDM Systems

Jiangnan Xiao, Zizheng Cao, Fan Li, Jin Tang, and Lin Chen

(Hunan University, Changsha 410082, China)

Abstract

In this paper, we describe a novel technique based on the flipped-exponential (FE) Nyquist pulse method for reducing peak-to-average power ratio (PAPR) in an optical direct-detection orthogonal frequency-division multiplexing (DD-OFDM) system. The technique involves proper selection of the FE Nyquist pulses for shaping the different subcarriers of the OFDM. We apply this technique to a DD-OFDM transmission system to significantly reduce PAPR. We also investigate the sensitivity of a received OFDM signal with strong nonlinearity in a standard single-mode fiber (SMF).

Keywords

optical fiber communication; orthogonal frequency-division multiplexing (OFDM); flipped-exponential Nyquist pulse; PAPR

1 Introduction

Orthogonal frequency-division multiplexing (OFDM) is widely used in wireless communications and has also been considered for use in fiber-optic systems [1]–[10]. The reason OFDM has been applied to optical communications is that it is extremely tolerant to chromatic dispersion (CD) [1]–[10]. However, one inherent defect of optical OFDM is its high peak-to-average power ratio (PAPR) [11], [12]. Because of this, an optical OFDM signal has high nonlinearity in the transmission fiber. In addition, if the PAPR is too high, a Mach-Zehnder modulator (MZM) and digital-to-analog/analog-to-digital (DAC/ADC) converter will also introduce high nonlinearity. Therefore, reducing the PAPR of the OFDM signal is an urgent issue. Many techniques have been developed to reduce PAPR, including selective clipping, coding, scrambling, and companding. However, most of these cause signal distortion or redundancy, which results in increased need for transmission bandwidth. In this paper, we propose and experimentally demonstrate optical direct-detection OFDM (DD-OFDM) that uses the flipped-exponential (FE) Nyquist pulse technique. This can reduce the PAPR of the OFDM signal without affecting bandwidth efficiency, and it does not close off the possibility of using other techniques for channel

protection. Increasing spectral efficiency (SE) is essential for future large-capacity optical transmission systems and networks. Several industry research proposals on spectrally efficient channel multiplexing and filtering techniques, such as optical OFDM and Nyquist-WDM, have been put forward [13]–[15].

In the proposed system, we study the transmission of 2.5 Gbit/s QPSK-OFDM signals over 100 km single-mode fiber (SMF). The FE Nyquist technique is used for transmission.

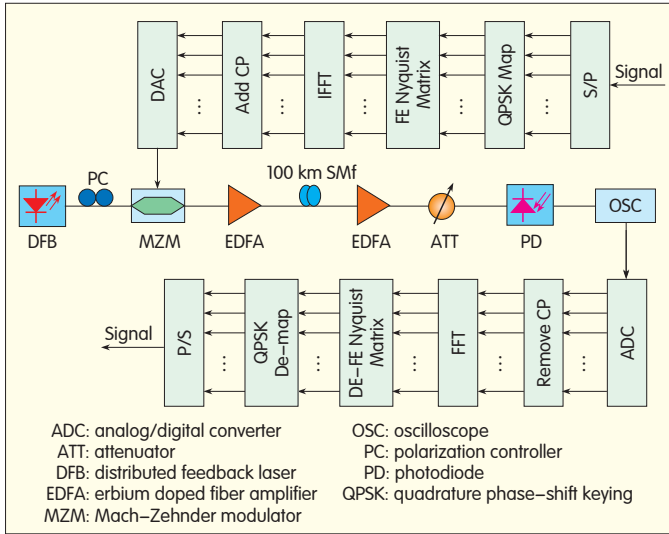
2 Principle of Operation

2.1 OFDM System with FE Nyquist Pulse Technique

Fig. 1 shows an intensity-modulation and direct-detection (IM-DD) OFDM transmission system with FE Nyquist pulse technique. PAPR of the OFDM signals can be reduced if the subcarrier waveforms have different shapes [6]. We choose the FE Nyquist pulse. The FE Nyquist pulse technique is used to reduce PAPR of the OFDM signal, and its pulse shapes are very flexible and can control the correlation between the OFDM block samples without destroying orthogonality between the subcarriers of the modulated OFDM signal.

2.2. OFDM System Model with FE Nyquist Pulse Technique

Fig. 2 shows the transmitter schematic. The incoming signal



▲ Figure 1. Intense modulation and direct-detection (IM-DD) OFDM transmission system with FE Nyquist pulse technique.

is modulated on baseband by using a bandwidth-efficient modulator.

The total number of orthogonal subcarriers is N . The baseband modulated stream has a data rate $1/T$, where T is the symbol duration, and is split into N parallel streams. Each stream is shaped by a time waveform and is transmitted over a subcarrier. The equivalent transmitted OFDM signal can be written as

$$s(t) = \sum_{n=0}^{N-1} a_n p_n(t) \exp(j2\pi f_n t) \quad 0 \leq t \leq T \quad (1)$$

where a_n is the modulated data symbol of the n th subcarrier. The waveform $p_n(t)$ is the pulse shape, which has duration T at subcarrier f_n and has a bandwidth less than or equal to the bandwidth of the OFDM signals $s(t)$. To maintain orthogonality of the subcarriers, the shaping pulses $p_n(t)$ should have the following properties [16]:

$$T = \int_0^T |p_n(t)|^2 dt \quad (2)$$

$$\int_0^T p_m(t) p_n(t) \exp[j2\pi(f_m - f_n)t] dt = \begin{cases} T, & m = n \\ 0, & m \neq n \end{cases} \quad (3)$$

The PAPR of the OFDM signal is given by

$$\text{PAPR} = \max_{0 \leq t \leq T} [|s(t)|^2] / E_{0 \leq t \leq T} [|s(t)|^2] \quad (4)$$

The summing of the in-phase orthogonal frequencies causes high PAPR. A possible way of reducing this PAPR is to correlate the different OFDM samples of the same block. By making cross-correlation close to one, a multicarrier signal with very low PAPR is obtained. The cross-correlation function of the OFDM signal is

$$R_s(t_1, t_2) = \sum_{n=0}^{N-1} \sum_{m=0}^{N-1} E[a_n a_m^*] p_n(t_1) p_m^*(t_2) \exp\{j2\pi(nt_1 - mt_2)/T\} \quad (5)$$

The autocorrelation function is a function of the modulated

signal symbol and the subcarrier waveforms. Therefore, increasing the correlation between the OFDM signal samples at the same block can be achieved with these two parameters.

If the pulse shape is different, the cross-correlation function is

$$R_s(t_1, t_2) = \sum_{n=0}^{N-1} \sum_{m=0}^{N-1} E[a_n a_m^*] p_n(t_1) p_m^*(t_2) \exp\{j2\pi(nt_1 - mt_2)/T\} \\ = \begin{cases} E_a N^2 p(t_1) p^*(t_2), & t_1 = t_2 \\ E_a N^2 p(t_1) p^*(t_2) \left(\frac{1 - e^{j2\pi t_1/T}}{1 - e^{j2\pi t_2/T}} \right) \left(\frac{1 - e^{j2\pi t_2/T}}{1 - e^{j2\pi t_1/T}} \right), & t_1 \neq t_2 \end{cases} \quad (6)$$

Thus, shaping the different subcarriers using the same pulse shape increases the peak amplitude of the transmitted signal without affecting the correlation properties between the different samples. If the pulse shape is different, the cross-correlation function is

$$R_s(t_1, t_2) = \sum_{n=0}^{N-1} \sum_{m=0}^{N-1} E[a_n a_m^*] p_n(t_1) p_m^*(t_2) \exp\{j2\pi(nt_1 - mt_2)/T\} \quad (7)$$

Thus, a proper selection of the subcarrier time waveforms increases the cross-correlation function and reduces PAPR. A set of broadband pulse waveforms was proposed in [6] to reduce PAPR. We define the following set of Nyquist pulses:

$$\begin{cases} p_i = 0, & |t - T/2| > T/2 \quad (i=0, 1, \dots, N-1) \\ p_m(t) e^{j2\pi \frac{m}{T} t} = p_n(t - \tau_{m-n}) e^{j2\pi \frac{m}{T} (t - \tau_{m-n})} \end{cases} \quad (8)$$

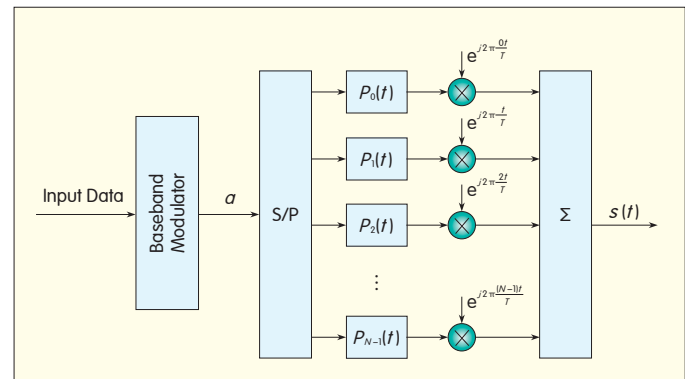
where $t - \tau_{m-n} = [(m-n) \bmod N] T_s$. Then,

$$\text{PAPR} = \frac{1}{N} \max_{0 \leq t \leq T} \left(\sum_{m=0}^{N-1} |p_m(t)| \right)^2 \leq \frac{1}{N} \left(\max_{0 \leq t \leq T} \sum_{m=0}^{N-1} |p_m(t)| \right)^2 \quad (9)$$

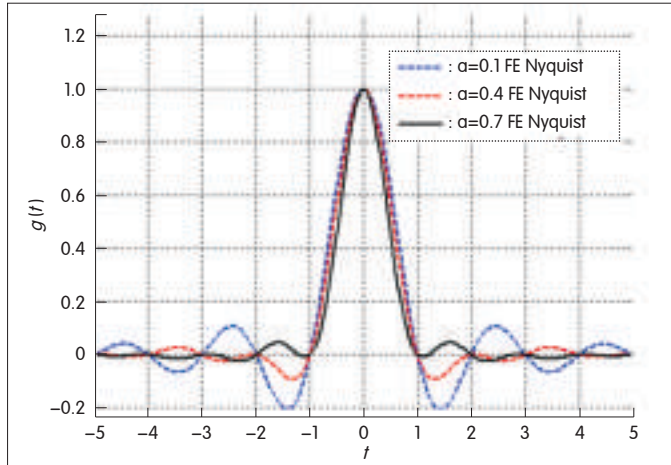
where $p(kT_s) = \begin{cases} 1, & k=0 \\ 0, & \text{else} \end{cases}$ (T_s is the sampling instant).

This shows that the different subcarriers using the set of FE Nyquist pulses shapes do not increase the peak amplitude of the transmitted signal. The peak amplitudes of the different waveforms shaped by the FE Nyquist pulse set, which is formed according to (1), do not occur at the same time. This is also the ISI-free property of a Nyquist pulse.

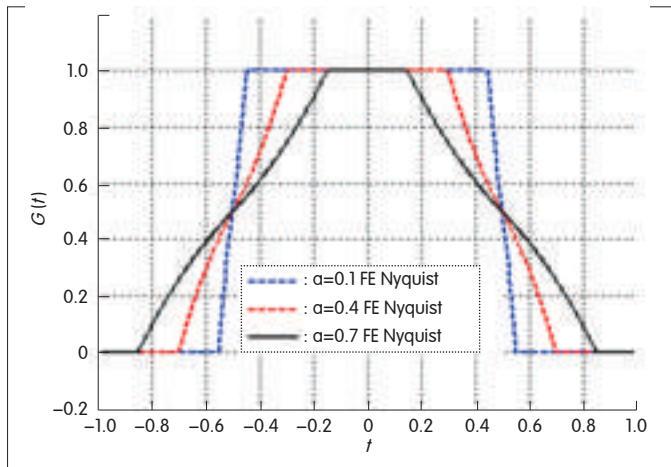
An FE Nyquist pulse is specified by the frequency spectrum [17], [18]:



▲ Figure 2. OFDM scheme based on pulse shaping.



▲ Figure 3. Impulse response of FE Nyquist pulses.



▲ Figure 4. Frequency response of FE Nyquist pulses.

$$S(f) = \begin{cases} 1, & 0 \leq f \leq B(1-\alpha) \\ \exp\left\{\frac{\ln 2}{\alpha B} [f - B(1-\alpha)]\right\}, & B(1-\alpha) \leq f \leq B \\ 1 - \exp\left\{\frac{\ln 2}{\alpha B} [f - B(1+\alpha)]\right\}, & B \leq f \leq B(1+\alpha) \\ 0, & B(1+\alpha) \leq f \end{cases} \quad (10)$$

The corresponding impulse responses are

$$P_z(t) = \frac{1}{T_s} \text{sinc}\left(\frac{t}{T_s}\right) \frac{4 \frac{\ln 2}{\alpha B} \pi t \sin\left(\frac{\pi \alpha t}{T_s}\right) + 2 \left(\frac{\ln 2}{\alpha B}\right)^2 \cos\left(\frac{\pi \alpha t}{T_s}\right) - \left(\frac{\ln 2}{\alpha B}\right)^2}{(2\pi t)^2 + \left(\frac{\ln 2}{\alpha B}\right)^2} \quad (11)$$

where B is the bandwidth that corresponds to the symbol repetition rate $T = 1/(2B)$. The roll-off factor is α .

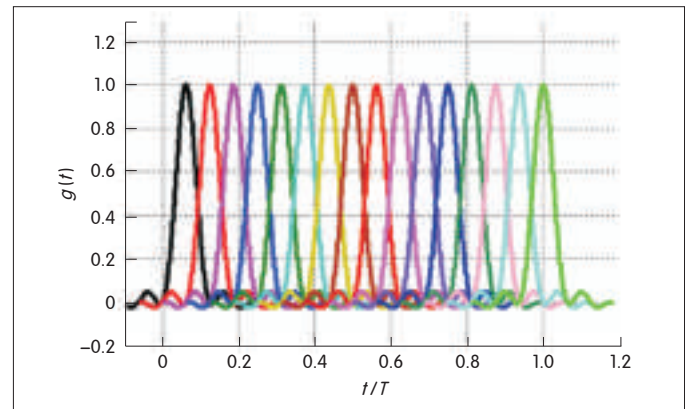
Fig. 3 and Fig. 4 show the impulse and frequency response of FE Nyquist pulses with different α respectively. These pulses are real, even, and ISI free with optimal time sampling. Furthermore, the FE Nyquist pulses asymptotically decay as t_n and the amplitude of the main side lobes decrease and as the roll-off factor α increases.

Fig. 5 shows the shape of these subcarrier waveforms for $N=16$ and $\alpha=0.7$. This set of waveforms reduces PAPR of the OFDM signal because the peak amplitudes of the waveforms do not occur at the same time. This is also the ISI-free property of the Nyquist pulse and shows that each FE Nyquist pulse is orthogonal to each other. Fig. 6 shows the corresponding spectrum.

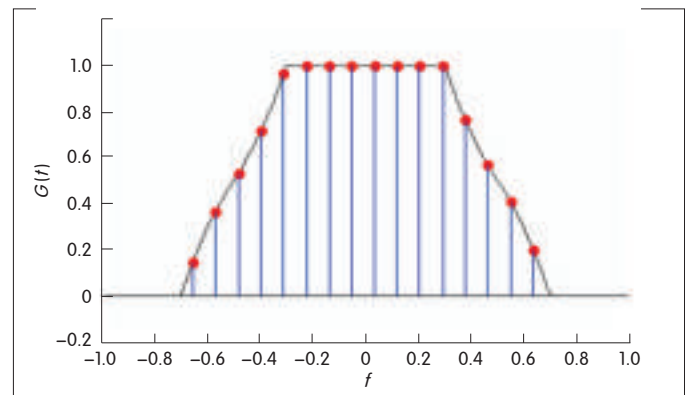
Fig. 7 shows the complementary cumulative distribution functions (CCDFs) of the original OFDM and OFDM with FE Nyquist. Our proposed method reduces peak power more than conventional OFDM. The reason why more PAPR is reduced with a larger roll-off factor is because the magnitude of the side lobe of a Nyquist pulse is smaller with a larger roll-off factor. The improvement on original OFDM is 1.9 dB for $\alpha = 0.1$, 2.4 dB for $\alpha = 0.4$, and 2.9 dB for $\alpha = 0.7$ when CCDF is 1×10^{-4} .

3 Experimental Setup and Results

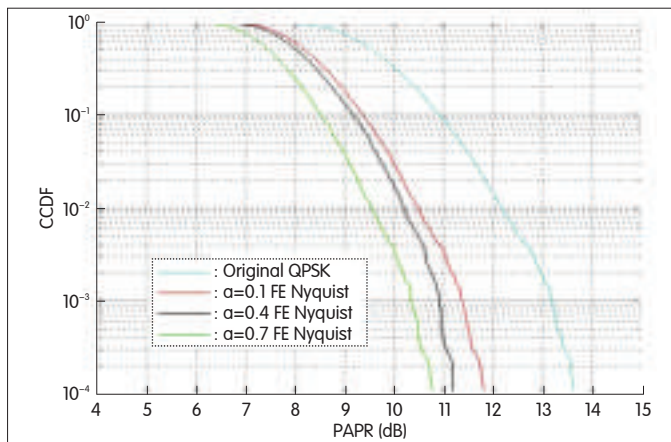
In this experiment, the number of OFDM subcarriers is 256. Of these subcarriers, 192 are used for data; 8 are used for pilots; and 56 are used for guard intervals. The cyclic prefix is 1/8 of the OFDM symbol duration, which is 32 samples in each OFDM frame. QPSK is used for the subcarrier modulation scheme. The OFDM signal is generated offline



▲ Figure 5. The new set of waveforms with FE Nyquist as the main pulse for $N=16$ subcarriers.



▲ Figure 6. The spectrum with FE Nyquist pulse for $N = 16$ subcarriers.



▲ Figure 7. CCDF of conventional OFDM and OFDM with transmission FE Nyquist pulse technique.

and uploaded into an arbitrary waveform generator (AWG). The waveforms produced by the AWG are continuously output at sample rate of 2.5 GSa/s. In the receiver, we use Matlab to process a waveform recorded by a real-time oscilloscope. There are two types of OFDM signals in this experiment: original QPSK-OFDM signal and OFDM signal with FE Nyquist. We measure the BER of the OFDM signals at different power levels into the transmission fiber.

Fig. 8(a) shows the waveforms of the original OFDM signal. Fig. 8(c), (e), and (g) shows the OFDM signal with FE Nyquist when $\alpha = 0.1$, 0.4, and 0.7, respectively. The waveforms of the FE Nyquist OFDM signal are have a smaller range than those of the original OFDM signal. Moreover, the range becomes smaller as increases.

Fig. 4(b) shows the spectra of the original OFDM signal. Fig. 4(d), (f), and (h) shows the FE Nyquist OFDM signal when $\alpha = 0.1$, 0.4, and 0.7, respectively. Spectral broadening is clearly observed, and this broadening is introduced when a larger roll-off factor is used.

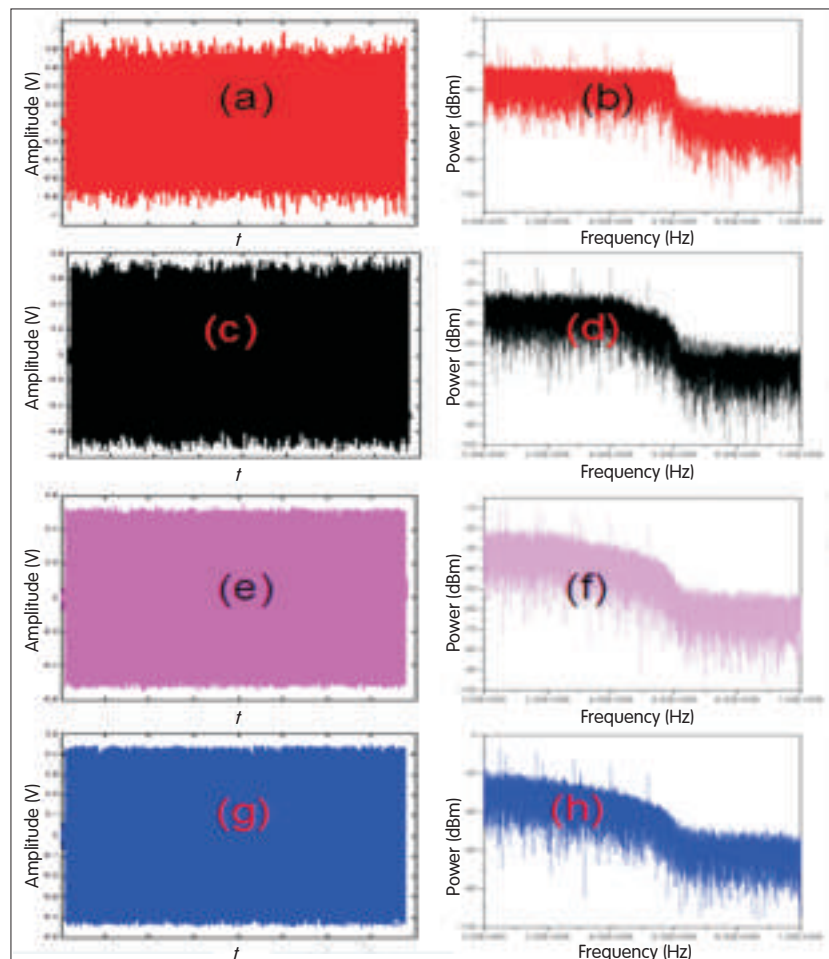
Fig. 9 shows that α significantly affects BER, because a large α can greatly decrease ICI power and dramatically improve BER. The signal is transmitted over 100 km standard SMF, and the launch power is -2 dBm. For the 2.5 Gbit/s FE Nyquist OFDM signal transmitted over 100 km standard SMF, the receiver sensitivity at BER = 10^{-4} is 2 dB, 1.5 dB, and 1 dB better than that of OFDM without FE Nyquist when $\alpha = 0.7$, 0.4, and 0.1, respectively. Because it uses a unity roll-off factor, the new method outperforms original schemes.

Fig. 10 shows the BER of the FE Nyquist OFDM signal transmitted 100 km standard SMF with a launch power of 3 dBm. It also shows that the BER of the FE Nyquist OFDM signal improves as α increases. However, the BER of the FE Nyquist OFDM signal with launch power of 3 dBm is better

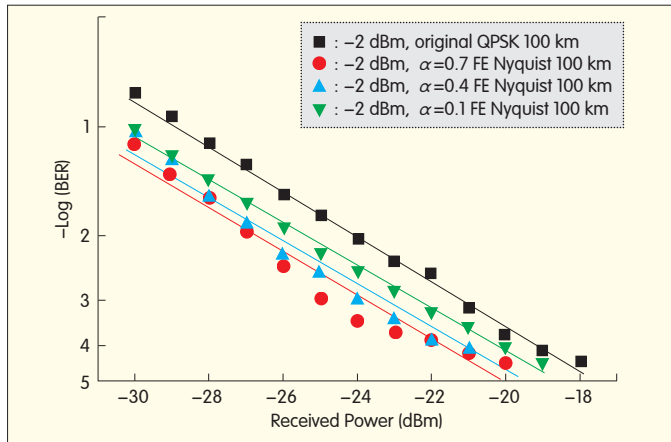
than that of the FE Nyquist OFDM signal with launch power of -2 dBm. The receiver sensitivity at BER = 10^{-4} over 100 km SMF transmission is 3 dB, 2 dB, and 1 dB better than that of the OFDM signal without FE Nyquist when $\alpha = 0.7$, 0.4, and 0.1, respectively.

Fig. 11 shows the BER of the FE Nyquist OFDM signal transmitted over 100 km standard SMF with a launch power of 8 dBm. It also shows that the BER of the FE Nyquist OFDM signal improves as α increases. However, the BER of the FE Nyquist OFDM signal with launch power of 8 dBm is better than that of the FE Nyquist OFDM signal with a launch power of -2 dBm or 3 dBm. The receiver sensitivity at BER = 10^{-4} 100 km SMF transmission is 3 dB, 2 dB, and 1dB better than that of the OFDM signal without FE Nyquist when $\alpha = 0.7$, 0.4, and 0.1, respectively.

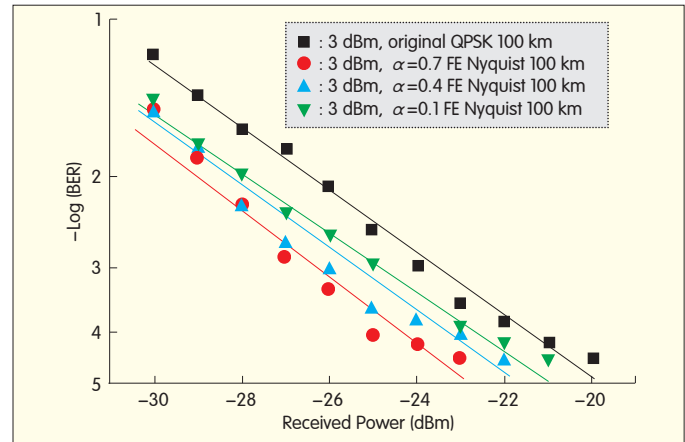
Fig. 12 shows the BER of the FE Nyquist OFDM signal when $\alpha = 0.7$. The signal is transmitted over 100 km standard SMF transmission, and the launch power is -2, 3, and 8 dBm. The received optical power of FE Nyquist OFDM with $\alpha = 0.7$ at BER = $10^{-4.5}$ is -24 dBm, -23 dBm, and -20 dBm for launch powers of 8 dBm, 3 dBm, and 2 dBm, respectively. However, the required optical power of the original OFDM signal at BER



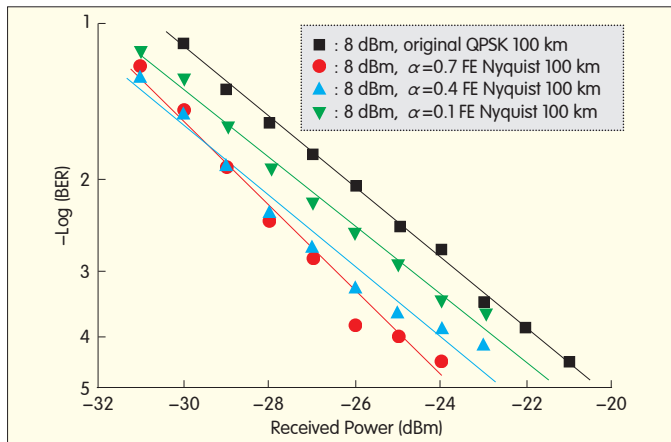
▲ Figure. 8 Spectra and waveforms of the original OFDM signal and OFDM signal with FE Nyquist pulses technique when $\alpha = 0.1$, 0.4 and 0.7, respectively, over 100 km SMF.



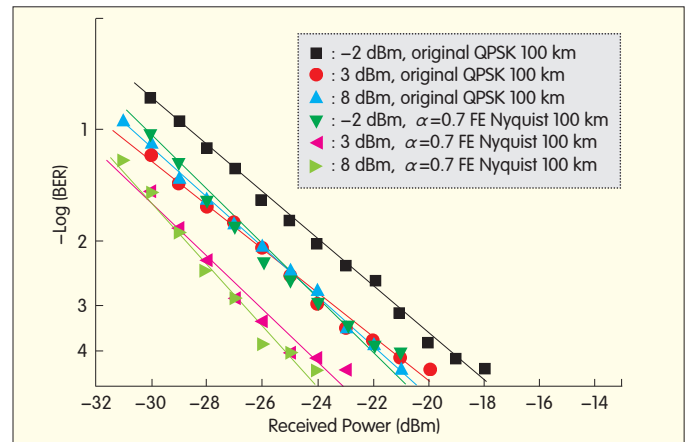
▲ Figure 9. BER curves for OFDM signal with FE Nyquist pulse when $\alpha = 0.1, 0.4, 0.7$ and fiber launch power is 2 dBm.



▲ Figure 10. BER for OFDM signal with FE Nyquist pulse when $\alpha = 0.1, 0.4, 0.7$ and fiber launch power is 3 dBm.



▲ Figure 11. BER for OFDM signal with FE Nyquist pulse when $\alpha = 0.1, 0.4, 0.7$ at 8 dBm fiber launch power.



▲ Figure 12. BER for an OFDM signal with FE Nyquist pulse when $\alpha = 0.7$ at different launch powers.

of 10^{-4} is -20.5 dBm, -20 dBm, and -18 dBm for 8 dBm, 3 dBm, and -2 dBm launch powers, respectively. Fig. 12 shows that the receiver sensitivity significantly increases for the FE Nyquist OFDM signal when α remains the same and the launch power increases.

4 Conclusion

We have proposed a novel PAPR reduction method for optical DD-OFDM systems. The flipped-exponential Nyquist pulse technique is experimentally shown to be effective in reducing the PAPR in an OFDM system. Our proposed technique is very effective and flexible for any number of carriers. We have analyzed the BER of an FE Nyquist OFDM signal with different roll-off factors α . The signal was transmitted over 100 km SMF with fiber launch powers of -2 dBm, 3 dBm, and 8 dBm.

These experimental results show that the BER of an OFDM signal with FE Nyquist pulse technique improves when α increases and the launch power stays the same. The receiver sensitivity at BER = 10^{-4} after 100 km SMF transmission is

2 dB, 1.5 dB, and 1 dB better than that of the original OFDM signal when $\alpha = 0.7, 0.4$, and 0.1, respectively, and when the fiber launch power is -2 dBm. The receiver sensitivity is 3 dB, 2 dB, and 1 dB better than that of the original OFDM signal when $\alpha = 0.7, 0.4$, and 0.1, respectively, and when the launch power is 3 dBm. The receiver sensitivity is 3 dB, 2 dB, and 1 dB better than that of the original OFDM signal when $\alpha = 0.7, 0.4$, and 0.1, respectively, and when the launch power is 8 dBm. Moreover, the receiver sensitivity significantly increases for the FE Nyquist OFDM signal when the roll-off factor remains the same and the launch power increases. These experimental results show that the FE Nyquist pulse technique efficiently improves the performance of an IM-DD optical OFDM system. Using the technique, the BER and receiver sensitivity of optical OFDM are better than the BER and receiver sensitivity of the original optical OFDM, which does not use the technique.

Acknowledgements

This work has been partly supported by the National Science Foundation of China (Grant Nos. 60977049), the

National "863" High Tech Research and Development Program of china (Grant No. 2009AA01Z220, 2009AA01Z222), Program for Hunan Provincial Science and technology.

References

- [1] Lowery, A.J., Liang Banguan Du, Armstrong, J., "Performance of Optical OFDM in Ultralong-Haul WDM Lightwave Systems," *Journal of Lightwave Technology*, vol.25, no.1, pp.131–138, Jan. 2007.
- [2] W. Shieh, X. Yi, Y. Ma, and Y. Tang, "Theoretical and experimental study on PMD-supported transmission using polarization diversity in coherent optical OFDM systems," *Opt. Express* (15), 9936–9947 (2007).
- [3] Yiran Ma, Qi Yang, Yan Tang, Simin Chen, Shieh, W., "1-Tb/s Single-Channel Coherent Optical OFDM Transmission With Orthogonal-Band Multiplexing and Subwavelength Bandwidth Access," *Journal of Lightwave Technology*, vol.28, no.4, pp.308–315, Feb.15, 2010.
- [4] Armstrong, J., "OFDM for Optical Communications," *Journal of Lightwave Technology*, vol.27, no.3, pp.189–204, Feb.1, 2009.
- [5] Shieh, W., "PMD-Supported Coherent Optical OFDM Systems," *IEEE Photonics Technology Letters*, vol.19, no.3, pp.134–136, Feb.1, 2007.
- [6] W. Shieh, H. Bao, and Y. Tang, "Coherent optical OFDM: theory and design," *Opt. Express* (16), 841–859 (2008).
- [7] Takahashi, H., "Coherent OFDM transmission with high spectral efficiency," *Optical Communication*, 2009. ECOC '09. 35th European Conference on, pp.1–4, Sept. 2009.
- [8] Schuster, M. Randel, S. Bunge, C.A.; Lee, S.C.J. Breyer, F. Spinnler, B. Petermann, K., "Spectrally Efficient Compatible Single-Sideband Modulation for OFDM Transmission with Direct Detection," *IEEE Photonics Technology Letters*, vol.20, no.9, pp.670–672, May1, 2008.
- [9] Schmidt, B.Lowery, A.J.Armstrong, J., "Impact of PMD in Single-Receiver and Polarization-Diverse Direct-Detection Optical OFDM," *Journal of Lightwave Technology*, vol.27, no.14, pp.2792–2799, July15, 2009.
- [10] Schmidt, B.J.C., Lowery, A.J.; Armstrong, J., "Experimental Demonstrations of Electronic Dispersion Compensation for Long-Haul Transmission Using Direct-Detection Optical OFDM," *Journal of Lightwave Technology*, vol.26, no.1, pp.196–203, Jan.1, 2008.
- [11] Armstrong J., "Peak-to-average power reduction for OFDM by repeated clipping and frequency domain filtering," *Electronics Letters*, vol.38, no.5, pp.246–247, 28 Feb 2002.
- [12] Wonjeong Jeong, Hyuncheol Park; Hyuckjae Lee, Sunghyun Hwang, "Performance improvement techniques for CCK-OFDM WLAN modem," *IEEE Transactions on Consumer Electronics*, vol.49, no.3, pp. 602– 605, Aug. 2003.
- [13] Jianjun Yu, Ze Dong, Hung-Chang Chien, Zhensheng Jia, Di Huo, Hong Yi, Meng Li, Zhiliang Ren, Nan Lu, Li Xie, Kai Liu, Xiaochao Zhang, Yan Xia, Yao Cai, Gunkel, M.Wagner, P., Mayer, H.; Schippel, A., "Field trial Nyquist-WDM transmission of 8x216.4Gb/s PDM-CSRZ-QPSK exceeding 4b/s/Hz spectral efficiency," *Optical Fiber Communication Conference and Exposition (OFC/NFOEC)*, 2012 and the National Fiber Optic Engineers Conference, pp.1–3, 4–8 March 2012.
- [14] Zhou, X. Nelson, L. E. Isaac, R. Magill, P. D. Zhu, B.; Peckham, D. W. Borel, P. Carlson, K. "4000 km transmission of 50GHz spaced, 10x494.85-Gb/s hybrid

- 32–64QAM using cascaded equalization and training-assisted phase recovery," *Optical Fiber Communication Conference and Exposition (OFC/NFOEC)*, 2012 and the National Fiber Optic Engineers Conference, pp.1–3, 4–8 March 2012.
- [15] Cai, J.-X. Cai, Y. Sun, Y. Davidson, C.R., Foursa, D.G. Lucero, A.; Sinkin, O. Patterson, W. Pilipetskii, A. Mohs, G. Bergano, N.S., "112x112 Gb/s transmission over 9,360 km with channel spacing set to the baud rate (360% spectral efficiency)," *Optical Communication (ECOC)*, 2010 36th European Conference and Exhibition on, pp.1–3, 19–23 Sept. 2010.
- [16] SB Slimane, "Peak-to-average power ratio reduction of OFDM signals using broadband pulse shaping," *Proc. IEEE VTC '02*, pp. 889–893, Sep. 2002.
- [17] Beaulieu, N.C., Tan, C.C., Damen, M.O., "A "better than" Nyquist pulse," *IEEE Communications Letters*, vol.5, no.9, pp.367–368, Sept. 2001.
- [18] Assalini, A.; Tonello, A.M., "Improved Nyquist pulses," *IEEE Communications Letters*, vol.8, no.2, pp. 87– 89, Feb. 2004.

Manuscript received: December 15, 2011

B iographies

Jiangnan Xiao (xjn2302@163.com) is pursuing his PhD degree at Hunan University, Changsha, China. His research interests include impairment compensation of orthogonal frequency-division multiplexing (OFDM) radio-over-fiber system, signal processing—including synchronization, equalization coding—in coherent OFDM systems, and PDM.

Zizheng Cao (oigangeo@163.com) received his ME degree in information and communication engineering from Hunan University, Changsha, China, in 2010. He is currently pursuing his PhD degree at Hunan University. His research interests include impairment compensation of orthogonal frequency-division multiplexing (OFDM) radio-over-fiber systems, and high-spectra efficiency direct-detection OFDM transmission systems.

Fan Li (fanli0809@sina.com) is pursuing his PhD degree at Hunan University, Changsha, China. His research interests include optical orthogonal frequency-division multiplexing (OFDM) transmission, and impairment compensation in OFDM radio-over-fiber systems.

Jin Tang (jltangjin@hotmail.com) is pursuing his PhD degree at Hunan University, Changsha, China. His research interests include optical orthogonal frequency-division multiplexing (OFDM) transmission, signal processing in coherent OFDM systems, and coherent optical communication systems.

Lin Chen (liliuchen12@126.com) received his PhD degree in optical communications from Beijing University of Posts and Telecommunications in June 2004. He is currently a professor at Hunan University, Changsha, China. He has authored or coauthored more than 40 journal papers. His research interests include polarization-mode dispersion compensation, new modulation format techniques, radio over fiber, and coherent optical communication systems.

ZTE Partners with KPN Group Belgium to Deploy Packet-Switched Core Network

27 August 2012—ZTE Corporation has signed a deal on a packet-switched core network (CN) for KPN Group Belgium (KPNGB). KPNGB will deploy ZTE's packet-switched CN equipment, which supports unified radio access. The contract is the second of its kind between ZTE and KPN follows from a construction project with KPN Germany (E-Plus) that was completed in September 2010.

ZTE's Uni-Core solution allows seamless evolution from 2G/3G packet core to evolved packet core (EPC) and assists operators support unified 2G, 3G and 4G access. ZTE helps operators build a smart pipe that supports service differentiation and traffic distribution and enables a flexible policy mechanism. This will help KPNGB deliver differentiated services and enhance its service innovation capability and competitive edge.

As of Q1 2012, ZTE has secured more than 20 EPC commercial contracts, deployed more than 80 trial networks globally, and has cooperation with mainstream operators. (ZTE Corporation)

100 Gbit/s Nyquist-WDM PDM 16-QAM Transmission over 1200 km SMF-28 with Ultrahigh Spectrum Efficiency

Ze Dong

(ZTE USA, Morristown, NJ 07960, USA)

Abstract

Nyquist wavelength-division multiplexing (N-WDM) allows high spectral efficiency (SE) in long-haul transmission systems. Compared to polarization-division multiplexing quadrature phase-shift keying (PDM-QPSK), multilevel modulation, such as PDM 16 quadrature-amplitude modulation (16-QAM), is much more sensitive to intrachannel noise and interchannel linear crosstalk caused by N-WDM. We experimentally generate and transmit a 6×128 Gbit/s N-WDM PDM 16-QAM signal over 1200 km single-mode fiber (SMF)-28 with amplification provided by an erbium-doped fiber amplifier (EDFA) only. The net SE is 7.47 bit/s/Hz, which to the best of our knowledge is the highest SE for a signal with a bit rate beyond 100 Gbit/s using the PDM 16-QAM. Such SE was achieved by DSP pre-equalization of transmitter-side impairments and DSP post-equalization of channel and receiver-side impairments. Nyquist-band can be used in pre-equalization to enhance the tolerance of PDM 16-QAM to aggressive spectral shaping. The bit-error ratio (BER) for each of the 6 channels is smaller than the forward error correction (FEC) limit of 3.8×10^{-3} after 1200 km SMF-28 transmission.

Keywords

16-QAM; coherent detection; Nyquist wavelength-division multiplexing; Nyquist-band; pre-equalization; spectral efficiency; signal transmission

1 Introduction

With the commercialization of 100G Ethernet, spectral efficiency (SE) needs to be increased to meet the bandwidth requirements of next-generation optical transmission networks [1]–[4]. Recent experiments have shown that a polarization-division multiplexing quadrature phase-shift keying (PDM-QPSK) transmission system can achieve a maximum SE of 4 bit/s/Hz [5], [6]. To further increase SE, we can combine multilevel modulation formats such as 16 quadrature-amplitude-modulation (16-QAM), 32-QAM, or 64-QAM with PDM. These modulation formats carry more than 4 bits per symbol. However, multilevel modulation not only requires larger optical signal-to-noise ratio (OSNR), it is more sensitive to nonlinear propagation impairments and laser phase noise. Thus, as a tradeoff, PDM 16-QAM that

carries 8 bits per symbol is a promising candidate for improving SE. The potential of PDM 16-QAM has already been shown in both simulations [7]–[9] and experiments [10].

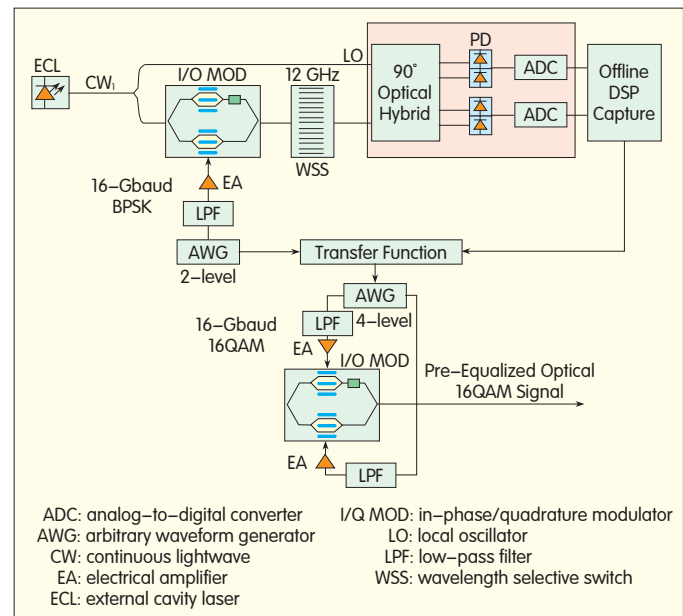
Two different schemes have been proposed for achieving very high SE with PDM 16-QAM. The first scheme uses coherent optical orthogonal frequency-division multiplexing (CO-OFDM) [11]. In experiments carried out in [12], a 485 Gbit/s CO-OFDM superchannel with PDM 16-QAM transmitted over 1600 km ultralarge-area fiber (ULAF) and standard single-mode fiber (SSMF) links. The second scheme is Nyquist wavelength-division multiplexing (N-WDM), which is based on optical pulses that have an almost-rectangular spectrum, and the bandwidth is ideally equal to the baud rate [13]. Although these two schemes have the potential to perform the same, CO-OFDM requires channels to be synchronized, and the analog-to-digital converters (ADCs) need large receiver bandwidth. In practical implementation, N-WDM is much more robust to receiver

constraints [14]. Therefore, a combination of N-WDM and PDM 16-QAM is a promising solution for future large-capacity, high-SE optical transmission systems and networks.

In conventional direct-detection receivers, linear distortion caused by fiber chromatic dispersion (CD) in the optical domain is converted into a nonlinear distortion in the electrical domain. Using a linear baseband equalizer based on one received baseband signal only improves performance a little. In coherent-detection receivers, distortion caused by CD is converted linearly into the electrical domain. This explains why, in the case of CD only, fractionally spaced equalizers with complex coefficients can potentially extend the system reach to distances that are only limited by the number of equalizer taps [15]. However, when CD is ideally compensated, nonlinear propagation impairments and laser phase noise (which PDM 16-QAM is very sensitive to) eventually limits the maximum achievable transmission distance. Most of the complexity of building an equalizer in a coherent receiver can be avoided by adopting pre-equalization at the transmitter, where the data is still in its uncorrupted form.

The large constellation size of PDM 16-QAM also makes the system sensitive to transmitter impairments such as nonlinear drive in the optical modulator and imbalance between the frequency responses of the in-phase (I) and quadrature (Q) channels. These cause signal distortion and deteriorate system performance. Transmitter impairments in PDM 16-QAM can be precompensated with pre-equalization, which is not difficult to implement in the digital-to-analog converter (DAC) at the transmitter. Some studies have focused on electronic pre-equalization, which is now a well-known technique in optical communication [16]–[18]. A further benefit of pre-equalization is that the transmitted spectrum can be optimized using Nyquist-band preshaping pulses, which allow narrower channel spacing and higher SE [18].

In this paper, we use PDM 16-QAM to generate a 16 Gbaud signal in an N-WDM channel on a 16 GHz grid. In section 2, we describe the principle of pre-equalization and compare bit-error ratio (BER) of a single channel with that of an N-WDM channel when both channels have Nyquist-band pre-equalization or no Nyquist-band equalization. Pre-equalization can compensate for transmitter impairments and reduce the effects of nonlinear propagation and laser phase noise. N-WDM with Nyquist-band pre-equalization is tolerance of narrowband filtering and crosstalk caused by adjacent channels. In section 3, we describe the setup of an experiment for generating and transmitting 6×128 Gbit/s N-WDM PDM 16-QAM signals over 1200 km SMF-28. Amplification is provided by an erbium-doped fiber amplifier (EDFA) only. In this experiment, spectral efficiency (SE) of 7.47 bit/s/Hz was achieved. To the best of our knowledge, this the highest SE ever achieved for a signal with a bit rate beyond 100 Gbit/s and using PDM 16-QAM. The BER for all channels (with the average OSNR of 23.6 dB) is smaller than the forward-error-correction (FEC) limit of 3.8×10^{-3} over



▲ Figure 1. The principle of pre-equalization.

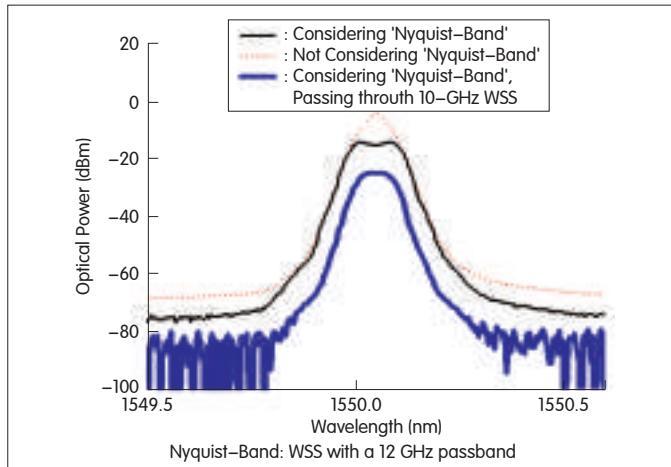
1200 km SMF-28 transmission. Section 4 concludes the paper.

2 Pre-Equalization

2.1 Principle

Instead of only building the equalizer at the receiver, the equalizer can also be built at the transmitter. Compared with a binary phase-shift keying (BPSK) signal, a high-level signal has much more uncontrolled nonlinearity because of imperfections in the DAC, electrical amplifier (EA), in-phase/quadrature modulator (I/Q MOD), optical filter, and ADC. Therefore, we first transmit a BPSK signal in the back-to-back (B2B) link in order to calculate the transfer function. This function is then used to pre-equalize the high-level signal and reverse the channel distortion.

Fig. 1 shows the principle for pre-equalization. One of the parallel Mach-Zehnder modulators (MZMs) in an I/Q MOD is driven by a 16 Gbaud binary signal so that BPSK is generated. This signal has $1.5 \times$ samples and a word length of $2^{15}-1$, and it is generated by an arbitrary waveform generator (AWG). An electrical lowpass filter (LPF) with 3 dB bandwidth of 7.5 GHz is used to suppress out-of-band noise from the AWG, which operates in the interleaver mode with a sample rate of 24 GSa/s. The continuous wavelength lightwave (CW) generated by an external cavity laser (ECL) with a linewidth of less than 100 kHz and output power of 14.5 dBm is used as both the signal source and the local oscillator (LO) source in self-homodyne coherent detection. Then, the optical BPSK signal passes through a wavelength selective switch (WSS) with a 12 GHz passband before coherent detection. A real-time scope with 3 dB bandwidth of 16 GHz captures the detected electrical signal, which is used to calculate the



▲ Figure 2. Optical spectra (0.02 nm resolution) of the pre-equalized 16 Gbaud PDM 16-QAM signal.

transfer function of the transmitter in the frequency domain. The transfer function is then used to pre-equalize the 4-level signal with a word length of $2^{15}-1$. This signal is used to generate the optical 16-QAM via the I/Q MOD. A raised-cosine (R-C) filter with a roll-off factor of 0.99 is used to pulse shape the 4-level signal. Pre-equalization of the I and Q output of the AWG makes the performance of both outputs similar to each other; therefore, we simply choose the I output of the AWG to implement pre-equalization in our experiment.

The WSS has a 12 GHz passband and is used for pre-equalization. This WSS is different from the WSS with 10 GHz passband used for the WDM channel in the next section. The reason for setting WSS at a different bandwidth for pre-equalization and for WDM channel shaping is to balance the pre-equalization effect and crosstalk from the neighboring channels. After pre-equalization, we show by experiment the generation and transmission of the 6×128 Gbit/s N-WDM PDM 16-QAM signal over 1200 km SMF-28 with EDFA-only amplification. The spectral efficiency is 7.47 bit/s/Hz if we assume 7% FEC overhead.

2.2 Experimental Results and Discussion

Fig. 2 shows the optical spectra for 16 Gbaud PDM 16-QAM in the case of pre-equalization with and without Nyquist band. Nyquist band is the definition of the WSS with a 12 GHz passband. Compared to pre-equalization without Nyquist band (Fig. 3, dotted line), pre-equalization with Nyquist band results in a PDM 16-QAM optical spectrum that has the function of a Nyquist-like filtering profile. This can sufficiently compensate for narrowband filtering effects. After passing through the 10 GHz WSS, the PDM 16-QAM optical spectrum with Nyquist-band pre-equalization is much narrower.

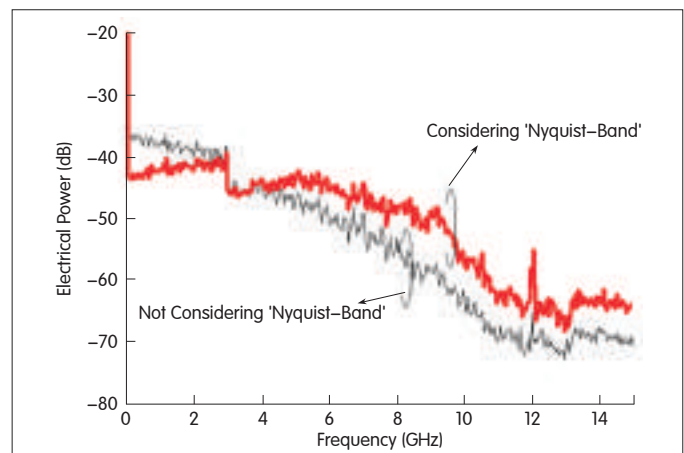
Fig. 3 shows the measured electrical spectrum for the generated 16 Gbaud 4-level signal from the AWG in the case of pre-equalization with and without Nyquist band. Certain high-frequency components that are lost because of

aggressive spectral filtering are pre-recovered. The 5 dB dip at 3 GHz in both traces is the reflection of the pre-distortion caused by the 7.5 GHz LPF shown in Fig. 1.

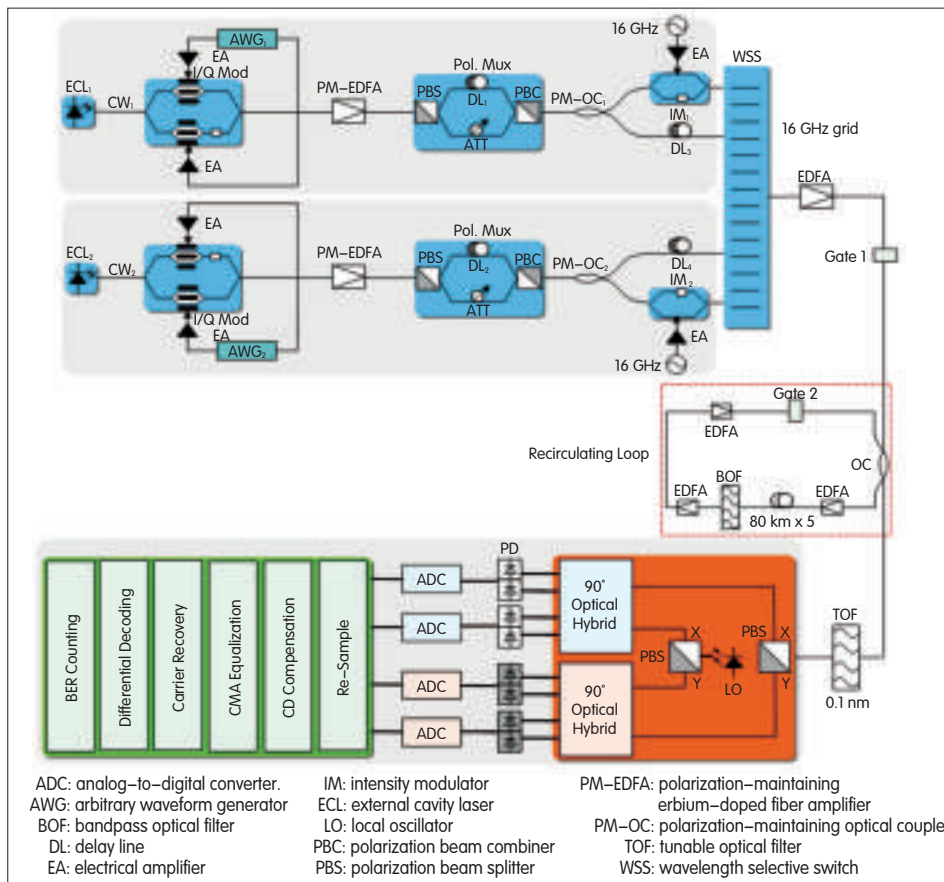
3 Generation and Transmission of a 6×128 Gbit/s N-WDM PDM 16-QAM Signal

3.1 Experimental Setup

Fig. 4 shows the experimental setup for generating and transmitting a 6×128 Gbit/s N-WDM PDM 16-QAM signal. The two 16 Gbaud electrical 16-QAM signals are generated from AWG₁ and AWG₂. CW₁ has a frequency spacing of 1550.10 nm at 48 GHz, and CW₂ has a frequency spacing of 0.384 nm at 48 GHz. Both are generated by two ECLs, each with a linewidth of less than 100 kHz and output power of 14.5 dBm. Two I/Q MODs are used to modulate CW₁ and CW₂ with the I and Q components of the 64 Gbit/s, 16 Gbaud electrical 16-QAM signals. This occurs after power amplification using four broadband electrical amplifiers (EA). To generate an optical 16-QAM signal, the two parallel MZMs in an I/Q MOD are biased at the null point and driven at full swing to achieve zero-chirp, 0-phase and π -phase modulation. The phase difference between the upper and lower branches of the I/Q MOD is controlled at $\pi/2$. After boosting the power with polarization-maintaining EDFAs (PM-EDFAs), PDM for each path is realized by the polarization multiplexer. This comprises a polarization beam splitter (PBS), which halves the signal, an optical delay line (DL), which provides a delay of 150 symbols, and a polarization beam combiner (PBC), which recombines the signal. In the upper path, the optical PDM 16-QAM signal is then halved again by a polarization-maintaining optical coupler (PM-OC1). Here, the signal passing through the upper branch is handled by an intensity modulator (IM1) that is driven by a 16 GHz sinusoidal radio frequency (RF) signal and that is DC-biased at the null point. The signal passing



▲ Figure 3. Electrical spectrum of the pre-equalized 16 Gbaud 4-level (in-phase of 16-QAM) signal considering and not considering the Nyquist-band.



▲ Figure 4. Experimental setup for the generation and transmission of a 6 × 128 Gbit/s N-WDM PDM 16-QAM signal.

through the lower branch is handled by DL3. So do the operation for the lower path. IM1 and IM2 are used for optical carrier suppression (OCS) modulation [19]; in other words, the function of IM1 and IM2 is to produce two copies of the original signal that are +16 GHz and -16 GHz relative to the original signal center. The four branches, with the uppermost and lowermost branches each including two subcarriers, are spectrally filtered and combined using a programmable 4-channel WSS with a 10 GHz passband on a 16 GHz grid. The insertion loss of the WSS is 7 dB.

The WDM signals are launched into the recirculating loop of 5 × 80 km SMF-28 with three circles. Each span has an average loss of 18 dB and chromatic dispersion of 17 ps/km/nm at 1550 nm when there is no optical dispersion compensation. EDFA is used to compensate for the loss of each span. The total launched power (after EDFA) into each span is 10 dBm, which corresponds to approximately 1 dBm per channel at 128 Gbit/s. A tunable optical bandpass filter (BOF) with a bandwidth of 1.27 nm is used in the loop to remove the ASE noise from each circle of the recirculating loop. At the receiver, a tunable optical filter (TOF) with 3 dB bandwidth of 0.35 nm is used to choose the desired channel. An ECL with a linewidth of less than 100 kHz is used as the LO. A polarization-diverse 90 degree hybrid is used for

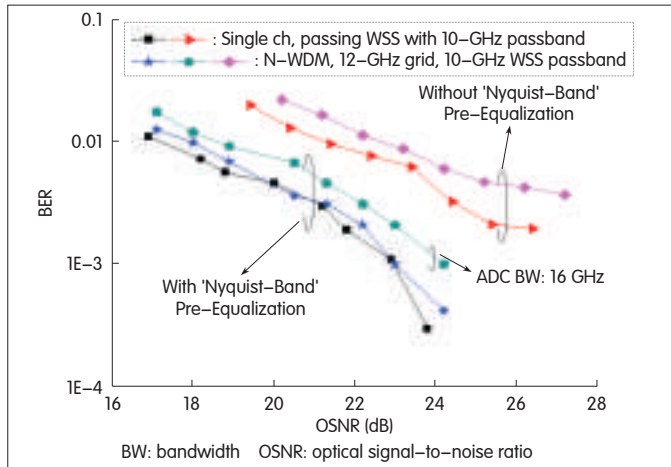
polarization- and phase-diverse coherent detection of the LO and received optical signal prior to balanced detection. The digital scope performs ADC at 50 GSa/s with an electrical bandwidth of 9 GHz.

In the DSP, electrical polarization recovery is performed using a three-stage blind equalization scheme. First, the clock is extracted using the square-and-filter method, and the digital signal is resampled at twice the baud rate of the recovered clock. Second, a T/2-spaced time-domain finite impulse response (FIR) filter is used to compensate for CD. The filter coefficients are calculated using the known fiber CD transfer function and the frequency-domain truncation method. Third, two complex 13 tap, T/2-spaced adaptive FIR filters are used to retrieve the modulus of the 16-QAM signal. The two adaptive FIR filters are based on the classic constant modulus algorithm (CMA) and are followed by a three-stage CMA for multimodulus recovery and polarization demultiplexing. Carrier recovery is performed in the subsequent step. The 4th power is used to estimate the frequency offset between the LO and the received optical signal. Phase recovery is achieved by using feed-forward and least-mean-square (LMS) algorithms for offset compensation. Finally, differential decoding is used to calculate the BER after the decision.

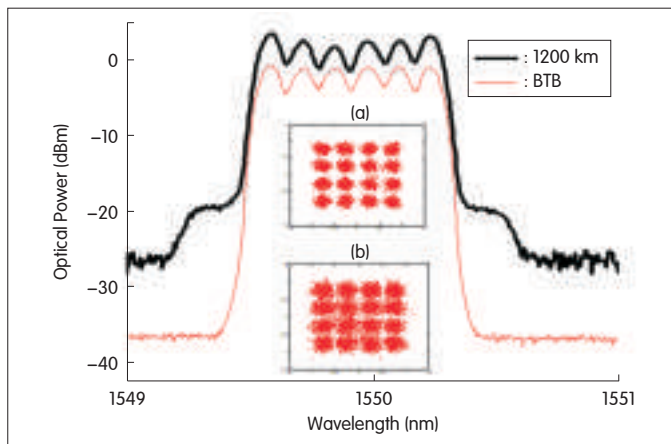
3.2 B2B Experimental Results and Discussion

Fig. 5 shows B2B BER versus OSNR for 16 Gbaud PDM 16-QAM at the N-WDM channel of 1550.10 nm. The scope has a bandwidth of 9 GHz and a sample rate of 50 GSa/s. There are four different cases: B2B single channel with and without Nyquist-band pre-equalization, and N-WDM PDM 16-QAM with and without Nyquist-band pre-equalization.

In the cases involving WDM, the six-channel 16 Gbaud PDM 16-QAM is on a 16 GHz grid, and all the channels of the previously mentioned four cases pass through the WSS with a 10 GHz passband. In the case of Nyquist-band pre-equalization, the required OSNR at the BER of 3.8×10^{-3} is 20.6 dB for a single channel. For the corresponding WDM case, the required OSNR penalty can be neglected because pre-equalization can precompensate for transmitter impairments as and reduce the effects of nonlinear impairments and laser phase noise. Our experiments indicate that 10 GHz filtering bandwidth with 12 GHz Nyquist-band pre-equalization is narrow enough to avoid crosstalk from



▲ Figure 5. B2B BER versus OSNR for a 16 Gbaud PDM 16-QAM signal at the N-WDM channel of 1550.10 nm.



▲ Figure 6. Optical spectrum (0.1 nm resolution) before and after 1200 km SMF-28 transmission with EDFA-only amplification, and (a) the obtained signal constellations before transmission and (b) the obtained signal constellations after transmission.

adjacent channels. The required OSNR penalty at BER of 1×10^{-3} increases to 1 dB when the ADC bandwidth is 16 GHz. The required bandwidth of the ADC plays an important role in detecting the N-WDM PDM 16-QAM signal. An ADC with bandwidth of half the baud rate frequency is beneficial for suppressing the noise and neighboring channel signal. For a single channel that passes through the 10 GHz WSS and has no Nyquist-band pre-equalization, the required OSNR at BER of 3.8×10^{-3} is 24 dB, and the required OSNR penalty is approximately 4 to 5 dB. PDM 16-QAM is quite sensitive to narrow filtering effects and noise. For N-WDM without Nyquist-band pre-equalization, there is an extra 1.5 dB OSNR penalty caused by crosstalk from adjacent channels.

3.3 Experimental Results for Transmission over 1200 km SMF-28

Fig. 6 shows the optical spectra before and after 1200 km

Figure 7. BER versus launch power for an N-WDM channel at 1550.10 nm after transmission over 1200 km SMF-28.

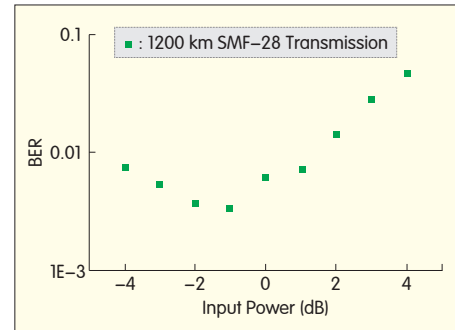


Figure 8. BER versus transmission distance for an N-WDM channel at 1550.1 nm.

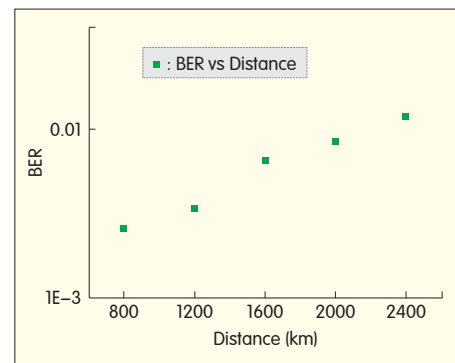
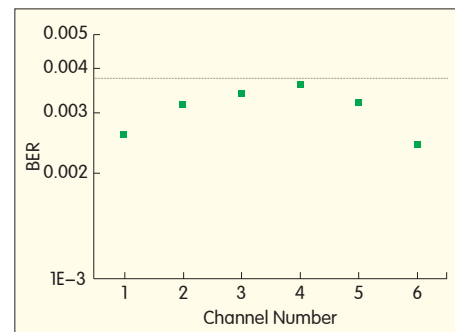


Figure 9. BER for each of the 6 channels after transmission over 1200 km SMF-28 at the optimal launch power.



SMF-28 transmission with EDFA-only amplification. The corresponding constellations are shown in Fig. 6(a) and (b). The OSNR of the signal is 23.6 dB after transmission over 1200 km SF-28. Fig. 7 shows BER versus power launched into each fiber span for an N-WDM channel at 1550.10 nm after 1200 km SMF-28 transmission. Launch power of -1 dBm gives the best BER performance. Fig. 8 shows BER versus transmission distance for an N-WDM channel at 1550.10 nm after transmission. The launched power of -1 dBm per channel is optimal. After transmission over 1200-km SMF-28, the BER for each of the six channels (with average OSNR of 23.6 dB) is smaller than the FEC limit of 3.8×10^{-3} (Fig. 9) [20].

4 Conclusion

We have experimentally demonstrated the generation and transmission of a 6×128 Gbit/s N-WDM PDM 16-QAM signal on a 16 GHz grid over 1200 km SMF-28 with EDFA-only amplification. The net SE is 7.47 bit/s/Hz, which to

the best of our knowledge is the highest SE for a signal with a bit rate beyond 100 Gbit/s using PDM 16-QAM. Such SE was achieved by DSP pre-equalization of transmitter-side impairments and DSP post-equalization of channel and receiver-side impairments. The benefit of Nyquist-band pre-equalization scheme has been shown experimentally. BER for all channels is smaller than the FEC limit of 3.8×10^{-3} over a 1200 km SMF-28 transmission link.

References

- [1] C. R. S. Fludger, T. Duthel, D. van den Borne, C. Scholien, E. -D. Schmidt, T. Wuth, J. Geyer, E. De Man, G. -D. Khoe, and H. de Waardt, "Coherent equalization and POLMUX-RZ-DQPSK for robust 100-GE transmission," *J. Lightw. Technol.*, vol. 26, no. 1, pp. 64-72, Jan. 1, 2008.
- [2] J. -X. Cai, Y. Cai, Y. Sun, C. R. Davidson, D. G. Foursa, A. Lucero, O. Sinkin, W. Patterson, A. Pilipetskii, G. Mohs, and N. S. Bergano, "112x112 Gb/s transmission over 9360 km with channel spacing set to the baud rate (360% spectral efficiency)," in *Proc. ECOC 2010*, Torino, Italy, Sep., pp. 1-3, PD2.1.
- [3] J. Yu, X. Zhou, Y. -K. Huang, S. Gupta, M. -F. Huang, T. Wang, and P. Magill, "112.8-Gb/s PM-RZ-64QAM optical signal generation and transmission on a 12.5GHz WDM grid," in *Proc. OFC 2010*, San Diego, CA, paper OThM1.
- [4] Z. Dong, J. Yu, H. -C. Chien, S. Shi, Y. Xia, and C. Ge, "24Tb/s (24x1.3Tb/s) WDM transmission of terabit PDM-CO-OFDM superchannels over 2400 km SMF-28," in *Proc. OECC 2011*, PDP6.
- [5] J. -X. Cai, Y. Cai, C. R. Davidson, D. G. Foursa, A. Lucero, O. Sinkin, W. Patterson, A. Pilipetskii, G. Mohs, and N. S. Bergano, "Transmission of 96x100-Gb/s bandwidth-constrained PDM-RZ-QPSK channels with 300% SE over 10610 km and 400% SE over 4370 km," *J. of Lightw. Technol.*, vol. 29, no. 4, pp. 491-498, 2011.
- [6] Z. Dong, J. Yu, Z. Jia, H. -C. Chien, and G. -K. Chang, "7 x 224 Gb/s/ch N-WDM transmission over 1600-km SMF-28 using PDM-CSRZ-QPSK modulation," *IEEE Photon. Technol. Lett.*, unpublished.
- [7] V. Curri, A. Carena, G. Bosco, P. Poggiolini, and F. Forghieri, "Nonlinear propagation of 1 Tbps superchannels based on 240 Gbps PM-16QAM subcarriers on PSCF with hybrid Erbium/Raman fiber amplification," in *Proc. of ECOC 2010*, Torino (Italy), paper P4.11, Sep. 2010.
- [8] G. Bosco, V. Curri, A. Carena, P. Poggiolini, and F. Forghieri, "On the performance of N-WDM terabit superchannels based on PM-BPSK, PM-QPSK, PM-8QAM or PM-16QAM subcarriers," *J. of Lightw. Technol.*, vol. 29, no. 1, pp. 53-61, Jan. 2011.
- [9] K. Kikuchi, "Ultra-long-haul optical transmission characteristics of wavelength-division multiplexed dual-polarisation 16-quadrature-amplitude-modulation signals," *Electron. Lett.*, vol. 46, no. 6, pp. 433-434, Mar. 2010.
- [10] A. H. Gnauck, P. J. Winzer, S. Chandrasekhar, X. Liu, B. Zhu, and D. W. Peckham, "Spectrally efficient long-haul WDM transmission using 224-Gb/s polarization-multiplexed 16-QAM," *J. of Lightw. Technol.*, vol. 29, no. 4, pp. 373-377, Feb. 2011.
- [11] W. Shieh and C. Athaudage, "Coherent optical orthogonal frequency division multiplexing," *Electron. Lett.*, vol. 42, no. 10, pp. 587-589, May 2006.
- [12] B. Zhu, S. Chandrasekhar, X. Liu, and D. W. Peckham, "Transmission performance of a 485-Gb/s CO-OFDM superchannel with PDM-16QAM subcarriers over ULAF and SSMF-based links," *IEEE Photon. Technol. Lett.*, vol. 23, no. 19, pp. 1400-1402, Oct. 2011.
- [13] R. Cigliutti, A. Nespola, D. Zeolla, G. Bosco, A. Carena, V. Curri, F. Forghieri, Y. Yamamoto, T. Sasaki, and P. Poggiolini, "Ultra-Long-Haul Transmission of 16x112 Gb/s Spectrally-Engineered DAC-Generated Nyquist-WDM PM-16QAM Channels with 1.05x(Symbol-Rate) Frequency Spacing," in *Proc. OFC 2012*, paper OTh.3A.3.
- [14] G. Bosco, A. Carena, V. Curri, P. Poggiolini, and F. Forghieri, "Performance limits of N-WDM and CO-OFDM in high-speed PM-QPSK systems," *IEEE Photon. Technol. Lett.*, vol. 22, no. 15, pp. 1129-1131, Aug. 1, 2010.
- [15] J. Winters, "Equalization in coherent lightwave systems using a fractionally spaced equalizer," *J. Lightw. Technol.*, vol. 8, no. 10, pp. 1487-1491, Oct. 1990.
- [16] X. Zhou, and J. Yu, "Multi-level, multi-dimensional coding for high-speed and high-spectral-efficiency optical transmission," *J. Lightw. Technol.*, vol. 27, no. 16, pp. 3641-3653, Aug. 2009.
- [17] X. Zhou, J. Yu, M. -F. Huang, Y. Shao, T. Wang, L. Nelson, P. Magill, M. Birk, P. I. Borel, D. W. Peckham, R. Lingle, Jr., and B. Zhu, "64-Tb/s, 8 b/s/Hz, PDM-36QAM Transmission Over 320 km using both pre- and post-transmission digital signal processing," *J. Lightw. Technol.*, vol. 29, no. 4, pp. 571-577, Feb. 2011.
- [18] T. Sugihara, T. Kobayashi, Y. Konishi, S. Hirano, K. Tsutsumi, K. Yamagishi, T. Ichikawa, S. Inoue, K. Kubo, Y. Takahashi, K. Goto, T. Fujimori, K. Uto, T. Yoshida, K. Sawada, S. Kametani, H. Bessho, T. Inoue, K. Koguchi, K. Shimizu, and T. Mizuocho, "43 Gb/s DQPSK pre-equalization employing 6-bit, 43GS/s DAC integrated LSI for cascaded ROADM filtering," in *Proc. OFC 2010*, paper PDPB6.
- [19] J. Yu, Z. Jia, L. Yi, Y. Su, G. -K. Chang and T. Wang, "Optical millimeter-wave generation or up-conversion using external modulators," *IEEE Photon. Technol. Lett.*, vol. 18, no. 1, pp. 265-267, Jan. 1, 2006.
- [20] ITU-T Recommendation G.975.1, "Forward error correction for high bit-rate DWDM submarine system," 2004.

Manuscript received: June 12, 2012

Biography

Ze Dong (zdong9@mail.gatech.edu) received his BS degree in electronic information science and technology from Hunan Normal University, China, in 2006. He received his PhD degree in electrical engineering from Hunan University, Changsha, in 2011. From 2009 to 2011, he was a PhD exchange scholar at Georgia Institute of Technology, Atlanta. He is currently a postdoctoral fellow in the School of Electrical and Computer Engineering, Georgia Institute of Technology. His research areas are broadband optical communication and optical coherent communications. He has authored or co-authored more than 40 papers and conference proceedings on coherent optical transmission, passive optical networks, and broadband radio-over-fiber systems.

ZTE Wins Contract to Provide LTE Wireless Uifi Set to UNE

2 August 2012—ZTE Corporation today announced it has won a project to provide UNE with an MF821 LTE Dongle and MF821+MF20 LTE Wireless Uifi set. UNE is Colombia's biggest telecommunications operator.

The MF821 LTE wireless network card supports LTE FDD (100 Mbps download and 50 Mbps upload). It has a Micro SD slot up for storage of up to 32 GB and supports all major operating systems. MF20 is a new datacard adapter. Its main function is to change datacard access for WiFi coverage. It is portable, battery powered, and can also be used as a wired router.

ZTE is a world-leader in LTE technology. ZTE Cikey, a multiple access terminal, won the "Best LTE Device/Handset" award at the 2012 Mobile World Summit in Barcelona. ZTE holds approximately 2000 LTE patents, seven per cent of the worldwide total. To date, the company has built seven TD-LTE commercial networks across the globe. The company also has signed LTE-FDD/TDD construction agreements with Hutchison Whampoa Hi3G and provides services across a number of northern European countries. (ZTE Corporation)

Field Transmission of 100G and Beyond: Multiple Baud Rates and Mixed Line Rates Using Nyquist-WDM Technology

Zhensheng Jia, Jianjun Yu, Hung-Chang Chien, Ze Dong, and Di Huo
(ZTE USA, Morristown, NJ 07960, USA)

Abstract

In this paper, we describe successful joint experiments with Deutsche Telecom on long-haul transmission of 100G and beyond over standard single mode fiber (SSMF) and with in-line EDFA-only amplification. The transmission link consists of 8 nodes and 950 km installed SSMF in DT's optical infrastructure. Laboratory SSMF was added for extended optical reach. The first field experiment involved transmission of 8×216.8 Gbit/s Nyquist-WDM signals over 1750 km with 21.6 dB average loss per span. Each channel, modulated by a 54.2 Gbaud PDM-CSRZ-QPSK signal, is on a 50 GHz grid, which produces a net spectral efficiency (SE) of 4 bit/s/Hz. We also describe mixed-data-rate transmission coexisting with 1T, 400G, and 100G channels. The 400G channel uses four independent subcarriers modulated by 28 Gbaud PDM-QPSK signals. This yields a net SE of 4 bit/s/Hz, and 13 optically generated subcarriers from a single optical source are used in the 1T channel with 25 Gbaud PDM-QPSK modulation. The 100G signal uses real-time coherent PDM-QPSK transponder with 15% overhead of soft-decision forward-error correction (SD-FEC). The digital post filter and 1-bit maximum-likelihood sequence estimation (MLSE) are introduced at the receiver DSP to suppress noise, linear crosstalk, and filtering effects. Our results show that future 400G and 1T channels that use Nyquist WDM can transmit over long-haul distances with higher SE and using the same QPSK format.

Keywords

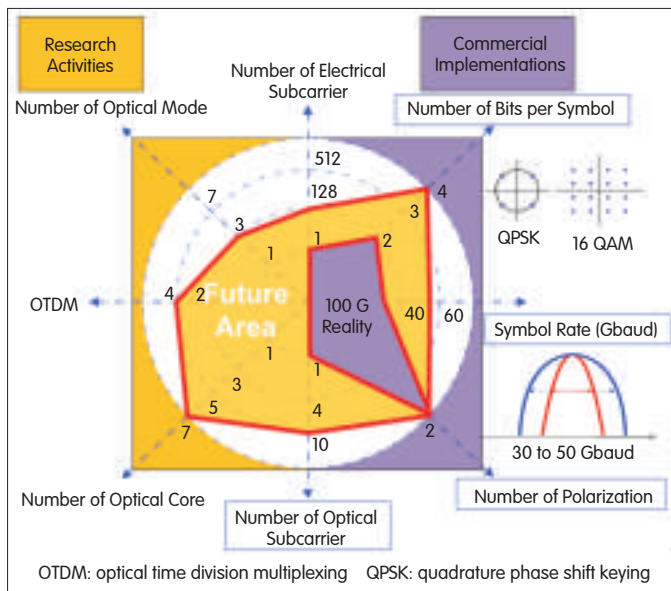
coherent detection; field trial; coherent optical OFDM; Nyquist WDM; MLSE

1 Introduction

The demand for bandwidth is being driven by more and more video streaming and proliferation of cloud computing, social media, and mobile data delivery [1]–[4]. Along with the need for reduced cost per bit per hertz, this trend has led to high-speed underlying optical transmission interfaces. At present, 100 Gbit/s long-haul systems, whether being developed or deployed, are all based on a single-carrier polarization-division multiplexed quadrature phase-shift keying (PDM-QPSK) modulation format that is associated with coherent detection and digital signal processing (DSP) [5]–[6]. Spectral efficiency (SE) over a conventional 50 GHz optical grid is 2 bit/s/Hz; thus, the system capacity is around 10 Tbit/s in a fiber C-band transmission window. Corresponding standardization for client-side 100GE, transport layer optical transport unit 4 (OTU4), and key electro-mechanical aspects has been completed to make end-to-end system connection and interoperability

possible [7].

Optical transmission at 100G+ per channel is the logical next step to sustaining future traffic growth. Much research has been done on trading off capacity, data rate, and optical reach (Fig. 1) [8]–[9]. Optical time-division multiplexing (OTDM) is one of the classic approaches to increasing the channel data rate. A recent experiment with OTDM resulted in a symbol rate of 1.28 Tbaud and a single-channel bit rate of 10.2 Tbit/s with return-to-zero (RZ) modulation [10]. Another recent experiment with OTDM resulted in 640 Gbaud and a line rate of 1.28 Tbit/s with non-return-to-zero (NRZ) modulation [11]. However, the commercial reality is that OTDM provides limited system stability and compactness and is generally considered a useful interim technique to explore the limits of high-bit-rate transmission. It was replaced by electrical time-division multiplexing (ETDM) when the bandwidth of optoelectronic components allowed the desired bit-rate. Spatial-division multiplexing (SDM) that uses multicore fiber (MCF) or few-mode fiber (FMF) coupled with multiple-input multiple-output (MIMO) signal processing is



▲ Figure 1. Research directions of scaling channel capacity beyond 100G.

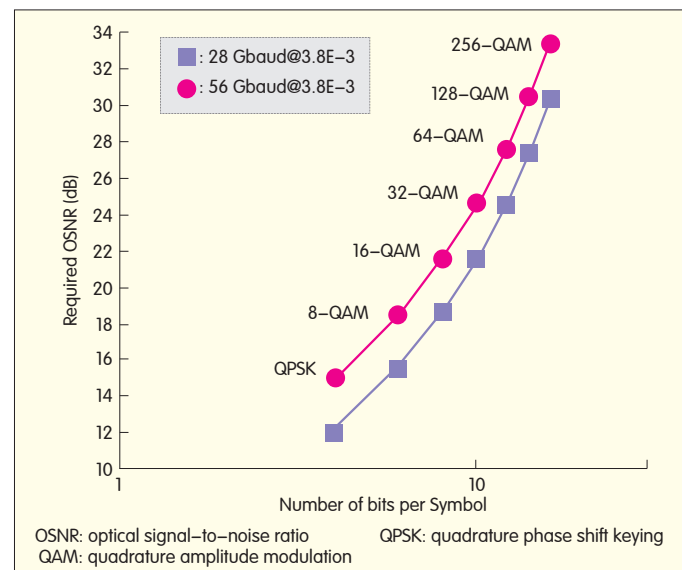
being investigated. With recent advances in the fabrication of special fiber and in transmission performance, SDM shows promise [12]–[14]. However, as well as design and manufacturing challenges, there are other significant challenges—such as fan in/out devices, connector/splice, and amplifier and transceiver integration—that show there is still long way to go before SDM becomes a commercial reality.

There are three main ways to increase channel bit rate when PDM and coherent detection are being used. The first way is ETDM, which increases symbol rate so that full advantage can be taken of mature electronic technologies (Fig. 1). Using differential phase-shift keying (DPSK), symbol rates of up to 40 Gbaud have been achieved in field deployments [15], and using NRZ, a symbol rate of 100 Gbaud has been achieved in experimental conditions [16]. Both these scenarios involve direct detection. With 30 Gbaud symbol rate, today's 100 Gbit/s commercial systems or 400 Gbit/s dual-carrier prototypes are limited in their ability to transport QPSK or 16 quadrature amplitude modulation (16-QAM) signals in coherent detection [17]. In the laboratory, 16-QAM signals with symbol rates of up to 56 Gbaud have been reported, but this comes at the expense of reduced transmission distance [18].

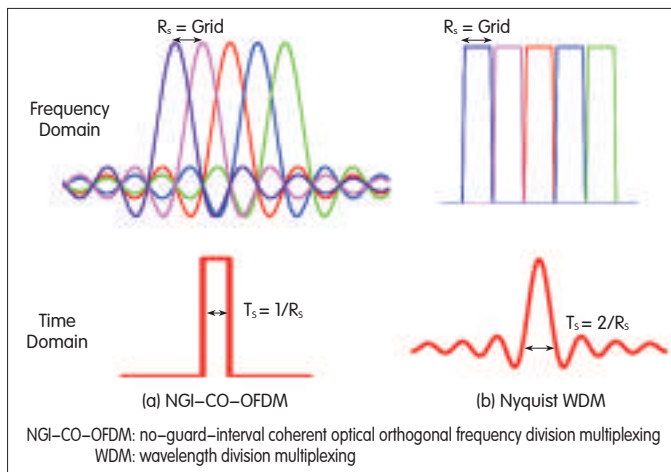
The second way is to use higher-level QAM formats because they provide higher SE than PDM-QPSK, but this comes at the expense of higher implementation penalty, a higher requirement for receiver sensitivity, and reduced optical reach. The required optical signal-to-noise ratio (OSNR) of a 16-QAM signal is 6 dB larger than that of a QPSK signal and grows exponentially as the constellation points increase (Fig. 2) [22]. In a recent laboratory experiment, the implementation penalty for a 16-QAM signal with BER = 10^{-3} was as great as 8 dB compared to around 1 dB for a QPSK signal [18]. In a field experiment, 512 Gbit/s dual-carrier 16-QAM signals were transmitted over a limited distance of

734 km. Dispersion-compensated standard single-mode fiber (SSMF) were used with 10 Gbit/s neighbors on a 200 GHz grid [17]. These experiments prove how challenging it is to increase SE with a 16-QAM format.

The third way is to use multiple optical carriers (superchannels) to overcome the speed and bandwidth limitations of optoelectronic components. These superchannels are ultra-densely packed 100–200 Gbit/s channels. So far, the transmission reach achievable using a single, high-SE PDM-QPSK superchannel is 7200 km [23], which implies that QPSK constellations reflect a good trade-off between SE and distance. As opposed to using single-carrier transmission in each channel, using multicarrier transmission requires a shift from fixed spacing grids to flexible spacing grids in optical nodes. Among different multicarrier technologies, no-guard-interval coherent optical orthogonal frequency-division multiplexing (NGI-CO-OFDM) and Nyquist wavelength-division multiplexing (Nyquist WDM) have the greatest potential for higher SE without sacrificing too much transmission distance [24], [25]. Comparisons of the time and frequency domains of the two technologies are shown in Fig. 3(a) and (b). The basic idea of NGI-CO-OFDM is that the subcarrier spacing is equal to the baud rate in the frequency domain, and in Nyquist WDM, the subcarriers are spectrally shaped so that their occupancy is close or equal to the Nyquist limit for transmission that is free of intersymbol interference (ISI). The spectra of the optical subcarriers overlap, but the signals remain separable after optical detection because of their orthogonality in NGI-CO-OFDM. The need for higher sampling speed and bandwidth of the analog-to-digital converter (ADC) is also a challenge in demultiplexing [23]. In Nyquist WDM, spectral shaping at the transmitter (Tx) is needed using either a specific optical filter in optical domain or Tx DSP with digital-to-analog converter (DAC) in electrical domain. Nyquist WDM and NGI-CO-OFDM have been theoretically and experimentally



▲ Figure 2. Challenges in increasing constellation points and baud rate.



▲ Figure 3. Multicarrier superchannel realization using (a) NGI-CO-OFDM and (b) Nyquist-WDM.

compared in [26] and [27]. The results show that Nyquist WDM is much more robust and practical in terms of ICI tolerance and implementation constraints.

Many laboratory experiments have been done on different system configurations with varying technologies. These technologies include electrical OFDM [28], [29] and optical OFDM [30] based on fast Fourier transform (FFT) and inverse fast Fourier transform (IFFT). The electrical OFDM has a single optical carrier with electrical OFDM signal modulation, and the optical OFDM has optical IFFT at Tx and FFT at Rx. Other technologies include electrical-optical OFDM with multiple optical carriers and electrical OFDM signal modulation [31], coherent WDM [32], and maximum a posteriori (MAP) or maximum likelihood sequence estimation (MLSE) algorithm for strong filtering and equalization of ISI [33]. The factors that determine which technology is adopted include SE, nonlinear tolerance, cost, and integration compactness.

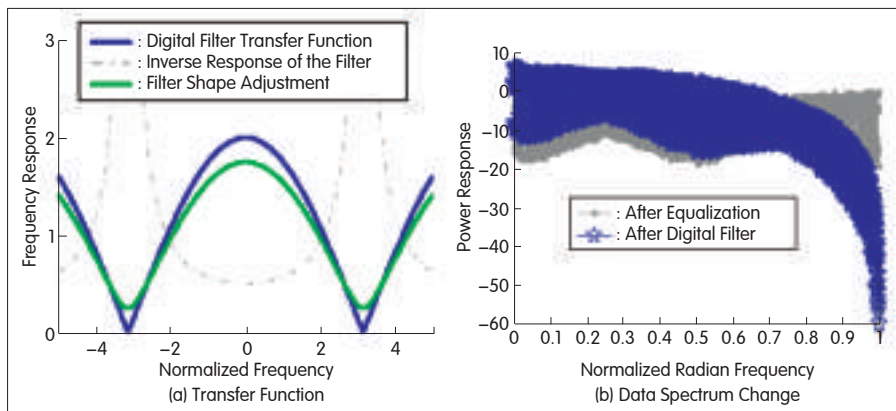
Although many experiments are adequate for proof-of-concept, field trials impose more rigorous and realistic requirements on the system and are much closer to real implementation. For example, the system must automatically adjust to changes in chromatic dispersion (CD) and polarization-mode dispersion (PMD) caused by temperature and mechanical disturbance in different locations. Other unknown factors also affect the performance of blind equalization at the receiver. Operators need to characterize different technologies in order to better understand system-level implications of latest approaches for a real fiber network. In the past three years, there several field trials have been done to test and evaluate commercial 100G and beyond optical systems. In 2010, AT&T assessed the feasibility of upgrading their network with a 100G channel over 1800 km with dispersion compensation module (DCM) and neighboring 10G and 40G DWDM systems [34]. In 2012, they then successfully demonstrated 3760 km transmission of a 1100G channel with soft-decision forward-error correction (SD-FEC) over uncompensated 40G-optimized DWDM reconfigurable optical add-drop multiplexing (ROADM)

systems for 80 km SSMF spans [35]. Verizon completed the first trial of end-to-end native IP 100G single-carrier coherent detection transmission over 1520 km. 100GE router cards and 100GBASE-LR4 C form-factor pluggable (CFP) interfaces were used [7]. They performed the first mixed-channel (112 Gbit/s, 450 Gbit/s, and 1.15 Tbit/s) transmission based on coherent OFDM with spectral efficiency of up to 3.3 bits/s/Hz [36], and they also achieved the highest capacity in a field trial: 21.7 Tbit/s with 8-QAM and QPSK [37]. Deutsche Telekom conducted a field experiment on 253 Gbit/s electrical OFDM channels over 764 km SSMF [38] and another field experiment on 512 Gbit/s 16-QAM channels over 734 km [17]. British Telecom conducted the first gridless optical networking field trial with geographically scattered flexible-spectrum-switching nodes linked over 620 km. The nodes were capable of spectrum defragmentation [39].

In this paper, we describe a field trial conducted over Deutsche Telekom's G.652 SSMF link between Darmstadt and Nuremberg. To investigate long-haul transmission, we used additional lab SSMF to extend the optical transmission distance [34], [35]. We report several results for 100G and beyond transmission over the same optical link. These include results for multiple baud rates (25 Gbaud, 28 Gbaud, and 54.2 Gbaud) and line rates (120 Gbit/s, 216.8 Gbit/s, 448 Gbit/s, and 1.3 Tbit/s) over different transmission distances. The 120 Gbit/s signals have PDM-QPSK format and real-time coherent detection with SD-FEC capability, and the 448 Gbit/s and 1.3 Tbit/s superchannels use PDM-QPSK modulation for each optical subcarrier but with Nyquist-WDM technology. The 8×216.8 Gbit/s signals use 54.2 Gbaud PDM-carrier suppression return-to-zero (CSRZ)-QPSK format on a 50 GHz optical grid. The electrical-digital post filter is introduced at the Rx to shape the binary signal into a duo-binary signal for suppressing noise, crosstalk, and combined filtering effects given spectral shaping after a wavelength selective switch (WSS), bandwidth-limited ADC chips, and other optical/electrical components. This makes possible the use of MLSE with 1 bit memory length for further signal decoding and error correction.

2 Digital Post-Finite Impulse Filter

The requirements on the optical filter in a real implementation are far different from those of an optical filter under the ideal condition of Nyquist spectral shaping. To avoid the need for a high-bandwidth, high-sampling-speed DAC at the Tx, an optical multiplexer with narrowband optical filtering is typically used to perform aggressive spectrum shaping and multiplexing. This is necessary to obtain Nyquist signals, where the symbol bandwidth equals the channel spacing, or faster-than-Nyquist-WDM signals, where the symbol bandwidth is less than the channel spacing. However, spectral shaping induces crosstalk for the intrachannels and interchannels and greatly limits transmission performance. This means that innovative signal processing techniques are



▲ Figure 4. Transfer profile of digital filter and data spectrum after equalization and filtering.

needed at the receiver to realize high SE and counter ISI.

Partial response signaling, also called duobinary signaling or correlative coding [22], involves introducing a controlled amount of ISI into the signal rather than trying to eliminate it completely. This can be compensated for at the receiver, and an ideal symbol-rate packing of 2 symbols per Hertz can be achieved without the need for unrealizable filters based on Nyquist. Optimal multisymbol detection schemes such as MAP and MLSE are necessary to take advantage of the symbol correlation in the received partial response signals. In [36], successful transmission of $198 \times 100\text{G}$ bandwidth-constrained PDM RZ-QPSK channels with an SE of 4 bit/s/Hz over long-haul ultralarge-effective-area (ULEA) fiber is reported. The challenge is that the number of states and transitions grow exponentially in relation to memory length. An MLSE length of 10 means 4^{10} states and 4^{11} transitions in lane-dependent PDM-QPSK signals [33], which imposes significant computational complexity in practical implementation. On the other hand, the noise in high-frequency components of the signal spectrum is enhanced when a conventional linear impairment equalization algorithm, such as conventional constant modulus algorithm, is used in a bandwidth-constrained optical coherent system [40]. The simulated spectrum of data after linear equalization is shown in Fig. 4(b). The high-frequency part is strongly recovered and mixed with enhanced noise.

A linear electrical delay-and-add digital filter is a simple way of achieving partial response while mitigating the enhanced noise [40]. The MLSE algorithm is still used for symbol decoding and optimal detection, but the memory length is significantly reduced. Filtering is performed after carrier phase estimation in the conventional DSP flow of the coherent receiver. The effect of filtering on the high-frequency components is shown in Fig. 4(b). The transfer function of the digital filter is shown in Fig. 4(a). The second-tap coefficient of the filter is adjusted so that its performance with the following MLSE detection algorithm is

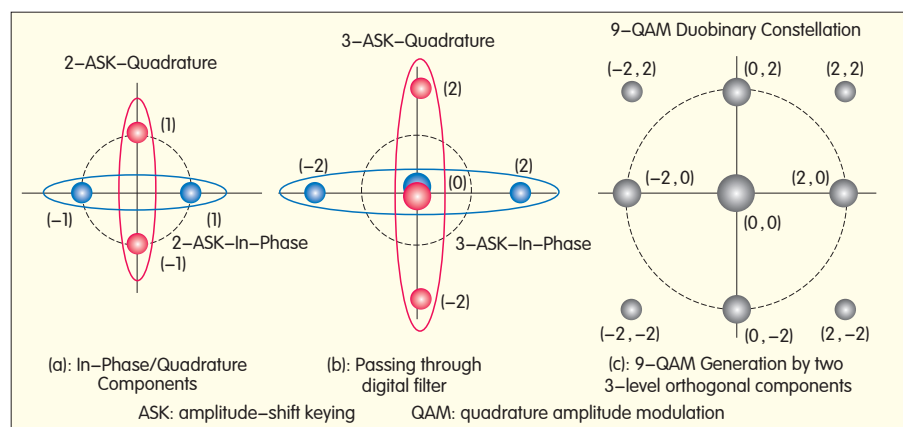
optimized. After filtering, the enhanced noise and ISI are suppressed.

The digital filter turns 4-point QPSK signals into 9-point quadrature duobinary signals. This transformation is shown in Fig. 5. As a result of the delay-and-add effect, the 2-amplitude-shift keying (ASK) in-phase and quadrature components disappear and change into two 3-ASK symbol series. The generation mechanism of 9-QAM signals can be considered a superposition of two 3-ASK vectors on a complex plane. The size of constellation points reflects the relative number of points generated after the digital filter.

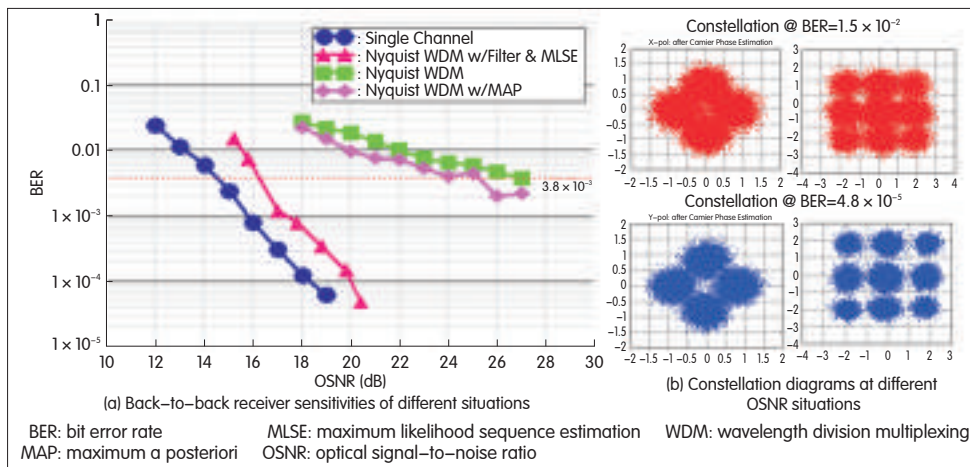
We conducted a lab experiment to

determine the effectiveness of this technology. Fig. 6 shows the back-to-back (BTB) BER performance for Nyquist WDM using different demodulation schemes with and without adjacent subchannels. The signal is 28 Gbaud, and the channel spacing in the case of WDM is 25 GHz. The ADC is operated at 50 GSa/s with a 13 GHz bandwidth for all measurements. The digital signal is resampled at twice the symbol rate based on the recovery clock. A $T/2$ -spaced time-domain FIR filter (where T is the sampling time period) is used for electronic dispersion compensation (EDC). Then, polarization recovery is performed using classic CMA with 21-tap, $T/2$ -spaced adaptive FIR filters. Carrier recovery, including frequency offset estimation by FFT method and carrier recovery by 4th power Viterbi-Viterbi algorithm, is then performed. It is then additionally equipped with the filter and is followed MLSE with a memory length of 1 bit [22].

By turning adjacent subchannels off, at BER = $3.8\text{e-}3$ the single PM-QPSK subchannel at 112 Gbit/s achieves a minimal OSNR requirement of 14.4 dB. Typical Nyquist WDM suffers a large 12.6 dB OSNR penalty because of the deteriorated filtering effect. Although that penalty may be reduced by 3 dB by introducing 3-tap MAP estimation at the receiver, the received OSNR of 24 dB is still too high for long-haul transmission. By using the new processing technique with digital filter and 1 bit MLSE, the OSNR penalty



▲ Figure 5. 9-QAM signal generated by a digital filter.



▲ Figure 6. Lab experimental measurement.

is dramatically cut down to 1.8 dB (16.2 dB OSNR). We also investigate 25 Gbaud WDM under the same 25 GHz optical filtering effect. A 0.5 dB OSNR improvement is obtained compared with 28 Gbaud case.

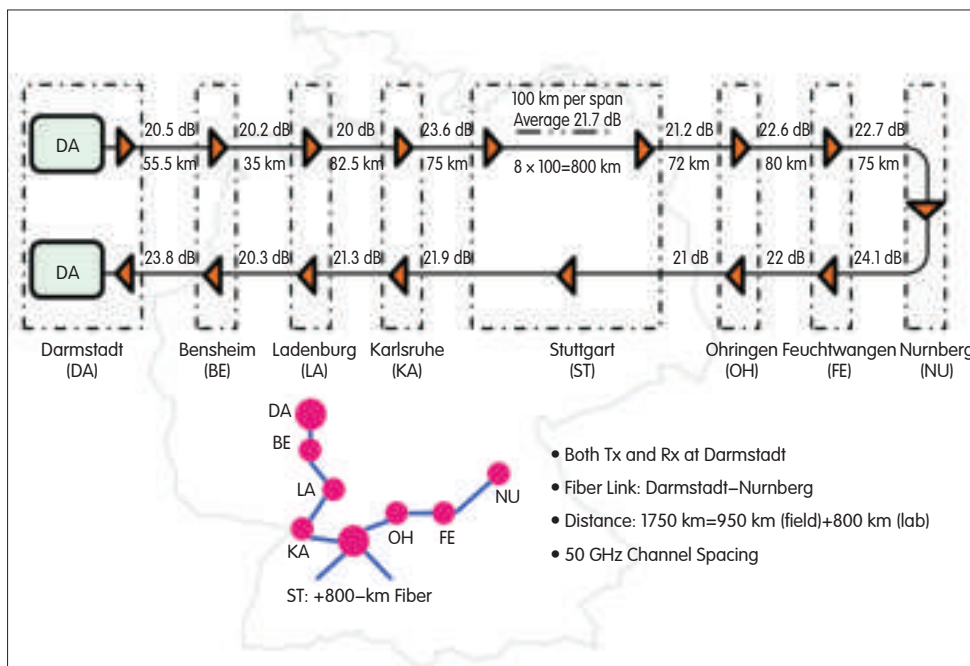
3 The 54.2 Gbaud Signals on 50 GHz Optical Grid

This field experiment was conducted to investigate the feasibility of higher baud rate on the 50 GHz optical grid and with the same PDM-QPSK format. QPSK constellations provide lower implementation penalty and the best trade-off between SE and distance compared with 16-QAM or higher-level QAM formats. Recent experiments have been done on hybrid transmission of asymmetrically interleaved

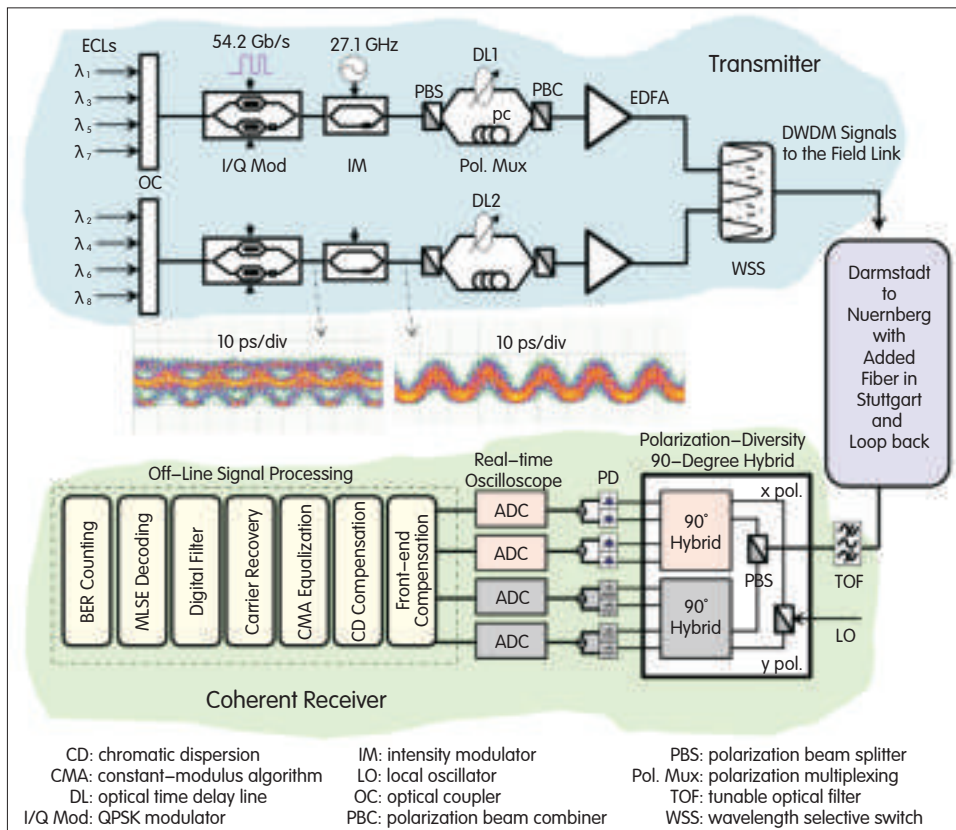
losses are 20 dB and 24.1 dB, respectively. In order to extend the transmission distance, additional 8×100 k. 652 fiber spans are inserted in Stuttgart to increase the total distance to 1750 km. Commercial gain-flatten inline EDFAs are used so that fiber span loss can be compensated for without the need for additional gain equalizers in the link. The average loss of the 22 fiber spans is 21.6 dB. The test center, where both the transmitters and receivers were installed, was located at the Deutsche Telekom research center in Darmstadt.

Fig. 8 shows the experimental setup of 8×216.8 Gbit/s PDM-CSRZ-QPSK signal generation and transmission over 1750 km G.652 fiber deployed in the field and in the laboratory. The 54.2 Gbaud binary electrical signals are generated from a 4:1 electrical mux after multiplexing four-channel 13.55 Gbit/s binary signals. Eight ECLs with a

linewidth of less than 100 kHz, with neighboring wavelength spacing of 50 GHz, and with output power of 14.5 dBm are divided into odd and even carriers. Each I/Q modulator is driven by two 54.2 Gbit/s pseudorandom binary sequence (PRBS) electrical signals with a word length of $(2^{13}-1) \times 4$. These modulators modulate the odd or even carriers. The 67% CSRZ pulse carver is realized by using a single-arm Mach-Zehnder intensity modulator (IM) that is driven by a 27.1 GHz sinusoidal RF signal and that is DC-biased at the null points. Each path is polarization multiplexed by the polarization multiplexer. This comprises a polarization beam splitter (PBS) to split signal, an optical delay line (DL1 and DL2) to provide a delay of more than 100 symbols, and a polarization beam



▲ Figure 7. Field-trial link configuration in DT's optical infrastructure.



▲ Figure 8. Experimental setup for generating and transmitting 8×216.8 Gbit/s PDM-CSRZ-QPSK over 1750 km fiber. Eye diagrams of PDM-CSRZ-QPSK before (a) and after (b) CSRZ pulse curving.

combiner (PBC) to recombine the signal. The odd and even channels are spectrally filtered and combined using a programmable WSS with 50 GHz fixed grid. The optical spectrum of the single-channel 54.2 Gbaud PDM-CSRZ-QPSK signal before and after 50 GHz grid WSS is shown in Fig. 9. The spectrum shape at the high-frequency edge is significantly affected by the strong optical filtering.

The generated 8×216.8 Gbit/s PDM-CSRZ-QPSK signal is launched into a 22-span G.652 fiber transmission link (Fig. 7). At the receiver, a tunable optical filter (TOF) with 3 dB bandwidth of 1 nm is used to select the desired channel to be further evaluated. An ECL with a linewidth of less than 100 kHz is used as the local oscillator (LO).

A polarization-diverse 90° hybrid is used for polarization-diverse and phase-diverse front end of the balanced coherent detection. Sampling and digitization (A/D) is performed in the digital scope with 80 GSa/s sampling rate and 30 GHz electrical analog bandwidth. DSP is performed offline. Electrical impairment equalization and polarization demultiplexing is performed using the following blind equalization steps:

Step 1: The clock is extracted using the square-and-filter method, and the digital signal is resampled at twice the baud rate of the recovery clock.

Step 2: A T/2-spaced time-domain finite impulse-response (FIR) filter is used to compensate for

chromatic dispersion. The filter coefficients are calculated from a known fiber CD transfer function using the frequency-domain truncation method.

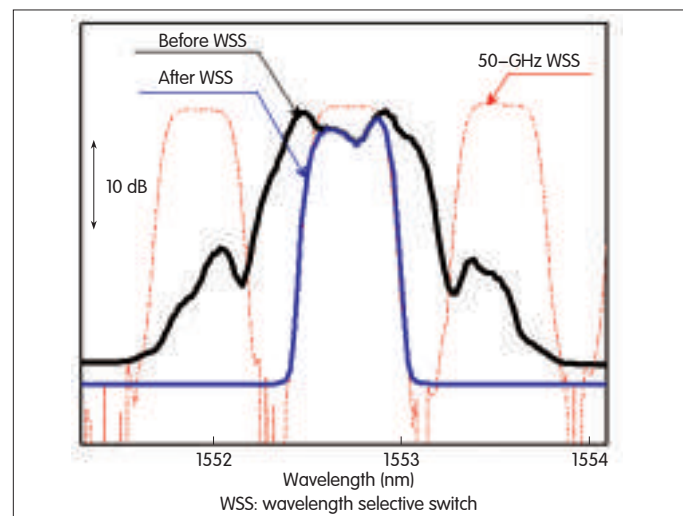
Step 3: Two complex-valued, 13-tap, T/2-spaced adaptive FIR filter banks, found on a classic CMA, is used to demultiplex the QPSK signal and compensate for the residual CD and polarization-mode dispersion (PMD). LO frequency offset compensation and carrier-phase estimation (CPE) follow using Viterbi-Viterbi algorithm. As a result of linear equalization of the spectral shaping signals, the noise and linear crosstalk at the high-frequency edge of signals is enhanced, which leads to the OSNR reduction.

Step 4: A digital postfilter, as discussed in section 2, is added and followed by the MLSE for the partial response estimation.

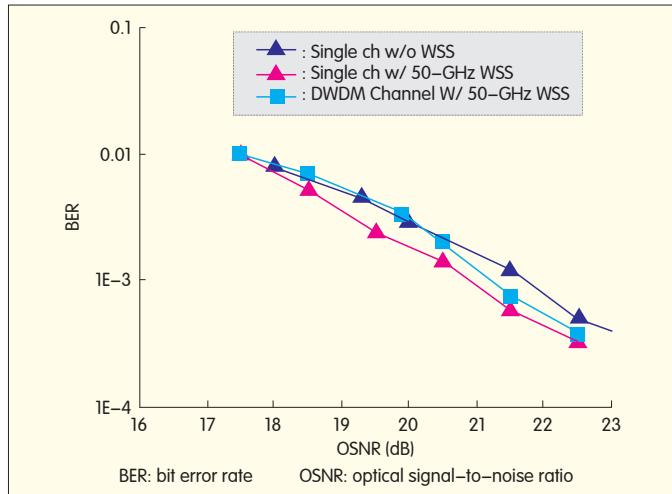
Because of the known pattern of duobinary signaling, only two states with 1 bit memory length) are needed for the signal decoding of the independent electrical lane. In this field experiment, errors are counted

over 12×10^6 bits (12 data sets, each data set contains 10^6 bits), and differential decoding is used to solve $\pi/2$ phase ambiguity.

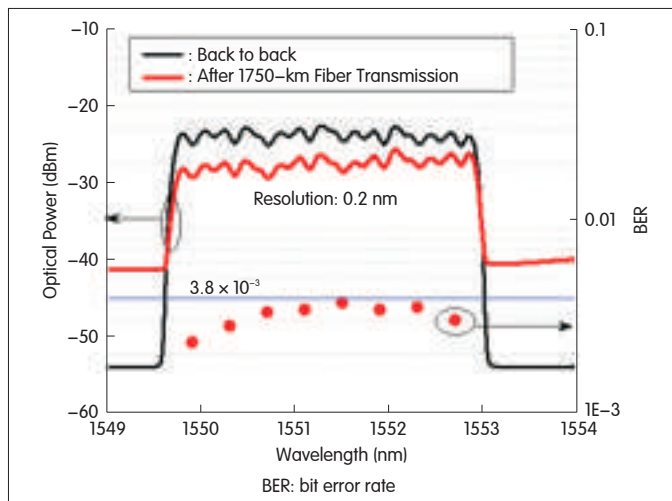
Fig. 10 shows the back-to-back BER as a function of OSNR with noise measured at 0.1 nm bandwidth. We measure the performance of the middle channel at 1551.51 nm while temporarily turning off the adjacent



▲ Figure 9. Spectrum before and after WSS (0.1 nm resolution).



▲ Figure 10. Back-to-back BER performance of the middle channel at 1551.51 nm in different situations.



▲ Figure 11. Optical spectra (left) and BER performance after transmission over 1750 km fiber.

Nyquist-WDM channels and bypassing the WSS. The required OSNR for this single carrier at $\text{BER} = 1 \times 10^{-3}$ is 21.6 dB/0.1 nm. This corresponds to the theoretical implementation penalty. After 50 GHz WSS filtering, a negative penalty of 0.8 dB is obtained. This penalty arises because the CS-RZ pulse has a very wide spectrum, and part of the optical power cannot be detected by the coherent receiver because of the limited bandwidth of the real-time oscilloscope [43]. By turning on the adjacent carriers, the measured OSNR requirement of $\text{BER} = 1 \times 10^{-3}$ for Nyquist WDM channels is about 21.4 dB. This means that a 0.6 dB penalty is caused by channel crosstalk. We also confirmed that all other channels perform similarly except that the side channel has 0.5 dB better OSNR tolerance.

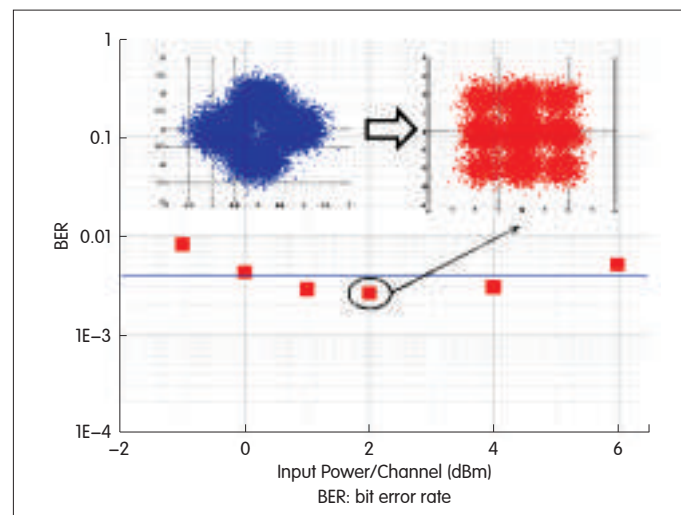
The optical spectrum before and after transmission over 1750 km with 2 dBm input power and 0.2 nm resolution is shown in Fig. 11. The measured BER after transmission, that

is, the average of both X and Y polarizations, is also shown in Fig. 11. The BER for all Nyquist-WDM channels is better than the hard-decision (HD) pre-FEC threshold of 3.8×10^{-3} . The average BER of all channels is 3.1×10^{-3} , with individual BER values ranging from 2.1×10^{-3} at the edge to 3.6×10^{-3} in the middle channel.

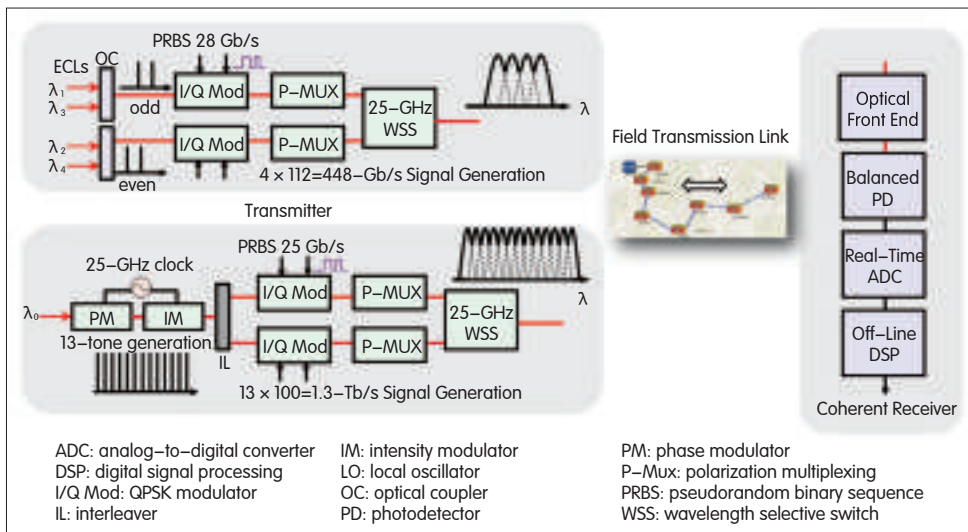
Fig. 12 shows the BER after transmission when the signal power into each span fiber is varied. The input power at 2 dBm per channel is the optimal launch power. The constellation diagrams of the transmitted signal before and after digital filtering are shown in Fig. 12 (insert). The binary QPSK signal is converted into duo-binary QPSK signal with less noise. The results from our field experimental show the potential for ultralong-haul transmission using the doubled baud rate and the relatively simple QPSK modulation format.

4 Mixed Transmission of 100G, 400G, and 1 T

In a similar optical link, we conducted another field trial on the mixed transmission of 120G signals and two multicarrier superchannels at 448 Gbit/s and 1.3 Tbit/s (Fig. 13). The 400G superchannel is generated using four independent ECLs with a linewidth of less than 100 kHz (Fig. 14). The PRBS rate is 28 Gbit/s for four electrical lanes. After the polarization multiplexing structure for odd and even channels, the PDM-QPSK signals pass through a WSS, which is programmed to operate at 25 GHz interleaving mode for spectral shaping of all input subchannels. This yields an SE of 4 bit/s/Hz. The generation of 13-subcarrier 1T signal is different. The CW light from an ECL with a linewidth of less than 100 kHz and output power of 14.5 dBm is modulated by a cascaded phase modulator (PM) and IM. The PM is driven by an RF clock at 25 GHz with a peak-to-peak voltage of 17 V. Its half-wave voltage and insertion loss is 4 V and 3.8 dB, respectively. After phase modulation, multiple coherent carriers spaced at 25 GHz are generated. The



▲ Figure 12. BER performances after 1750 km transmission at different input optical power per channel.



▲ Figure 13. Different generation schemes of 400G and 1T with similar coherent detection.

following IM is driven by a synchronized 25 GHz clock and is used to flatten the optical subcarriers generated by the PM. Then, the odd and even channels are separated using a 25/50 GHz optical interleaver (IL). The odd and even channels are independently I/Q modulated by a 25 Gbit/s PRBS signal and then polarization multiplexed. They are then combined by a 25 GHz WSS, which performs a similar function as in the 400G case. The signal occupies 325 GHz optical bandwidth. Significant linear crosstalk is expected to occur in the 400G and 1T cases. The digital filter and MLSE that follows are used to mitigate this impairment. The 100G line card used in this field experiment is a real-time coherent transceiver that is multisource agreement (MSA) package compliant. It consists of a 100GE CFP at the client side, OTU4 framing, PDM-QPSK modulation at line side, and coherent detection and DSP at receiver side (Fig. 14). A 40 nm CMOS ASIC is used with a four 8 bit, 63 GSa/s ADC on the receiver side. One of the key features of the MSA transceiver is that it has SD-FEC capability for correcting a pre-FEC BER of 1.9×10^{-2} to less than 1×10^{-15} , which corresponds to an 11.1 dB net coding gain. The total line rate is 120 Gbit/s with 15% SD-FEC overhead, which is based on Turbo-Product Code (TPC). Fig. 15(a) and (b) shows the back-to-back BER measurements as a function of OSNR for the 400G and 1T QPSK subchannel, respectively. The black square represents the performance of a single subcarrier without spectral shaping by the WSS. The subcarrier in 400G has 1.5 dB penalty at $\text{BER} = 1 \times 10^{-3}$, and the subcarrier in 1T has 1.4 dB penalty at the same BER. The difference in receiver sensitivity can be attributed to the 25 GHz spectral shaping of 25 Gbaud and 28 Gbaud signals. No substantial error floor is observed for both cases. Fig. 16(a) shows back-to-back pre-FEC BER as a function of OSNR for a 100G channel. A theoretical

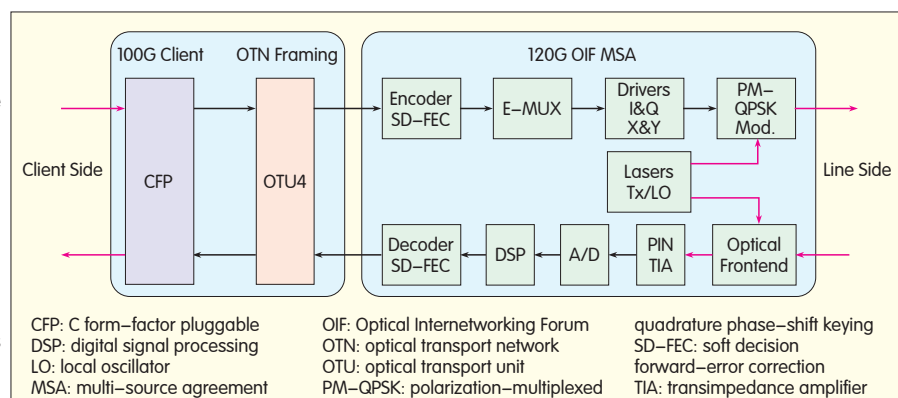
curve is also shown for comparison. OSNR of 15.5 dB is required for $\text{BER} = 1 \times 10^{-3}$, and only 1 dB implementation penalty is generated from the theoretical limit at SD-FEC threshold.

The 400G and 1T channels co-propagate with two 100G signals. The spectrum of the mixed signals after 1750 km transmission is shown in Fig. 16(b). The field experiment results are obtained for a launch power of 400G and 1T of -2 dBm per channel. The optimized launched power is -2 dBm and -1 dBm for 400G and 1T per channel, respectively. The average received OSNR is 17.5 dB. The two 100G channels are located at 1558.85 nm and 1557.25 nm. Fig.

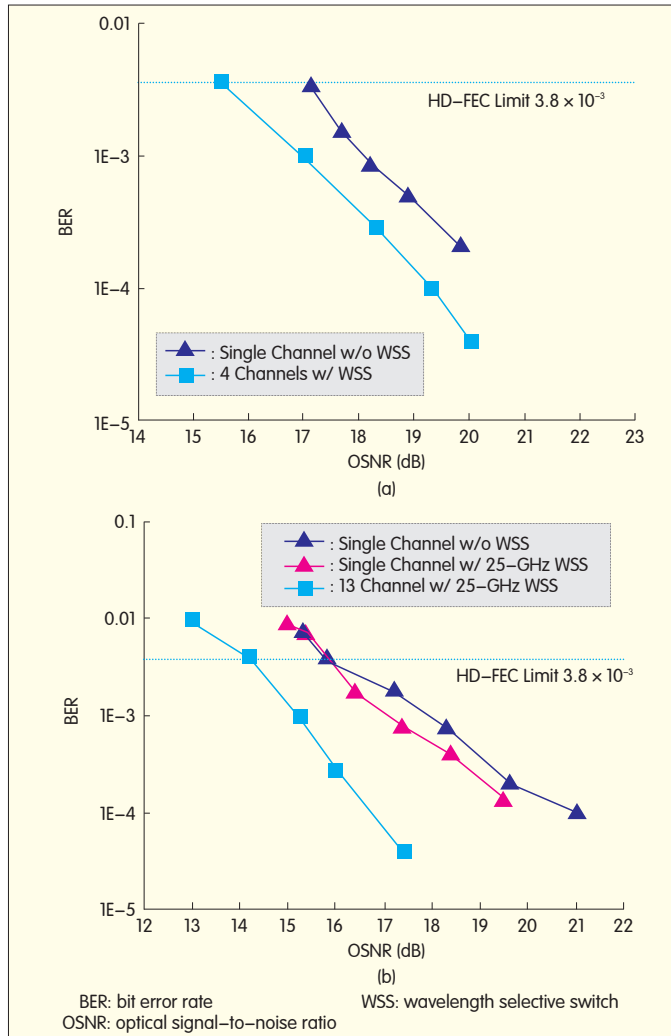
17 shows constellation diagrams and the corresponding measured BER after 1750 km transmission for both 400G and 1T signals. Fig. 18 shows BER as a function of the transmission distance in mixed-channel operation. Transmission distances of 950 km (all field fiber), 1750 km (950 km field + 800 km lab fiber in Stuttgart), and 2150 km (950 km field + 800 km lab fiber in Stuttgart + 400 km lab fiber in Darmstadt) are measured with the BER performance better than pre-SD-FEC threshold. After 2150 km transmission, the pre-FEC BER is 7.7×10^{-3} and 5.7×10^{-3} , respectively. This means that the encoding correction should be in the SD-FEC region. In the case of 100G transmission, a BER of 5.6×10^{-4} is achieved after 2150 km transmission. We also measured the transmission performance over 2450 km, the longest distance obtainable in our field trial with two 100G channels alone. A large BER margin still exists, even when pre-HD-FEC threshold and error-free transmission is verified on the client side.

5 Conclusion

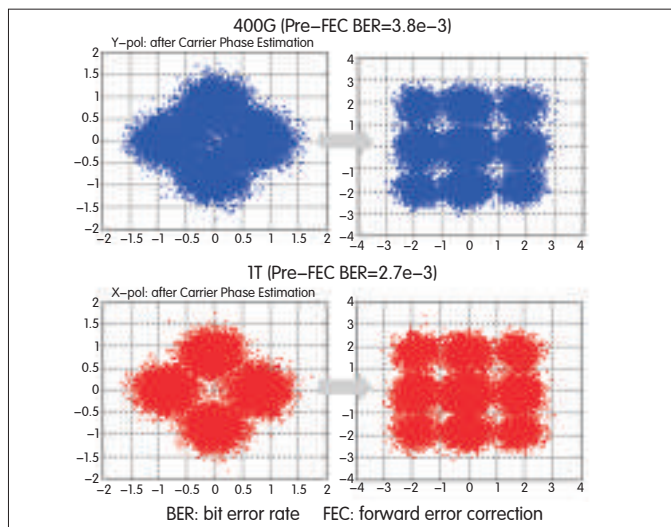
In our field trial, we successfully demonstrated the



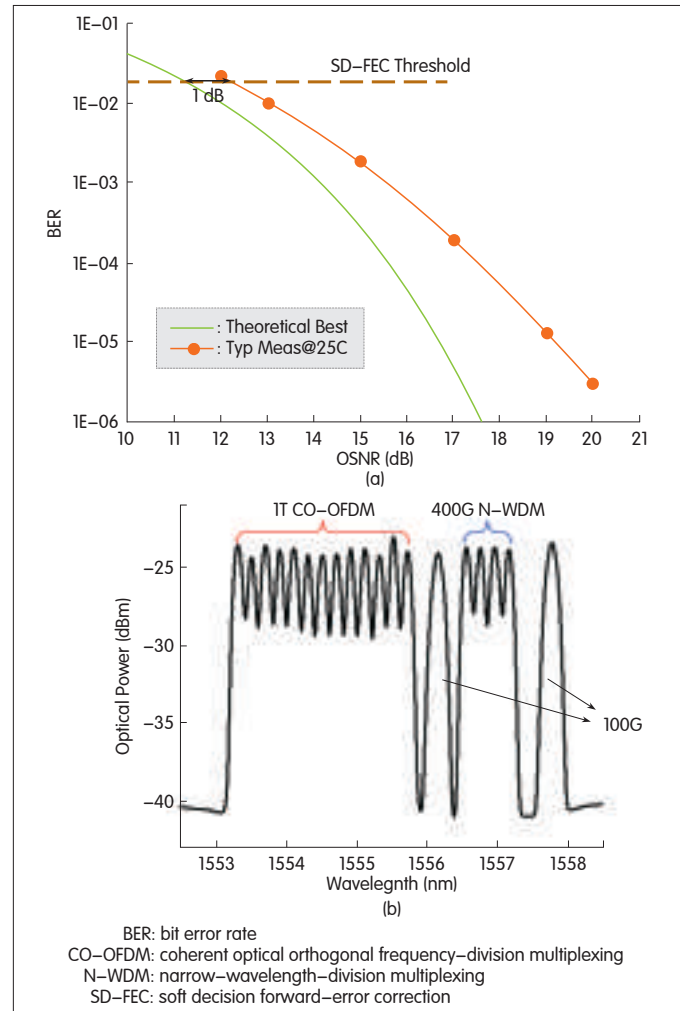
▲ Figure 14. 100G MSA transceiver with SD-FEC capability.



▲ Figure 15. Back-to-back receiver sensitivity of Nyquist (a) 400G and (b) 1T signals.

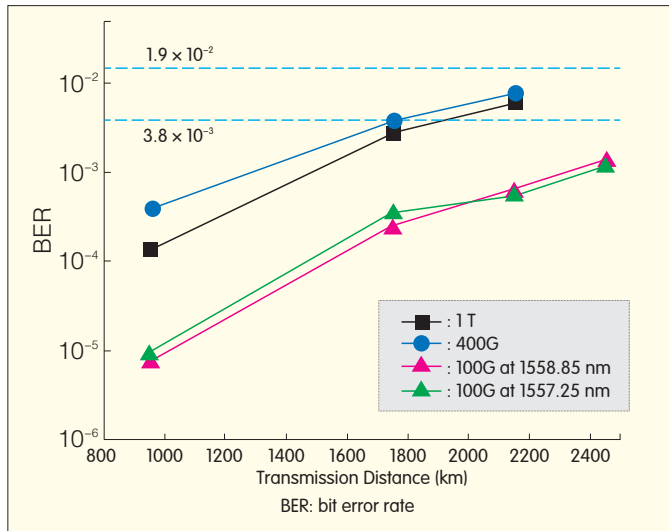


▲ Figure 17. Constellation diagrams after 1750 km transmission.



▲ Figure 16. (a) Measured back-to-back pre-FEC BER performance versus OSNR of the 100G channel, and (b) optical spectrum of a mixture of two 100G channels, one 400G, and a 1T channel after 1750 km transmission.

transmission of 100G and beyond over Deutsche Telecom's optical infrastructure. The first field experiment with 8×216.8 Gbit/s DWDM PDM-CSRZ-QPSK signals reached a record net SE of 4 bit/s/Hz over 22 SSMF spans with a total distance of 1750 km and with the BER of all channels smaller than the HD pre-FEC limit. This field experiment indicates that doubling the baud rate on the same 50 GHz grid with the same QPSK modulation is feasible to increase the capacity over long-haul transmission distances. In the case of mixed transmission, the 448 Gbit/s channel using Nyquist-WDM technology with PDM-QPSK modulation at each subcarrier achieved a net SE of 4 bit/s/Hz. Technology for generating multiple optical tones is used for the 1.3 Tbit/s superchannel creation with the same 25 GHz Nyquist spectral shaping and 325 GHz optical occupancy. These two superchannels—together with two neighboring real-time, SD-FEC based, 100G coherent transceivers—are successfully transmitted over 1750 km optical link for pre-HD-FEC and 2150 km for



▲ Figure 18. Transmission performance of 400G and 1T based on Nyquist technique.

pre-SD-FEC threshold with EDFA-only amplification in the link. The digital post filter and simplified MLSE algorithm are introduced in beyond-100G channels to mitigate the enhanced noise and crosstalk caused by strong spectral shaping. For the 100G transponder deployed in the real network, a large BER margin exists with respect to the pre-SD-FEC BER threshold after transmission over 2450 km field fiber. These field experiments show that 100G technology with SD-FEC is capable of ultralong-haul transmission. Nyquist WDM with special signal processing is practically implementable and very promising for scaling channel capacity beyond 100G over longhaul distances.

Acknowledgment

The author would like to thank Matthias Gunkel, Paul Wagner, Heinz Mayer and Achim Schippel from Deutsche Telecom for supporting the field transmission link; thank Yi Hong, Meng Li, Zhiliang Ren, Nan Lu, Li Xie, Kai Liu, Xiaochao Zhang, Yan Xia, and Yao Cai from ZTE Corporation, Beijing, for their dedicated technical support, and thank Dr. Jianqiang Li for fruitful discussions.

References

- [1] B. Swanson and G. Gilder, "Estimating the Exaflood: The impact of video and rich media on the internet—A zettabyte by 2015?" Discovery Institute, Jan. 29, 2008.
- [2] R. Tkach, "Scaling optical communications for the next decade and beyond," in *Bell Labs Techn. J.*, vol. 14, no. 4, pp. 3–9, 2010.
- [3] R. J. Essiambre, R. Tkach, "Capacity trends and limits of optical communication networks," *Proc. IEEE*, vol. 100, no. 4, pp. 1–21, 2012.
- [4] C. V. N. Index, "Forecast and Methodology, 2010–2015," White Paper, Cisco Systems, San Jose, CA, Jun. 1, 2011. [Online]. Available: http://www.cisco.com/en/US/solutions/collateral/ns341/ns525/ns537/ns705/ns827/white_paper_c11-481360_ns827_Networking_Solutions_White_Paper.html
- [5] K. Roberts, M. O'Sullivan, K.-T. Wu, H. Sun, A. Awadalla, D. J. Krause, and C. Laperle, "Performance of Dual-Polarization QPSK for Optical Transport Systems," in *J. Lightwave Technol.*, vol. 27, no. 16, pp. 3546–3559, Aug. 2009.
- [6] J. Renaudier, O. Bertran-Pardo, H. Mardoyan, P. Tran, G. Charlet, S. Bigo, M. Lefrançois, B. Lavigne, J.-L. Auge, L. Piriou, O. Courtois, "Performance comparison of 40G and 100G coherent PDM-QPSK for upgrading dispersion managed legacy systems," in *Proc. Opt. Fiber Commun. Conf./Nat. Fiber Opt. Eng. Conf. (OFC/NFOEC '09)*, San Diego, CA, 2009, paper NWD5.
- [7] T. J. Xia, G. Wellbrock, B. Basch, S. Kotria, W. Lee, T. Tajima, K. Fukuchi, M. Cvijetic, J. Sugg, Y. Ma, B. Turner, C. Cole, C. Urricariet, "End-to-end native IP data 100G single carrier real time DSP coherent detection transport over 1520 km field deployed fiber," in *Proc. Opt. Fiber Commun. Conf./Nat. Fiber Opt. Eng. Conf. (OFC/NFOEC '09)*, San Diego, CA, 2009, paper PDPD4.
- [8] S. Gringeri, E. B. Basch, T. J. Xia, "Technical considerations for supporting data rates beyond 100 Gb/s," in *IEEE Commun. Mag.*, vol. 50, no. 2, pp. 21–30, Mar. 2012.
- [9] J. Renaudier, O. Bertran-Pardo, M. Salsi, H. Mardoyan, P. Tran, G. Charlet, S. Bigo, "Will 100 Gb/s resist higher bit rates?" in *Proc. Eur. Conf. Opt. Commun.*, Geneva, Switzerland, 2011, paper Th.11.B.3.
- [10] T. Richter, E. Palushani, C. Schmidt-Langhorst, M. Nolle, R. Ludwig, J. K. Fischer, C. Schubert, "Single wavelength channel 10.2 Tb/s TDM—data capacity using 16-QAM and coherent detection," in *Proc. Opt. Fiber Commun. Conf./Nat. Fiber Opt. Eng. Conf. (OFC/NFOEC '11)*, Los Angeles, CA, 2011, paper PDPA9.
- [11] H. Hu, P. Munster, E. Palushani, M. Gaili, K. Dalgaard, H. C. H. Mulvad, P. Jeppesen, and L. K. Oxenlowe, "640 Gbaud NRZ-OOK data signal generation and 1.19 Tbit/s PDM-NRZ-OOK field trial transmission," in *Proc. Opt. Fiber Commun. Conf./Nat. Fiber Opt. Eng. Conf. (OFC/NFOEC '12)*, Los Angeles, CA, 2012, paper PDP5C.7.
- [12] R. Ryf, S. Randel, A. H. Gnauck, C. Bolle, A. Sierra, S. Mumtaz, M. Esmaeelpour, E. C. Burrows, R.-J. Essiambre, P. J. Winzer, D. W. Peckham, A. H. McCurdy, and R. Lingle, Jr., "Mode-Division Multiplexing Over 96 km of Few-Mode Fiber Using Coherent 6 × 6 MIMO Processing," in *J. Lightwave Technol.*, vol. 30, no. 4, pp. 521–531, Feb. 2012.
- [13] P. J. Winzer and G. J. Foschini, "MIMO capacities and outage probabilities in spatially multiplexed optical transport systems," in *Opt. Exp.*, vol. 19, no. 17, pp. 16680–16696, 2011.
- [14] J. Sakaguchi, B. J. Puttnam, W. Klaus, Y. Awaji, N. Wada, A. Kanno, T. Kawanishi, K. Imamura, H. Inaba, K. Mukasa, R. Sugizaki, T. Kobayashi, M. Watanabe, "19-core fiber transmission of 19×100×172-Gb/s SDM-WDM-PDM-QPSK signals at 305Tb/s," presented at the *Opt. Fiber Commun. Conf./Nat. Fiber Opt. Eng. Conf.*, Los Angeles, CA 2012, Paper PDP5C.1.
- [15] T. Wuth, M. W. Chbat, V. F. Kamalov, "Multirate (100G/40G/10G) transport over deployed optical networks," in *Proc. Opt. Fiber Commun. Conf./Nat. Fiber Opt. Eng. Conf. (OFC/NFOEC '08)*, San Diego, CA, 2008, paper NTU83.
- [16] G. Raybon, P. J. Winzer, and C. R. Doerr, "1-Tb/s (10×107 Gb/s) electronically multiplexed optical signal generation and WDM transmission," in *J. Lightwave Technol.*, vol. 25, no. 1, pp. 233–238, Jan. 2007.
- [17] F. Buchali, K. Schuh, D. Rosener, E. Lach, R. Dischler, W. Idler, L. Schmalen, A. Leven, R.-P. Braun, A. Ehrhardt, C. Gerlach, L. Schurer, "512-Gb/s DP-16-QAM field trial over 734 km installed SSMF with co-propagating 10 Gb/s NRZ neighbors incorporating soft-FEC decoding," in *Proc. Opt. Fiber Commun. Conf./Nat. Fiber Opt. Eng. Conf. (OFC/NFOEC '12)*, Los Angeles, CA, 2012, paper OW4C.4.
- [18] P. J. Winzer, A. H. Gnauck, S. Chandrasekhar, S. Draving, J. Evangelista, and B. Zhu, "Generation and 1,200-km Transmission of 448-Gb/s ETDM 56-Gbaud PDM 16-QAM using a Single I/Q Modulator," in *Proc. Eur. Conf. Opt. Commun. (ECOC '10)*, Torino, Italy, 2010, paper PD2.2.
- [19] X. Zhou, J. Yu, M.-F. Huang, Y. Shao, T. Wang, L. Nelson, P. Magill, M. Birk, P. I. Borel, D. W. Peckham, R. Lingle, B. Zhu, "64-Tb/s, 8 b/s/Hz, PDM-36QAM transmission over 320 km using both pre- and post-transmission digital signal processing," in *J. Lightwave Technol.*, vol. 29, no. 4, pp. 571–577, Feb. 2011.
- [20] A. H. Gnauck, P. J. Winzer, A. Konczykowska, F. Jorge, J.-Y. Dupuy, M. Riet, G. Charlet, B. Zhu, and D. W. Peckham, "Generation and transmission of 21.4-Gbaud PDM 64-QAM using a novel high-power DAC driving a single I/Q modulator," in *J. Lightwave Technol.*, vol. 30, no. 4, pp. 532–536, Feb. 2012.
- [21] A. Sano, T. Kobayashi, S. Yamanaka, A. Matsuura, H. Kawakami, Y. Miyamoto, K. Ishihara, and H. Masuda, "102.3-Tb/s (224×548-Gb/s) C- and extended L-band all-Raman transmission over 240 km using PDM-64QAM single carrier FDM with digital pilot tone," in *Proc. Opt. Fiber Commun. Conf./Nat. Fiber Opt. Eng. Conf. (OFC/NFOEC '12)*, Los Angeles, CA, 2012, paper PDP5C.3.
- [22] J. G. Proakis, *Digital Communications*, 4 ed. New York: McGraw Hill, 2000.
- [23] S. Chandrasekhar, X. Liu, "Experimental investigation on the performance of closely spaced multi-carrier PDM-QPSK with digital coherent detection," in *Opt. Exp.*, vol. 17, no. 24, pp. 21350–21361, 2009.
- [24] B. Zhu, X. Liu, S. Chandrasekhar, D. W. Peckham, R. Lingle, Jr., "Ultra-long-haul transmission of 1.2-Tb/s multicarrier No-Guard-Interval CO-OFDM superchannel using ultra-large-area fiber," in *IEEE Photon. Technol. Lett.*, vol. 22, no. 11, pp. 826–828, June 2010.
- [25] A. Sano, E. Yamada, H. Masuda, E. Yamazaki, T. Kobayashi, E. Yoshida, Y. Miyamoto, R. Kudo, K. Ishihara, and Y. Takatori, "No-Guard-Interval Coherent Optical OFDM for 100-Gb/s long-haul WDM transmission," in *J. Lightwave Technol.*, vol. 27, no. 16, pp. 3705–3713 Aug. 2009.
- [26] G. Bosco, A. Carena, V. Curri, P. Poggolini, F. Forghieri, "Performance limits of Nyquist-WDM and CO-OFDM in high-speed PM-QPSK systems," *IEEE Photon. Technol. Lett.*, vol. 22, no. 15, pp. 1129–1131, Aug. 2010.
- [27] M. Yan, Z. Tao, W. Yan, L. Li, T. Hoshida, J. C. Rasmussen, "Experimental comparison of No-Guard-Interval-OFDM and Nyquist-WDM superchannels," in

- Proc. Opt. Fiber Commun. Conf./Nat. Fiber Opt. Eng. Conf.*, Los Angeles, CA, 2012, Paper OTh1B.2.
- [28] S. L. Jansen, I. Morita, T. C. W. Schenk and H. Tanaka, "121.9-Gb/s PDM-OFDM transmission with 2 b/s/Hz spectral efficiency over 1,000 km of SSMF," in *J. Lightwave Technol.*, vol. 27, no. 3, pp. 177–188, 2009.
- [29] W. Shieh, "OFDM for flexible high-speed optical networks," in *J. Lightwave Technol.*, vol. 29, no. 10, pp. 1560–1577, May 2011.
- [30] D. Hillerkuss, T. Schellinger, R. Schmogrow, M. Winter, T. Vallaitis, R. Bonk, A. Marculescu, J. Li, M. Dreschmann, J. Meyer, S. Ben Ezra, N. Narkiss, B. Nebendahl, F. Parmigiani, P. Petropoulos, B. Resan, K. Weingarten, T. Ellermeyer, J. Lutz, M. Möller, M. Huebner, J. Becker, C. Koos, W. Freude, J. Leuthold, "Single source optical OFDM transmitter and optical FFT receiver demonstrated at line rates of 5.4 and 10.8 Tbit/s," in *Proc. Opt. Fiber Commun. Conf./Nat. Fiber Opt. Eng. Conf. (OFC/NFOEC '08)*, San Diego, CA, 2008, paper PDP C1.
- [31] X. Liu, S. Chandrasekhar, B. Zhu, P. J. Winzer, A. H. Gnauck, D. W. Peckham, "448-Gb/s reduced-guard-interval CO-OFDM transmission over 2000 km of ultra-large-area fiber and five 80-GHz-grid ROADMs," in *J. Lightwave Technol.*, vol. 29, no. 4, pp. 483–490, Feb. 2011.
- [32] P. Frascella, C. Antony, S. J. Fabbri, F. C. G. Gunning, P. Gunning, W. McAuliffe, D. Cassidy, and A. D. Ellis, "Impact of Raman amplification on a 2-Tb/s coherent WDM system," in *IEEE Photon. Technol. Lett.*, vol. 23, no. 14, pp. 959–961, July 2011.
- [33] J.-X. Cai, C. R. Davidson, A. Lucero, H. Zhang, D. G. Foursa, O. V. Sinkin, W. W. Patterson, A. N. Pilipetskii, G. Mohs, N. S. Bergano, "20 Tbit/s transmission over 6860 km with sub-Nyquist channel spacing," in *J. Lightwave Technol.*, vol. 30, no. 4, pp. 651–657, Feb. 2012.
- [34] M. Birk, P. Gerard, R. Curto, L. E. Nelson, X. Zhou, and P. Magill, T. J. Schmidt, C. Malouin, B. Zhang, E. Ibragimov, S. Khatana, M. Glavanovic, R. Lo-and, R. Marcoccia, and R. Saunders, G. Nicholl, M. Nowell, and F. Forghieri, "Coherent 100 Gb/s PM-QPSK field trial," in *IEEE Commun. Mag.*, vol. 48, no. 7, pp. 52–60, July 2010.
- [35] G. Zhang, L. E. Nelson, Y. Pan, M. Birk, C. Skolnick, C. Rasmussen, M. Givach, B. Mikkelsen, T. Scherer, T. Downs, W. Keil, "3760km, 100G SSMF transmission over commercial terrestrial DWDM ROADM systems using SD-FEC," in *Proc. Opt. Fiber Commun. Conf./Nat. Fiber Opt. Eng. Conf. (OFC/NFOEC '12)*, Los Angeles, CA, 2012, paper PDP5D.4.
- [36] T. J. Xia, G. A. Wellbrock, Y.-K. Huang, E. Ip, M.-F. Huang, Y. Shao, T. Wang, Y. Aono, T. Tajima, S. Murakami, M. Cvijetic, "Field experiment with mixed-line-rate transmission (112-Gb/s, 450-Gb/s, and 1.15-Tb/s) over 3,560 km of installed fiber using filterless coherent receiver and EDFAs only," in *Proc. Opt. Fiber Commun. Conf./Nat. Fiber Opt. Eng. Conf. (OFC/NFOEC '11)*, Los Angeles, CA, 2011, paper PDP A3.
- [37] T. J. Xia, G. A. Wellbrock, Y.-K. Huang, M.-F. Huang, E. Ip, P. N. Ji, D. Qian, A. Tanaka, Y. Shao, T. Wang, Y. Aono, T. Tajima, "21.7 Tb/s field trial with 22 DP-8QAM/QPSK optical superchannels over 1,503-km of installed SSMF," in *Proc. Opt. Fiber Commun. Conf./Nat. Fiber Opt. Eng. Conf. (OFC/NFOEC '12)*, Los Angeles, CA, 2012, paper PDP5D.6.
- [38] R. Dischler, A. Klekamp, F. Buchali, W. Idler, E. Lach, A. Schippel, M. Schneiders, S. Vorbeck, R.-P. Braun, "Transmission of 3 × 253-Gb/s OFDM-superchannels over 764 km field deployed single mode fibers," in *Proc. Opt. Fiber Commun. Conf./Nat. Fiber Opt. Eng. Conf. (OFC/NFOEC '10)*, San Diego, CA, 2010, paper PDP D2.
- [39] N. Amaya, M. Irfan, G. Zervas, K. Banias, M. Garrich, I. Henning, D. Simeonidou, Y. Zhou, A. Lord, K. Smith, V. Rancano, S. Liu, P. Petropoulos, D. Richardson, "Gridless optical networking field trial: flexible spectrum switching, defragmentation and transport of 10G/40G/100G/555G over 620-km field fiber," in *Proc. Eur. Conf. Opt. Commun. (ECOC '10)*, Torino, Italy, 2010, paper Th.13. K.1.
- [40] J. Li, E. Tipsuwannakul, M. Karlsson, P. A. Andrekson, "Low-complexity duobinary signaling and detection for sensitivity improvement in Nyquist-WDM coherent system," in *Proc. Opt. Fiber Commun. Conf./Nat. Fiber Opt. Eng. Conf. (OFC/NFOEC '12)*, Los Angeles, CA, 2012, Paper OW3H.2.
- [41] Y.-K. Huang, E. Ip, T. J. Xia, G. A. Wellbrock, M.-F. Huang, Y. Aono, T. Tajima, and M. Cvijetic, "Mixed line-rate transmission (112-Gb/s, 450-Gb/s, and 1.15-Tb/s) over 3560 km of field-installed fiber with filterless coherent receiver," in *J. Lightwave Technol.*, vol. 30, no. 4, pp. 609–617, Feb. 2012.
- [42] J.-X. Cai, Y. Cai, C. R. Davidson, D. G. Foursa, A. J. Lucero, O. V. Sinkin, W. W. Patterson, A. N. Pilipetskii, G. Mohs, and N. S. Bergano, "Transmission of 96x100-Gb/s bandwidth-constrained PDM-RZ-QPSK channels with 300% spectral efficiency over 10610 km and 400% spectral efficiency over 4370 km," in *J. Lightwave Technol.*, vol. 29, no. 4, pp. 491–498, Feb. 2011.
- [43] J. Yu, X. Zhou, M. F. Huang, D. Qian, L. Xu, P. N. Ji, "Transmission of hybrid 112 and 44 Gb/s PolMux-QPSK in 25 GHz channel spacing over 1600 km SSMF employing digital coherent detection and EDFA-Only amplification," in *Proc. Opt. Fiber Commun. Conf./Nat. Fiber Opt. Eng. Conf. (OFC/NFOEC '09)*, San Diego, CA, 2009, paper OThR3.
- [44] C. Xie, G. Raybon, P. J. Winzer, "Transmission of mixed 224-Gb/s and 112-Gb/s PDM-QPSK at 50-GHz channel spacing over 1200-km dispersion-managed LEAF® spans and Three ROADMs," in *J. Lightwave Technol.*, vol. 30, no. 4, pp. 547–552, Feb. 2012.

- [45] J. Yu, Z. Dong, H.-C. Chien, Z. Jia, D. Huo, H. Yi, M. Li, Z. Ren, N. Lu, L. Xie, K. Liu, X. Zhang, Y. Xia, Y. Cai, M. Gunkel, P. Wagner, H. Mayer, A. Schippel, "Field trial Nyquist-WDM transmission of 8 × 216.8 Gb/s PDM-CSRZ-QPSK exceeding 4b/s/Hz spectral efficiency," in *Proc. Opt. Fiber Commun. Conf./Nat. Fiber Opt. Eng. Conf. (OFC/NFOEC '12)*, Los Angeles, CA, 2012, paper PDP5D.3.

Manuscript received: March 31, 2012

Biographies

Zhensheng Jia (zhensheng.jia@zteusa.com) received his BE and MSE degrees in physical electronics and optoelectronics from Tsinghua University, Beijing, in 1999 and 2002. He received his PhD degree from Georgia Institute of Technology, Atlanta, in 2002. From 2002 to 2004, he researched ultralong-haul optical links and backbone networks at China Telecom Beijing Research Institute. From 2008 to 2011, he was a senior research scientist at Telcordia Technologies and worked on the architecture of core optical networks and RF photonic signal processing. Currently, he works at the Optical Labs of ZTE USA and researches ultralong-haul optical transmission system and optical transport architecture. Dr. Jia has authored or co-authored more than 100 peer-reviewed journal articles and conference papers. He is an active reviewer for many technical publications. He was one a recipient of the 2007 IEEE/LEOS Graduate Students Fellowship Award and the 2008 PSC Bor-Jei Chen Memorial Scholarship Award. In 2011, he also received the Telcordia CEO Award.

Jianjun Yu received his PhD degree in electrical engineering from Beijing University of Posts and Telecommunications in 1999. From June 1999 to January 2001, he was an assistant research professor at the Research Center COM, Technical University of Denmark. From February 2001 to December 2002, he was a member of the technical staff at Lucent Technologies and Agere Systems, Murray Hill, NJ. He joined Georgia Institute of Technology in January 2003 as a research faculty member and director of the Optical Network Laboratory. From November 2005 to February 2010, he was a senior member of the technical staff at NEC Laboratories America, Princeton, NJ. He is currently the chief scientist on high-speed optical transmission and director of ZTE Optics Labs North America. He is a chair professor at Fudan University and adjunct professor and PhD supervisor at Georgia Institute of Technology, Beijing University of Posts and Telecommunications, and Hunan University. He has authored more than 200 papers for prestigious journals and conferences. Dr. Yu holds 11 US patents with 30 others pending. Dr. Yu is a fellow of the Optical Society of America. He is editor-in-chief of Recent Patents on Engineering and an associate editor for the Journal of Lightwave Technology and Journal of Optical Communications and Networking. Dr. Yu was a technical committee member at IEEE LEOS from 2005 to 2007 and a technical committee member of OFC from 2009 to 2011.

Hung-Chang Chien received his BSc and MSc degrees in electrical engineering from National Cheng Cheng University, Taiwan, in 1999 and 2001. He received his PhD degree in electro-optical engineering from National Chiao Tung University, Taiwan, in 2006. From 2007 to 2011, he was a research engineer in the School of Electrical and Computer Engineering, Georgia Institute of Technology, Atlanta. He is currently a senior member of technical staff at ZTE Optics Labs North America, Morristown, NJ. Dr. Chien has authored and co-authored more than 100 journal papers and conference proceedings. He holds one US patent with nine others pending in the fields of coherent DWDM optical transmission, microwave photonics, and passive optical networks.

Ze Dong received his BSc degree in electronic information science and technology from Hunan Normal University in 2006. He received his PhD degree in electrical engineering from Hunan University, China, in 2011. From 2010 to 2011, he was a visiting scholar at Georgia Institute of Technology. He is currently a postdoctoral fellow in the School of Electrical and Computer Engineering, Georgia Institute of Technology. His research interests include broadband optical communication and optical coherent communications. Dr. Dong has authored or co-authored more than 35 journal papers and conference proceedings in prestigious journals.

Di Huo has worked in telecommunications research and development for 20 years. He started with Mannesmann (Vodafone Arcor, Germany) and moved to Bell-Labs (Alcatel-Lucent, USA). He is now responsible for the forward-looking and international standard activities of ZTE. His research interests include physical layer (system, fiber, component), control plane (GMPLS), and network deployment (RSA, EON, field trials).

Open Augmented Reality Standards: Current Activities in Standards–Development Organizations

Christine Perey

(PEREY Research & Consulting, Route de Chermex 2B, 1820 Montreux, Switzerland)

Abstract

Augmented reality (AR) has emerged from research laboratories and is now being accepted in other domains as an attractive way of visualizing information. Before AR can be used in the mass market, there are a number of obstacles that need to be overcome. Several of these can be overcome by adopting open standards. A global grassroots community seeking open, interoperable AR content and experiences began to take shape in early 2010. This community is working collaboratively to reduce the barriers to the flow of data from content provider to AR end user. Standards development organizations and industry groups that provide open interfaces for AR meet regularly to provide updates, identify complementary work, and seek harmonization. The community also identifies deployer and implementer needs, communicates requirements, and discusses emerging challenges that could be resolved with standards. In this article, we describe current activities in international standards–development organizations. We summarize the AR standards gap analysis and shed light on special considerations for using standards in mobile AR.

Keywords

augmented reality, standards, open interfaces, AR reference model

work harder to define and protect their unique contributions to the AR ecosystem. In most markets, standards emerge once a sufficient number of organizations see market and business value in interoperating with the solutions or services of others. Standards frequently provide a shared platform for technology and market development. They ensure the smooth running of an ecosystem, in which different segments contribute to and benefit from the success of the whole, and they are commonly the basis for robust, economically viable value chains. Widespread adoption of standards throughout the AR ecosystem will ensure interoperability between traditional and emerging content–creation and management systems. It will also increase the variety and amount of data available for use in AR–enhanced end–user experiences.

At the time of writing of this article, interoperable, open–standards–based AR content creation and management platforms do not exist. Applications for experiencing AR using standards–compliant interfaces and protocols also do not exist. This is not to say that there has been no change in the AR ecosystem over the past year or that there has been a lack of progress towards open–standards–based AR experiences.

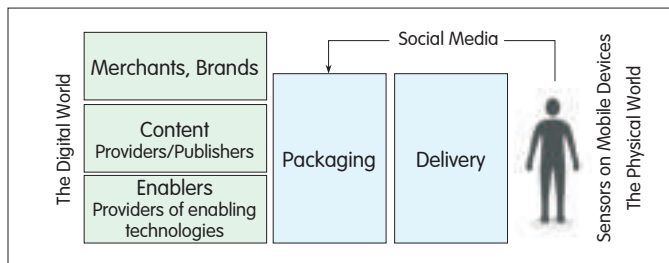
Over the past year, the number of single–vendor technology “silos” (technology that is closed and managed by a single vendor) has increased, and the challenge of publishing once for use across fragmented markets has grown more complex. At the same time, an increasing number of important industry groups and standards–development organizations (SDOs) have begun working on new, open frameworks and extensions of existing standards in which AR is the primary use case or one of the most important use cases. Finally, the number of users with AR–compatible devices has also increased, making the need for standards more clearly to participants in the ecosystem who seek to reach the mass market.

In 2012, there has been widespread interest in and increasing requests for standards–compliant AR solutions. Content publishers that can provide high–value AR experiences are motivated to make their data available to users of various devices that are connected to all types of networks or that are not connected at all. By adapting the assets used by many terminals, and by adapting content delivery options, publishers can monetize content for different

1 Introduction

Since late 2008, augmented reality (AR) has rapidly gone from being a topic of research and pilot projects to being a promising new way of providing value to almost any user scenario that involves the physical world and digital data. By providing digital information in real time and in tight association with the user’s physical surroundings, AR enhances the experience of “the present” for pleasure, learning, and professional goals.

As technologies mature and solutions for producing and experiencing the world with AR proliferate, companies must



▲ Figure 1. Ecosystem of mobile AR Segments.

use cases across substantially larger markets. This maximizes the audience size and potential revenue. Adoption of standards also reduces implementation costs and mitigates investment risks by making devices and use cases independent. By the beginning of 2013, leading technology providers will respond to these needs by introducing interfaces that comply with open standards and by introducing applications that provide AR experiences based on content authored in or delivered by platforms of competitors or partners.

2 Guiding Principles of an Open AR Industry

Open AR—interoperable systems for viewing content overlaid on the physical world in real time—is necessary for the continued evolution of the AR market. There are numerous standards that can be used to develop and deploy open AR; however, there are still interoperability gaps in the AR value chain. Work needs to be done on determining best practices for using existing international standards to build and deliver AR. Where there are interoperability gaps, new standards are being or need to be defined, documented, and tested. Pushing new standards through the development process of a standards organization may not suit the needs of the AR community, and profiles of existing standards may be more appropriate. Further, the development of a framework of standards for designing, building, and delivering AR is beyond the resources of any single body. Because AR requires the convergence of so many technologies, there are numerous interoperability challenges, and there will be no universal AR standard. Instead, AR will leverage hardware and software based on a suite of standards.

Many developers of AR technology seek to leverage existing standards that solve different interoperability issues. In order to address new issues raised by AR, we must extend standards that have been proven and optimized to permit applications to learn user locations, display objects on the screen, timestamp every frame of a video, and use inputs to manage behaviors.

One of the strongest motivations for cross-standard, multiconsortium, open discussions about standards and AR is time-to-market. Repurposing existing content and applications is critical. Existing standards (or profiles of standards) are used to avoid making mistakes, and currently deployed and proven technologies, including emerging

technologies, should be used to address urgent issues for AR publishers, developers, and users.

However, the time-to-market argument is only valid if most or all members of the ecosystem agree that having open AR, the opposite of technology silos, is a good thing. It is evident from the participation of academic and institutional researchers, companies of all sizes, and industry consortia representing technology groups, that there is agreement across many parts of the AR ecosystem about the need for standards [1].

2.1 Suggested Model of a General AR Ecosystem

The AR ecosystem comprises at least six interlocking, interdependent groups of technologies. Fig. 1 shows how these groups bridge the space between the digital and physical worlds.

On the far right of Fig. 1, there is the client device in the end-to-end system. The user holds or wears the client, which provides an interface for interacting with one or more services or applications in the digital world. The device also incorporates an array of real-time sensors, such as cameras, pressure sensors, or microphones. The sensors in the device detect the surrounding environment and, in some cases, also the user's input. There may also be sensors in the environment that could be accessed via the application. The client device is also the output for the user, permitting visualization or other forms of augmentation, such as sounds or haptic feedback.

Manufacturers of components and AR-capable devices such as smartphones may be present in both the client segment of the ecosystem as well as the enabler segment at the far left of Fig. 1. At the right side, client devices are frequently tightly connected to the networks.

Network providers, application store providers, government and commercial portals, social networks, spatial data infrastructures, and geo-location service providers provide the discovery and delivery channel by which the user experiences AR. This segment, like the device segment, overlaps with other segments so that companies may be content providers as well as device manufacturers.

Packaging companies provide tools and services that permit viewing of any published and accessible content. In this segment, there are subsegments such as AR SDK and toolkit providers, Web-hosted content platforms, and content developers who provide professional services to agencies, brands, and merchants.

Packaging companies provide technologies and services to organizations that have content suitable for context-driven visualization. Unlike other segments in the AR ecosystem, which existed prior to AR becoming possible on consumer devices, this segment is new. It developed rapidly between 2008 and the end of 2011. In this segment, there is the greatest number of proprietary AR solutions. The packaging segment must adapt rapidly in the near future because open-standard interfaces will be incorporated into client software, including the device operating systems, and will be used by content providers.

Packaging companies sometimes rely on providers of enabling technologies (Fig. 1). As with the packaging segment, there are subsegments of the enabler segment. These subsegments include semiconductor, sensor, and algorithm providers. The enabler segment is rich in existing standards that are being assimilated by the packaging segment companies.

Content providers have public, proprietary, and user–provided data. Traditionally, proprietary content was the primary content used in AR. More recently, content such as traffic data and base maps has been provided by government agencies, and content such as Open Street Map has been provided by volunteer sources. An excellent example of the evolution from proprietary to mixed–content platform is map data used in AR.

Traditional content providers, brands, and merchants seeking to provide digital information to users of AR–enabled devices were previously reluctant to enter the AR ecosystem because investment in a proprietary solution for a small audience was seen as a dead end. Two trends are stimulating content providers to examine AR more closely. First, companies have begun to realize that a dedicated application, such as an application for trying on glasses, gives real value to users and increases their engagement with a brand. This, in turn, increases sales. AR is now seen as a good investment for understanding end–user behavior and as a good investment for being perceived as forward–looking company. Second, in 2013, content providers will be looking carefully at how widely standards have been adopted for content encoding and for providing platforms and packaging companies with access to content. Content providers are waiting for this clear indication of market maturity. Standard interfaces and encoding will also allow content providers to access content from many more sources, including proprietary, user–provided, and government sources.

Content providers and those who experience AR will benefit when AR content standards are available to present the source content in a consistent and high–quality manner.

3 AR Requirements and Use Cases

For the proper development of AR standards, there needs to be a very clear understanding of AR requirements and use cases. Different domains have different AR requirements; for example, mass–market mobile AR used in tourism has different requirements from AR used by first responders in emergencies. However, analyses have been done to identify the most common requirements. By specifying use cases and requirements, standards organizations are beginning to obtain information about which standards are best for given situations or workflows. Given that different AR segments have different needs for standards, there are a number of different standards bodies and industry consortia that have been working on different aspects of the AR standards stack. Stronger collaboration between these bodies is required. By holding open, face–to–face meetings between parties such as AR DevCamps and the International AR Standards

Community, people from vastly different backgrounds are convening to exchange and share information about their successes and how these may be used to overcome challenges in interoperable and open AR. Having a common set of use cases and related requirements provides a lingua–franca for collaboration and discussion.

Collaboration between SDOs and their related expert communities is crucial at this juncture in the growth of AR. If we can benefit from the experience of those who have written, implemented, and optimized today’s most popular standards for AR–like applications such as OpenGL ES, JSON, HTML5, KML, GML, City GML, and X3D, the goal of interoperable AR will be more quickly achieved and many costly errors may be avoided.

In discussions on standards, it is generally agreed that developing standards specifically for AR applications is only necessary in a small number of cases. Instead, repurposing (creating profiles) and better understanding standards that have already been developed by organizations such as the Khronos Group, Web3D Consortium, World Wide Web Consortium (W3C), Open Geospatial Consortium (OGC), ETSI 3GPP, Open Mobile Alliance (OMA), National Information Standards Organization (NISO), British Information Standards Organization (BISO), and Society for Information Display (SID) will ensure the greatest impact, largest markets, and most stable systems in the future.

3.1 Requirements of AR Content Publishers

Publishers who produce and deploy AR content are extremely varied. They include multinational media conglomerates, device manufacturers, governments at all levels, users themselves, and individual content developers who wish to share their personal trivia or experiences. Publisher subsegments have needs that align with their specialized markets or use cases. Broadly speaking, a content publisher seeks to

- reach the maximum audience with the same content
- provide content in formats that are suited to special–use cases (also called repurposing)
- provide accurate, up–to–date content
- control access, for example, to billing, and limit pirating.

Content publishers desire a simple, lightweight mark–up language that is easily integrated into existing content–management systems and that attracts a large community of developers who will customize the content. Extending or creating profiles of the NISO information standards could be very useful; however, this has yet to be. Standards that specify the relationship between AR–ready content and KML could also be very useful. In 2011, members of the OGC, which is responsible for keyhole mark–up language (KML), initiated extensions to KML and ARML 2.0. This could be highly relevant to the content–provider segment.

3.2 Requirements of the Packaging Segment

This is the segment of the AR ecosystem in which proprietary technology silos are most evident and where control of content–development platforms is highly

competitive. The needs of providers of tools and platforms are significantly different from (and should be differentiated from) those of professional service providers, who use tools to gain their livelihoods.

Tools and platform providers seek to

- access and process content from distributed repositories and sensor networks. This may include repackaging for efficiency. However, for content such as maps or location content, the ability to access the content closest to the source gives the end user the latest, best quality.
- offer their tools and platforms to a large (preferably existing) community of developers who develop commercial solutions for customers
- integrate and fuse real-time sensor observations into the AR application
- quickly develop and bring to market new, innovative features that make their system more desirable than a competitor's or a free solution.

Professional developers of content are service providers who use the SDKs and platforms for publishing. They seek to

- make AR versions of (repurpose) existing tools and content. This helps manage costs and promote learning curves.
- provide end users with rich experiences that leverage an AR platform but, at the same time, have features that tie users to existing platforms for social networking, communications, navigation, content administration, and billing.

The packaging segment has a central role in designing and preparing AR experiences for end users. They also have a central role in the eventual propagation of open-standards-based tools and will be sensitive to and impacted by the development of standards in SDOs. Activities relevant to AR in OGC, W3C, Web3D Consortium, SID, Khronos Group, and OMA should proceed with strong input from this segment.

3.3 Discovery and Delivery Segment Requirements

Companies that provide connectivity (access and transport) between AR platforms and end-user devices have previously been defined as the “discovery and delivery” segment of the AR ecosystem. This segment provides value to ubiquitous AR experiences by ensuring that users can promptly and securely access the content necessary for AR. It also ensures that statistics about AR experiences are systematically and accurately captured.

Those in the delivery segment seek to

- receive and transmit requests from user devices to subscribe to/unsubscribe from AR experiences. These requests are processed according to the user's context, for example, location and detection of marker, in a manner that is scalable, reliable, and flexible to local network conditions.
- suspend and resume (hold/unhold) AR sessions in a way that makes optimal use of communications infrastructure
- access, cache, retrieve, and distribute content (assets) for use in AR experiences in a way that makes optimal use of distributed, low-cost resources
- adapt the AR content delivery to the capabilities of the

user device.

The OMA is working on a definition of the MobAR Enabler. In conjunction with W3C, OGC and other SDOs, they are taking into account the requirements of the delivery segment in the AR ecosystem [2].

3.4 AR System and Content Users

This is the most diverse segment in the AR ecosystem. Users include all people, related services, and organizations involved in future scenarios. It is natural that users of AR systems and content want to have experiences that leverage the latest technologies and the best, most up-to-date content without losing any of the benefits they have grown accustomed to.

Regardless of the use case or final objectives, end users seek to

- request and receive content in the context of their surroundings and in tight association with local points of interest. This may involve the use of filters, formats, and resolutions suited to the user's device and connectivity.
- receive content in AR view from multiple sources as part of a single, integrated AR experience
- rate and give feedback to the publisher about content
- create personal media and associate it with the real world (“social” AR).

In addition, the OMA has stated that end users should be able to

- personalize AR settings according to their preferences
- permit or prevent the collection of end-user metrics by AR content and system providers
- use AR in conjunction with reliable, secure billing mechanisms that are directly linked to the subscriber's account.

4 Approaches to the Challenge of AR Standards

To meet the needs of developers, content publishers, platform and tool providers, network operators, device providers, and users of the AR ecosystem, experts in hardware-accelerated graphics, imaging and computing, cloud computing and Web services, digital data formats, navigation, sensors, geospatial content and services management, and hardware and software devices must collaborate.

4.1 Basic Tools of the Standards Trade

Standards that are useful to AR segments leverage the know-how that is gained from creation of and experimentation with open-source, commercial and precommercial implementations. The process of recommending standardization usually begins with the development of a core set of requirements and use cases. This work is then followed by the establishment of a vocabulary (terms and definitions), information models, and abstract architectures. Principle objectives must also be agreed upon.

The results of one or more gap analyses, combined with known or emerging ecosystem requirements, reveal where the community should concentrate their standardization efforts. Guided by these directions, new standards work done by existing standards organizations can begin to fill the gaps and support AR experiences.

4.2 Standards Gap Analysis

A gap analysis begins with detailed examination of available standards in order to determine which standards are close to meeting AR ecosystem requirements and which are not. Gap analysis began as a community–driven activity involving developers and providers of tools and content. It began in October 2010 at the International AR Standards Meeting in Seoul and continued throughout 2011 and into the first half of 2012.

In gap analysis, problems are divided into those related to content and software and those related to infrastructure, such as device hardware and networks. The following describes the gap analysis to date.

5 Content–Related Standards

5.1 Declarative and Imperative Approaches to Content Encoding

First, for a gap analysis to succeed, it is important to clarify differences between the declarative and imperative approaches used in standards to describe and deliver content.

The imperative approach usually defines how something is computed; for example, it may define the code. Such definitions may cover storage, variables, states, instructions, and flow control. The imperative approach usually benefits from many options and user–centered variations. Imperative code can be designed in any manner as long as it conforms to the common rules of the interpreting background system. A typical example is JavaScript, which is a highly popular implementation of the ECMA Script (ECMA–262) language standard and a part of every Web browser on a mobile or desktop today.

Declarative approaches are more restrictive, and their design usually follows a strict behavior scheme and structure. They consist of implicit operational semantics that are transparent in their references and describe what is computed. Declarative approaches usually do not deliver states; thus, it is more difficult to create a dynamic system using a declarative approach. On the other hand, declarative approaches tend to be more transparent and easy to generate and use. A common declarative language in use today is the W3C XML standard, which defines a hierarchical presentation of elements and attributes. Another coding form for declarative data is JavaScript Object Notation (JSON), which is a lightweight, easy–to–port data interchange format. It builds on the ECMA Script specification.

Both approaches, either individually or in combination, are likely to be used to create AR content encoding and payload

standards.

5.2 Existing Standards

There are many standards related to content or payload encoding that could be used for AR applications. Fig. 2 shows an initial inventory of these standards and their possible relationships.

At the time of this analysis, there are at least ten mature standards based on geo–information system (GIS). These standards could be used in AR services and applications that rely on the user’s location. There are also another five to six ratified and widely adopted international standards that define the position and interactivity of digital objects in a user’s visual space.

5.3 New Standards Activities

In addition to the numerous existing standards, at least two new AR–specific standards are being developed.

The W3C Points of Interest Working Group is drafting the first version of the POI specification. The POI draft specification has been completed, will be voted on in late 2012, and is estimated to be available in early 2013. It will provide a simple data model for describing a POI that includes but is not limited to

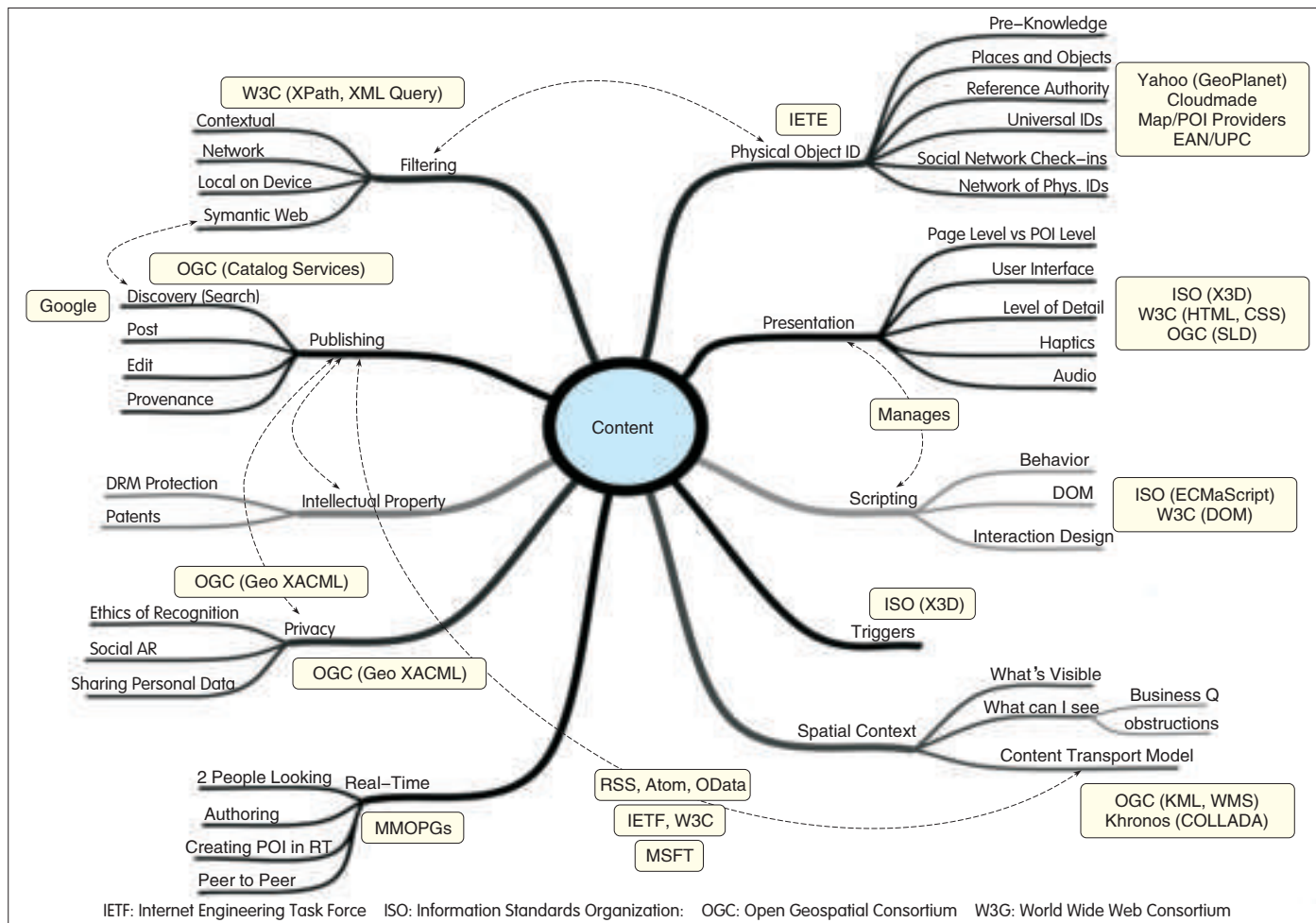
- an anchor
- an extent
- a URI
- a category
- an address.

In September 2011, the OGC ARML 2.0 Working Group began examining and harmonizing different approaches to using extensions or profiles of KML to create AR experiences. The charter of the ARML WG is to provide an open–standards approach to using KLM to encode the placement and interactivity of a digital object. The group’s work is advancing and results may be available for testing in late 2012.

5.4 Gap Analysis and Work in Progress

The gap analysis suggested in section 4.2 has been performed by the International AR Standards Community. The analysis revealed four very important issues in content–related standards:

- Terminology and architectural frameworks related to content (AR in particular) are not consistent across SDOs. This makes comparing standards, conducting ongoing activities, and using standards for open AR very difficult.
- There are multiple description systems for 3D that could be appropriate for AR, and these must be examined for suitability. Some of the existing 3D standards may be extended to describe AR experiences involving 3D objects.
- A suitable encoding standard for 3D object transmission is needed for many applications. This could be developed with minimal new investment, and it could be based on existing standards.
- An appropriate set of standards for indoor positioning and navigation are lacking. This is significantly hampering the development of certain AR use cases that require positioning



▲ Figure 2. Standards landscape and effect on mobile AR.

of the user both indoors and outdoors.

To address the first of these issues, the International AR Standards Community has begun to develop the Augmented Reality Reference Model to describe AR from perspectives defined by the ISO/IEC 10746 standard for reference models.

To address the second of these issues, the Declarative 3D Community Group of the W3C has begun holding meetings. It will discuss approaches with members of other WGs in the W3C as well as members of the Khronos Group, ISO/JTC1 SC 29 WG 11, and Web3D Consortium.

To address the third of these issues, the Khronos Group, Web 3D Consortium, and ISO/IEC JTC 1 SC 29 WG 11 (MPEG) began a dialog in December 2011. In March 2012, at the AR Standards Community meeting in Austin, TX, they drafted a joint proposal for development. Work on a new 3D compression and transmission standard is underway in a cross-SDO working group established through a series of liaison memorandums for this purpose. The subject of indoor positioning and navigation has begun to be discussed in standards groups. In January 2012, the OGC board approved the formation of the Indoor GML Standards Working Group, which conducted its first meeting in Austin, TX, in March 2012.

Further development of a middleware API for abstracting between the positioning technology and depiction of indoor spaces will be very valuable to the AR development community.

6 Considerations for Mobile AR Standards

Many promising technologies have been developed and integrated into mobile device hardware. New sensor technologies allow data for mobile AR applications to be delivered in a format that can be processed. The processing power of mobile devices has increased exponentially in recent years, as has network and memory bandwidth to support the latest mobile devices and applications. Software frameworks and platforms for mobile application development have also advanced greatly, permitting developers to create new user experiences very quickly. This creates huge potential for context- and location-aware AR experiences or applications to be extended to take advantage of new capabilities.

Although these developments have accelerated growth in the number and diversity of mobile AR-ready devices, this

growth has come at a cost. There are numerous standards available, but they are not well adapted for mobile platforms or use in AR. New work needs to be done to implement lighter profiles of these existing standards for use in mobile AR experiences so that content is delivered consistently across multiple, different platforms and in different use scenarios.

6.1 Mobile AR and Sensors

A sensor outputs information about an observed property. It uses a combination of physical, chemical, or biological means to estimate the underlying observed property. A sensor observes external phenomena and represents it with an identifier or description, usually in the form of an estimated value. Satellites, cameras, seismographs, water temperature and flow monitors, and accelerometers are examples of sensors. Sensors may be in-situ, such as those in an air pollution monitoring station, or they may be dynamic, such as a camera in an unmanned aerial vehicle. The sensor detects a property at a specific point in time and at a specific location, that is, within a temporal and spatial context. Further, the location of the sensor might be different from the location of the observed property. This is the case for all remote-observing sensors, such as cameras or radar.

From a mobile AR perspective, sensors may be in the device (onboard) or outside the device (external) and may be accessed by the AR application as required. Regardless, all sensors have descriptions of the processes by which observations and measurements are generated. They also have other related metadata, such as quality, time of last calibration, and time of measurement. Metadata, or characteristics, are critical for developers and applications that require sensor observations. A standard language for describing a sensor, its metadata, and processes will allow for greater flexibility and ease of implementation when accessing and using sensor observations in AR applications.

Sensors behave differently in different devices and platforms. Even when the same phenomenon is observed, dynamic (mobile) sensor observations may be inconsistent because of differences in manufacturing tolerances or measurement processes. Calculating a user's indoor location is one example where wide variation may occur. Different location-measurement technologies provide different levels of accuracy and quality. Inconsistency is exacerbated by factors such as interference from other devices and materials in the building.

Approaches that use computer-vision algorithms to improve the accuracy of geo-positioning data in mobile AR are promising. However, these approaches require new models for recognition, sensor-fusion, and pose reconstruction to be defined. Ideally, an abstraction layer that defines these different "sensor services" with a well-defined format and sensor characteristics would address existing performance limitations.

For some AR applications, real-time processing of vision data is crucial. In these cases, raw camera data cannot be processed in a high-level programming environment and should be processed on a lower level. When processing is

done at a lower level, algorithms that create an abstracted sensor-data layer for pose are beneficial.

Sensors with different processing needs can contribute to the final AR experience. At the same time, higher-level application logic may benefit by taking data from multiple sensors into account. Standards may provide direct access to sensor data or higher-level semantic abstractions of it.

A critical source of content for many AR experiences, regardless of domain, will be near-real-time observations from in-situ and dynamic sensors. In-situ sensors are used as traffic, weather, fixed video, and stream gauges. Dynamic sensors are used in unmanned aerial vehicles, mobile human contexts, and satellites. Already, some content used in AR is obtained via sensor technology, such as LIDAR. This content is processed and stored in a content management system. There are many other sources of sensor data that are, or will be, available on demand or by subscription. These sensor observations need to be fused into the AR environment in real time as well. There is a need for standards that enable the description, discovery, access, and tasking of sensors within the user's environment so that these sensors can be included in AR experiences.

6.2 Mobile AR Processing Standards

Considerable work has previously been done on standards for situational awareness, sensor fusion, and service workflows. This is a large field in which many existing standards are suitable for use by AR developers and content publishers. Some of these standards can be applied to processes in an AR workflow. For example, the OGC Web Processing Service provides rules for standardizing inputs and outputs (requests and responses) for geospatial processing services, such as polygon overlay. The standard also defines how a client can request the execution of a process and how the output of the process is handled.

Other approaches to describing vision-based tracking environments with visual (camera) constraints were first taken by Pustka et al., who introduced spatial relationship patterns for AR environment descriptions [3].

There are several standards that could be used for the presentation and visualization workflow stack for AR experiences. An AR-enabled application can use a service interface to access content such as a map. There are also lower-level standards for rendering content on the device.

Not all AR requires use of 3D. In some cases, especially in devices with low-power processors that cannot render 3D objects, 2D annotations are preferable. A very convenient declarative standard for describing 2D annotation is W3C's scalable vector graphic (SVG) standard or even HTML.

6.3 Mobile AR Acceleration and Presentation Standards

Augmented reality is highly demanding in terms of computation and graphics performance. Truly compelling AR on mobile devices requires advanced computation and graphics capabilities in today's smartphones.

Many mobile AR applications make direct and/or indirect use of hardware to accelerate computationally complex tasks.

Because device hardware varies, standard application programming interfaces (APIs) reduce the need to customize software for specific hardware platforms.

The Khronos Group is an industry standards body that defines open APIs that enable software to access high–performance silicon for graphics, imaging, and computation. A typical AR system with 3D graphics uses several Khronos standards and some that are under development.

6.4 Using HTML5 for a Universal Mobile AR Viewer

All smartphones and most other mobile devices have a Web browser. Many already support elements of the HTML5 standard, and the trend towards full HTML 5 support will continue. HTML5 is a very clear and simple option for AR developers. Within a Web browser, JavaScript allows access to the document object model (DOM) so that declarative elements can be observed, created, manipulated, and removed. An option for standardizing AR could be integrating declarative standards and data directly into the DOM.

X3Dom is a complete 3D renderer that uses JavaScript. It is built on WebGL, a JavaScript interface for encapsulating OpenGL ES 2. X3Dom is completely independent of the mobile platform on which the application runs. This does not imply that an output solution, such as X3Dom, is all that is needed to make a universal viewer for AR. A convenient interface extension for distributed access to real–time processed, concrete, or distributed sensor data is required.

7 Conclusions and Future Directions

In the creation of AR experiences, disciplines such as computer vision recognition and tracking, geospatial, and 3D converge. Algorithms for computer vision and sensor fusion are provided by researchers and software engineers, or they are provided as third–party services. Content for presentation and application logic is likely to be created by experienced designers. In this paper, we have discussed standards that can be used for interoperable and open AR. We have discussed issues in AR standards development and the use of international standards in AR applications and related services. We have identified the different standards bodies and players in different fields that already supply standards that are highly relevant to AR.

Although extending and using existing standards is highly beneficial to the objectives of the AR community, there must also be room for new ideas and evolving technologies. Therefore, standardization meetings such as International Standards Community meetings have been held to find the best interconnection and synergies between SDOs.

These standards coordination meetings enable all players in the AR ecosystem to discuss requirements, use cases, and issues and also establish focused working groups to address specific issues in AR standardization. This approach enhances AR standardization in specialized fields.

In the future, technologies will be able to filter reality to allow a user to see things differently. This implies that a person can

view a scene from different positions without having to move. Perspective and context are maintained in order to expose or diminish other elements in the scene. Work in this area will help maintain privacy, especially in collaborative applications, or help users focus their attention on the main task in the context.

Applying existing standards (or their extensions) for AR on the sensor side in mobile devices requires more research, specifically, on the delivery of improved context for fixed objects. Processing moving objects in the scene and processing variable light conditions also needs to be improved. Such improvements involve both hardware and software and are being researched in many laboratories.

These potential AR improvements and use cases require deep interoperability and integration of sensors so that data can be properly acquired and presented. AR improvements also require enhanced use of advanced silicon for imaging, video, graphics, and computational acceleration and must operate at battery–friendly power levels. AR will benefit greatly from the emergence of interoperable standards in divergent domains.

Acknowledgements

This article is an adaptation of “Current Status of Standards for Augmented Reality,” a chapter co–authored by Christine Perey and published by Springer in *Mobile collaborative augmented reality: Recent trends* (ISBN 978–1–4419–9844–6, pp.19–34). The author wishes to thank Neil Trevett (NVIDIA), Timo Engelke (Fraunhofer IGD), and George Percivall and Carl Reed (OGC) for their continued support and contributions to the international AR standards community.

References

- [1] This conclusion is based on the results of discussions at four meetings of the International AR Standards Community. [Online] Available: <http://www.arstandards.org>.
- [2] *Mobile Augmented Reality Enabler*. Open Mobile Alliance specification OMA–ER–MobAR–V1_0–20111017–D, Draft v.1.0, Oct. 2011. [Online]. Available: http://member.openmobilealliance.org/ftp/Public_documents/cd/Permanent_documents/
- [3] D. Pustka, M. Huber, M. Bauer, G. Klinker, “Spatial Relationship Patterns: Elements of Reusable Tracking and Calibration Systems,” in *Proc. 5th IEEE/ACM Int. Symp. Mixed and Augmented Reality (ISMAR 06)*, Santa Barbara, CA, pp. 88–97.

Manuscript received: December 29, 2011

Biography

Christine Perey (cperey@perey.com) is a Spine Wrangler and evangelist for augmented reality and the Internet of Things. She has 20 years experience in new multimedia communications markets and technologies. She received her BSc from Colorado State University in 1979. From 1991–1993, she worked in the technology industry as the publisher and editor of the QuickTime Forum and was the founder of the QuickTime Movie Festival. She was invited to speak at mobile industry events and serves on committees dedicated to the advancement of rich media experiences in business and consumer markets. Perey is engaged in market development work and regularly prepares custom research reports for clients. She organizes a variety of technology industry meetings and communities, including the International AR Standards Community <http://www.arstandards.org>. Perey chairs face–to–face meetings and leads programs to drive the adoption of open and interoperable AR.

Mobile Cloud for Personalized Any-Media Services

Bhumip Khasnabish

(Standards Development and Industry Relations, ZTE USA Inc., Morristown, NJ, 07960, USA)

Abstract

In this paper, we define mobile cloud computing and describe how it can be used for delivering advanced any-media services to both nomadic and mobile users. We focus on service delivery that is localized and personalized and suggest that virtualization and tighter cross-layer communication allows for convergence and seamless transition of services. These are also creating new and never-before seen ways of developing and delivering personalized any-media services. We discuss current paradigms for implementing cloud-based any-media services that generate revenue. Future research topics and requirements for evolving network and service elements are also discussed.

Keywords

mobile cloud; virtualization; cross-layer communications; any-media service; personalized services; localized services

1 Cloud Computing and Networking

Achieving better quality, cheaper, and faster any-media communication is not a dream anymore. Virtualization and tight cross-layer communication means any computing or communication solution can be established and used on demand. The beauty of this approach is that no significant capex¹ or opex² is incurred.

In cloud computing, there is no need to develop and own physical infrastructure because virtualized computing and communications elements such as virtual machines (computer systems) and network elements can be rented from a cloud service provider. This can be done through

¹ Capex is the capital expenditure associated with acquiring fixed assets such as computing equipment, equipment rooms and real estate, networks, and plants. These are necessary infrastructure for running a business.

² Opex is the operational expenditure of a business. This is the amount of money spent on running costs such as salaries and benefits; maintenance of systems, network, and equipment; and upgrades.

³ A data center is a collection of computing, communications, storage, application, and service resources that can be offered to internal and external customers through open APIs. Data centers are commonly installed on racks in a building with raised floors. They may also be stored in a secure trailer that has adequate communication bandwidth, ventilation, and power supply.

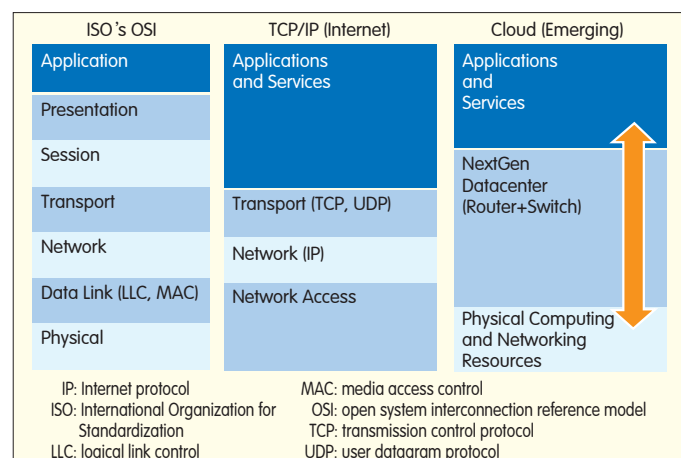
open-network application programming interfaces (APIs) or service APIs as long as the data centers³ of the cloud service provider can be accessed over the Internet. Further details about cloud-based systems and services can be found in [1]–[3].

With cloud computing, virtualization can be used to develop next-generation any-media services [4]. Cloud networks can deliver these services to nomadic or mobile users through virtualization and tight cross-layer communications [4].

A nomadic user moves from one location to another, but their device is in a fixed location. Therefore, they may be serviced by a different data center at a different time. When a service or session is initiated, it is hosted in the same data center for the duration of the session until the location changes.

A mobile user moves with their device from one location to another without service interruption. Consequently, a mobile user may initiate a session or service in one data center and then move to a neighboring data center during the same session. This is commonly done with a service handover or stitched session through specialized border gateways.

Increasingly, data-center network elements are capable of converting traditional four-layer TCP/IP Internet into a three-layer data-center network (Fig. 1). These data-center network elements support virtualized routing and switching, which allows traditional network and transport-layer functions to be mixed and matched. In this way, virtual machines can be seamlessly moved from one rack to another (distant) rack.

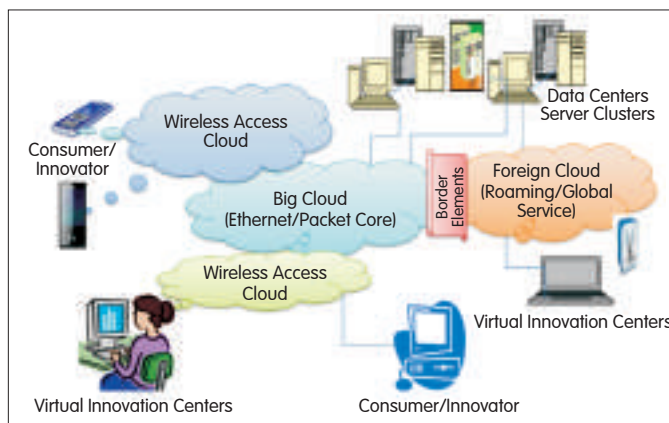


▲ Figure 1. Evolution of computer networking model, from seven-layer to three-layer system.

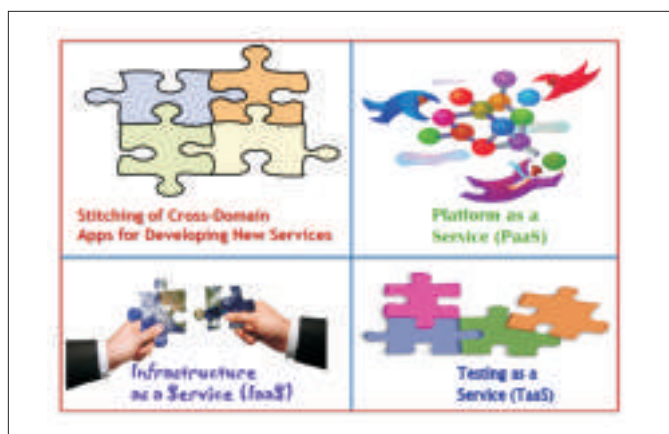
▼ Table 1. Emerging networking and service paradigms. Cloud computing and networking supports the emerging paradigm.

Existing	Emerging
Large- and mass-scale, broadcast, triple- and quad-play services	Personalized, mobile, any-media services
Long-term, well-thought-out, stable services	Short-term, 'try before you buy', continuously evolving services
Months of planning; weeks of development, testing, integration, and refinement	Weeks of planning, development, testing, integration, and refinement
Strategic planning and execution for long-term success	Strategic steering for survival
Pre-standard or standard implementations	Continuous innovation and customization of standards

Load balancing and service continuity can be achieved at minimal cost. Table 1 shows emerging networking and services paradigms. Cloud computing and networking supports the emerging paradigm. Fig. 2 shows the new network model. This is expected to be where seamless innovation in applications and services will occur. Fig. 3 shows how the cloud-based ecosystem will be used for continuous development of services. Creating cloud-based services is similar to piecing together a puzzle together; one best solution always exists.



▲ Figure 2. The new network is a playground for seamless innovation.



▲ Figure 3. An ecosystem for continuous development and innovation.

Cloud computing, networking, and service management (including grid computing) have recently emerged as viable computing and networking tools. These tools can be used to reduce infrastructure deployment and service management costs without sacrificing QoS and QoE [5].

At the heart of cloud computing is virtualized computing and networking resources. The self-organizing nature of the interconnections between these resources is similar to neural networks in the human brain.

However, the methods, mechanisms, and tools used to expose resources and their APIs for the purpose of developing XaaS are still ad-hoc and proprietary. Security, privacy, and multitenancy requirements add another dimension to the already-complex set of cloud management problems.

2 Why Mobile Cloud is Different

Mobile cloud refers to seamless delivery of cloud-based applications and services to clients with mobile or nomadic devices. With innovative mash-up of data, interface, service, and content as well as normalization of APIs, mobile cloud can seamlessly deliver real-time session and transaction-oriented services.

Mobile cloud delivers services from Internet and social networking platforms to clients. Such platforms include Google, Yahoo, Microsoft/Skype, and Facebook. Traditional and virtual network service providers such as AT&T, British Telecom, China Telecom, Deutsche Telekom, and France Telecom-Orange can offer these services.

Media-based sessions and calling-in to share virtual space will become commonplace. Dynamic sharing of computing, communications, and display resources between hand-held devices and networked servers will give rise to user experience beyond expectations. This trend will be equally applicable to the ICT and entertainment industries [4]–[6]. Mobile cloud is a new service-delivery paradigm currently being fleshed out at industry events and summits [7].

3 The Potential of Mobile Cloud

Mobile cloud is the best way of providing personalized services. Gathering information from mobile clients, devices, and ecosystems and effectively using this information to provide necessary, low-cost, customized services is a winning proposal. Policies can be steered in real-time, and gathered data can be micromined for charging purposes. This provides localized intelligence and allows services to be rapidly customized. Providing accurate, personalized real-time recommendations and assistance through any-media devices will strengthen customer loyalty and improve UE.

4 A Sample of Modern Mobile Cloud Services

This section gives a summary of emerging mobile cloud

services. Both transaction- and session-oriented services are discussed.

4.1 Personalized Spam Filter for SMS

In addition to keywords and flow rate, individual preferences can be the basis for dynamically setting and modifying spam filters. These filters can be based on personal profile, location, quality, or connection bandwidth. These services use micro data-mining as well as mini databases with virtual agents embedded in mobile clients.

4.2 On-demand Security for Transaction and Session

Mobile devices and clients are inherently vulnerable to impersonation and security threats. Mobile cloud immediately detects any impersonation or attack and mitigates these by allowing suitable agents to be embedded in mobile devices. An acceptable level of security during a transaction or session can be maintained by an independent, localized, trusted third-party platform.

4.3 Automated and Personalized Emergency Service

This service can be delivered through an embedded, local authorized proxy server. With appropriate agents and customer profiles, a mobile device can provide various personalized emergency services. Authenticating the mobile device and determining exact location are very important for such services, and mobile cloud is best suited for this purpose.

4.4 Automated Mobile Device Portability

This implies that hand-held clients and devices are seamlessly portable between carriers. No hardware—for example, SIM cards—need to be changed. The goal is to support dynamic provisioning and activation of devices and services. Also, billing and settlement for interservice providers can occur almost in real-time through intelligent service delivery.

5 Emerging Personalized Mobile Cloud Services

5.1 Mobile Transaction and Streaming Media Ecosystem

Mobile cloud can be used in health, banking, games, and entertainment where culture and location are important factors. For example, the McDonald's menu in Bangalore is different to that in Boston. A ubiquitous mobile service within a device may be able to sense location and act on behalf of the user if it is programmed to do so. Wearable devices can communicate with mobile devices so that important health and environment information can be relayed to a central location and assistance can be organized.

5.2 Services that Require Dynamic Creation and Restructuring of User Groups

A mobile cloud network can be used for vehicular communications and entertainment. It can also be used for

health monitoring.

5.3 Mobile Cloud that Offers Context-Aware Media Adaptation and Communications

This service can be used for energy saving, signaling, and processing in display and bandwidth management. QoE is not sacrificed; however, a broker or proxy agent may be needed to ensure QoE.

5.4 Instant Access to Up-to-Date Information Using Mobile Cloud

Database information, such as profile and personal information, automatically migrate from the home cloud to the user's current location. Secure and efficient mechanisms are needed to move personal databases and caches from one location to another in order to provide the same UE. Maintaining privacy and data integrity is of the utmost importance.

5.5 Cloud-Broker-Based Ubiquitous Access to Any-Media Services

Any-media services are delivered to devices anywhere in the world. Both private and public mobile cloud domains may be used for delivering services. To successfully deliver services, mobile devices must be capable of dynamically adjusting the required service and security profiles according to the service and the openness of the domain from where the resources are being borrowed.

5.6 Any-Media Content Downloading From Anywhere

Movies, video clips, and e-books are downloaded to a device from anywhere in the world, irrespective of the service or network access provider.

5.7 Location-Based Real-Time Maps and Traffic Update

This service is very similar to a navigation service provided over a mobile device. However, the device uses information about current location and personal habits and preferences to recommend direction-related services.

5.8 Seamless Tracking of Goods and Services

Goods can be seamlessly tracked throughout the transportation cycle.

5.9 Network-based Assisted Living

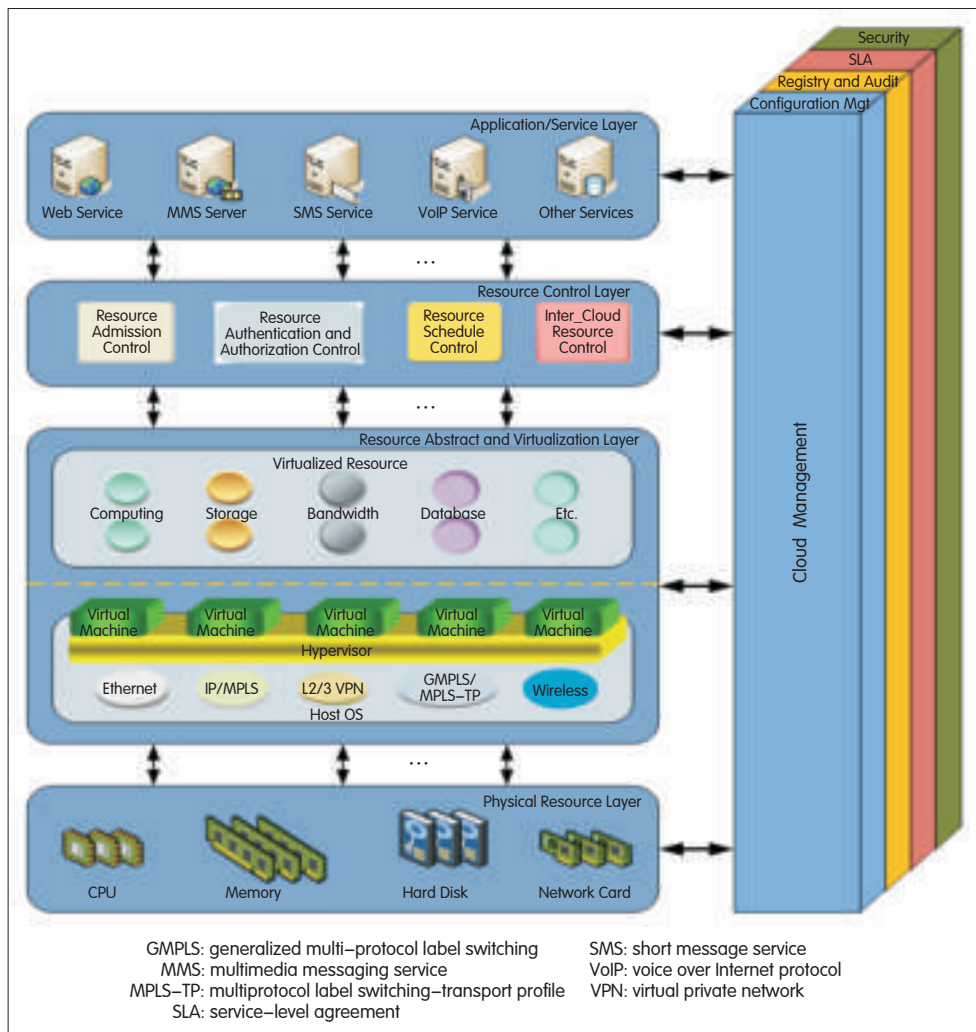
The mobile device intelligently and adaptively monitors the health requirements and location of the person carrying the device. It is sensitive to the requirements of the carrier and should support their computing and communications needs.

5.10 Location-Aware Mobile Wallet

This is equivalent to a near-field electronic-wallet service except that electronic cash is automatically converted to local currency through a banking service proxy.

5.11 Media Adaptation for Any-Media Cloud Services

Mobile cloud services often deliver audio, video, and



▲ Figure 4. Main elements of a CRF.

graphics to a variety of devices. The media may be encoded in a format that cannot be rendered or displayed on the device. Therefore, virtualized resource-based transcoding may be required for any-media-based services.

5.12 Virtualization of Clients and Services

Mobile cloud services sometimes require features and functions that are not easy to implement on the handset. Using virtualization and other embeddable features, it is possible to instantiate (emulate) advanced features and functions required by the service [8], [9]. These features may include 3D image viewing or multiparty video gaming.

5.13 Platforms for Mobile Cloud Services

Some platforms for mobile cloud services support virtualization and seamless mobility of virtual resources. These resources can be mobilized (according to specified arrangements) from one domain to another irrespective of physical location or ownership. Mobility can be triggered by proximity of the client, device, or user. It can also be triggered

by malfunctioning or overload of the service delivery platform (SDP) [6].

5.14 Incorporating Intelligence in Mobile Cloud Clients and Platforms

Using virtualization, intelligence can be incorporated into both mobile devices and platforms. A cloud-based mobile device can dynamically invoke cloud-host-based features to provide enriched audio, video, and gaming. Similarly, mobile SDPs can support normalization of APIs and invoke resources needed for enhancing UE on demand.

5.15 Innovative Business Models Using Mobile Clouds

Virtualization-enabled clients, SDPs, and associated components provide the agility and flexibility needed for innovation in the mobile cloud ecosystem.

6 A Cloud Reference Framework

The cloud reference framework (CRF) consists of four horizontal layers and one stacked vertical layer (Fig. 4). The four horizontal layers are 1) application/service layer, 2) resource control layer, 3)

resource abstraction and virtualization layer, and 4) physical resources layer. The stacked vertical layer is used for configuration management, registry, logging and auditing, security management, and service-level agreement (SLA) management. The CRF can be used to install cloud-based services (Fig. 5). It can also be used to describe the virtual resource management (VRM) (Fig. 6). Details about this CRF and its application can be found in [10].

7 Converging IT and Networking Services

Although there are specialized devices for voice, data, and video, device capabilities are converging rapidly. Traditionally, cell phones were only used for voice, but these devices are increasingly being used for email, SMS, IM, and streaming Internet radio and TV.

Such mentioned demands are the driving force behind convergence. Converged applications include map, picture, RBT, and video search. They also include e-ticket purchasing and mobile payment, bookings, banking, SMS-based

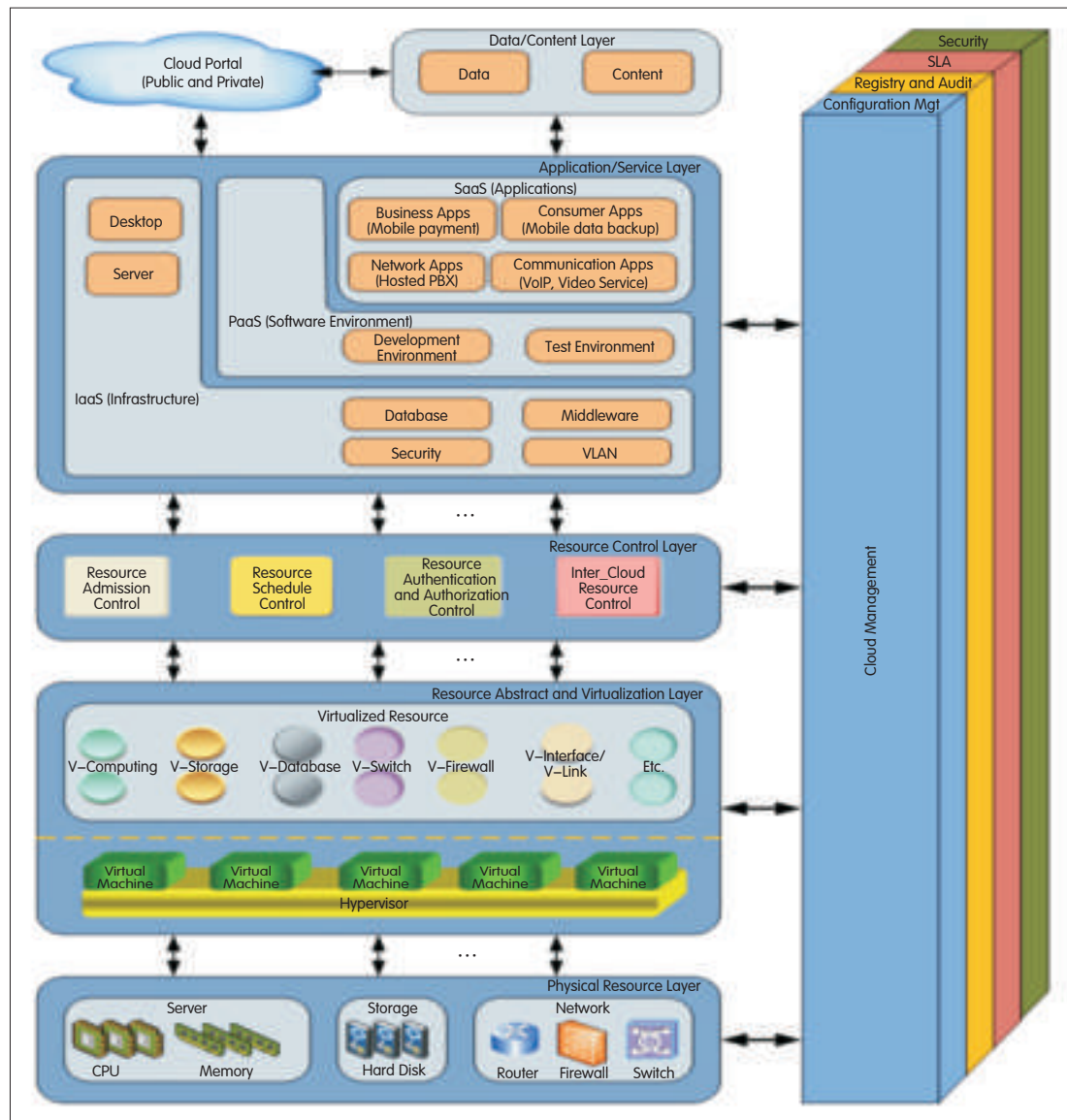
weather forecast, hospital registering, calendar reminders, mobile stock trading, and marketplace recommendations. Converged applications will cause an explosion in the number of devices that can support rich-media services and content over the mobile Internet.

Although such devices will have different sizes, shapes, and forms, they may run on the same operating system and virtual clients but have different features and functions. These features and functions may change many times throughout a day based on the applications and services they are supporting.

Fig. 8(a) shows how three-dimensional images and augmented-reality-based services can be delivered to the same hand-held device using network-based capability to a virtual client. Fig. 8(b) shows how adding, moving, changing, and updating can be easily facilitated

when a virtual client is available in a hand-held device. Further details on virtualized clients and their use in a cloud environment can be found in [8], [9], [11], and [12].

Telecom and IT operators (including ISPs and content delivery companies) are able to benefit from the new paradigm of convergence when delivering rich-media services with cloud-based infrastructures (as shown in Fig. 9). Hand-held device manufacturers need to support virtualized clients and cognitive access to networks and services (as shown in Fig. 2). Wireline and wireless telecom operators must support cognitive access to content and services regardless of the home network where the device originally registered for the service. This may require service-specific, policy-based interconnection with foreign networks and cloud data centers for the duration of a session. Privacy and security of everyone involved must not be



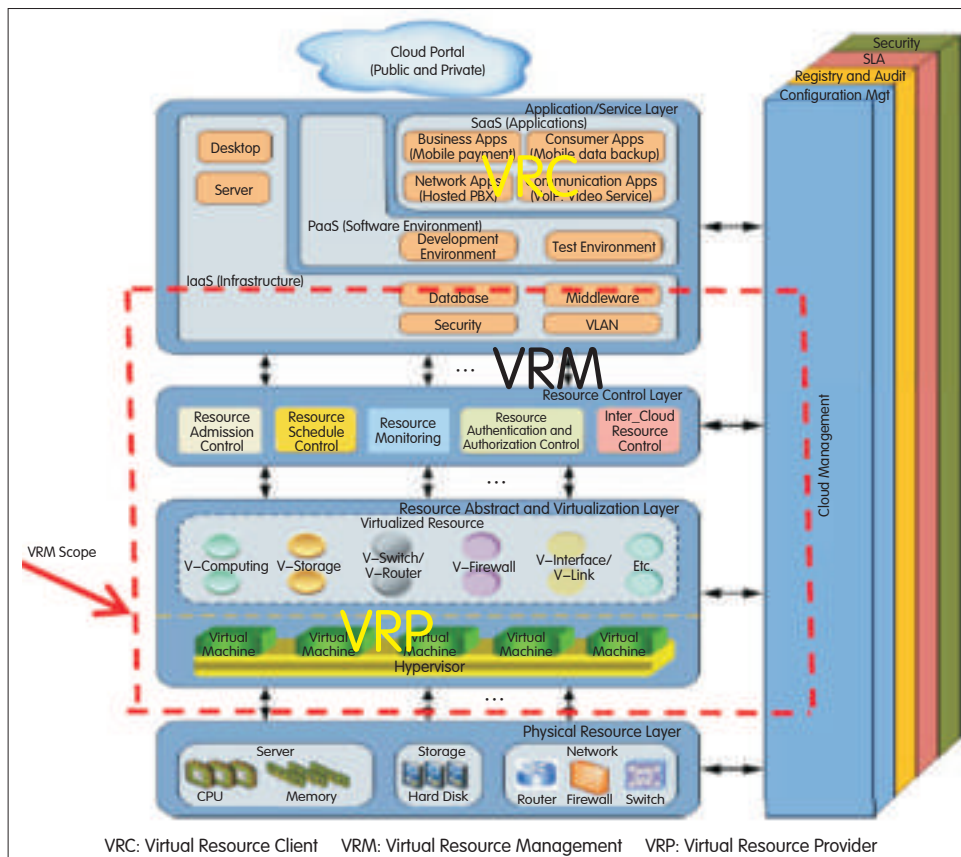
▲ Figure 5. CRF for describing service instantiation.

compromised.

8 Role of the Service Development Platform

Although devices come in the form of televisions, laptops, tablets, or mobile phones, they may use similar virtual clients with application-specific features and functions. The service may be hosted through an SDP to a service-specific application store

Application developers, however, want to develop applications for use in all devices and platforms. Therefore, a toolkit is needed that can provide an appropriate level of normalization and customization. Fig. 11 shows one such model. Unified network APIs, such as Parlay X and OMA RESTful, are desirable. Application and service developers also want seamless access to important information about



▲ Figure 6. CRF for VRM.

subscribers and users, for example, a verifiable address, location, and age. They also want identification, billing, and charging information about the subscribed service. Subscriber and service information can be used for unified messaging and session control, service discovery and delivery, and seamless migration of service from device to device as the user moves. Fig. 11 shows how developers can use open web-based APIs for customizing standard services offered by various service providers [4], [5], [13], and [14].

9 SDP and Cloud Storage Creates an Intelligent Application Store

SDP alone cannot seamlessly deliver all of desired applications and services across different access networks and devices. A variety of gateways, interconnecting devices, storage, and business process development and maintenance elements are required (Fig. 12).

Fig. 12 shows a business strategy and processes. Policy-based network operation and management needs to be implemented in order to generate direct and indirect revenue from mobile app stores.

These can be coupled with an interconnected multidomain service overlay network so that services can be dynamically created using service components from different domains. This coupling also allows for dynamic allocation of computing,

networking, and service resources across wired, wireless, private, and public domains to create unified and seamless UE. These resources can be offered by intelligent applications and service stores (Fig. 13), and this is what self-organizing and cloud-based systems (SOCS) and networks are expected to deliver [6], [14]. SOCS networks can also dynamically reconfigure networked platforms and devices in order to deliver customer-desired content and services with required security and QoS, irrespective of the location and ownership of the content and features.

An innovative business model needs high-quality and agile partners as well as excellent system and service integration. It also needs to be based on standard platforms that can be rapidly customized so that content and services from any provider can be abundantly and consistently supplied [6], [14].

10 Conclusion and Future Research Topics

Mobile cloud is about to transform the ICT and entertainment industries and create the ultimate UE. The effect of this transformation will be that device and equipment manufacturers, application and service developers, system integrators, and network and service operators will have to adapt rapidly to new business models. An infrastructure business model based on CAPEX and OPEX will disappear as will the line between wired and wireless services. Sharing of content, infrastructure, applications, and other resources will be widespread. Commoditization will trigger innovation in business models, services, and devices and will enable anyone with a broadband-capable device to provide any

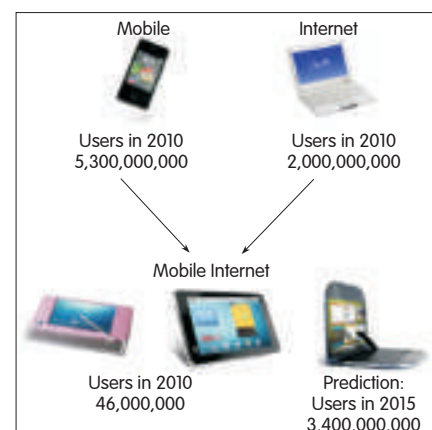
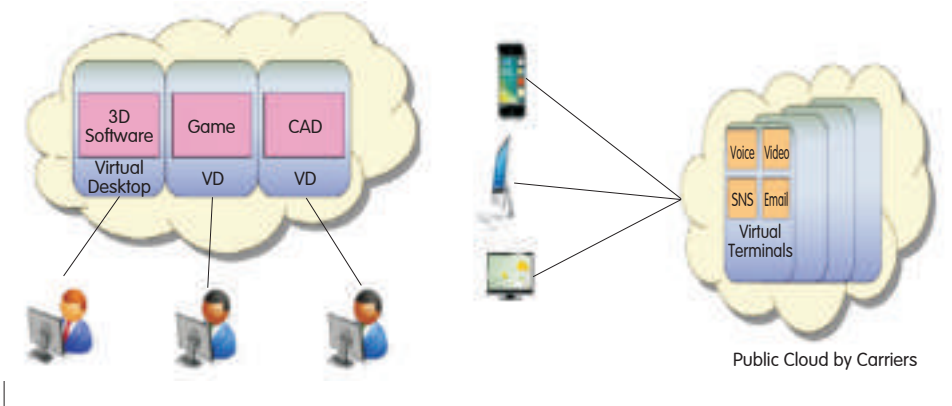
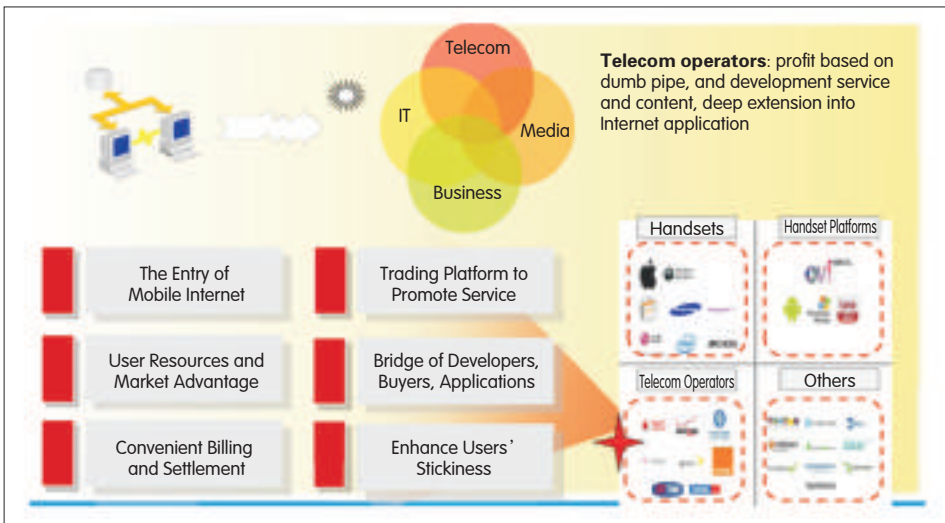


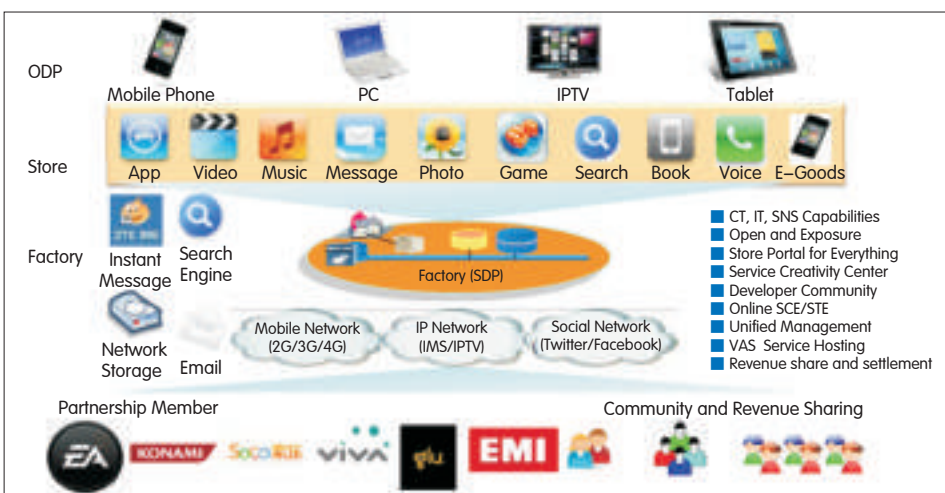
Figure 7. ▶ Market potential for mobile Internet devices and services will be enormous in the near future.



▲ Figure 8. Examples of XaaS. (a) 3D game, augmented reality, or CAD software as a service based on virtual desktop infrastructure. (b) Terminal hosting for seamless access to services using any device from anywhere (seamless add, move, change, and update).



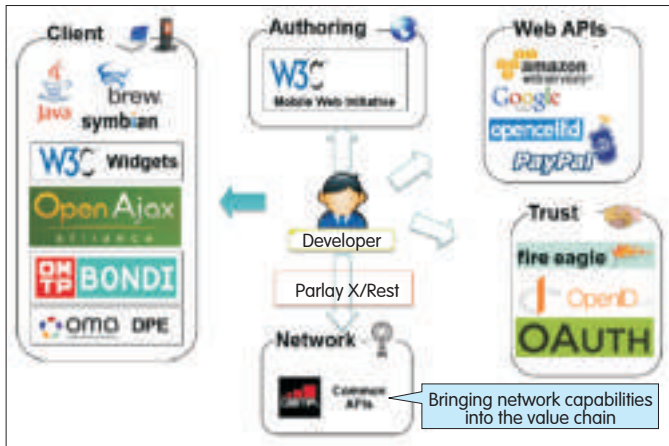
▲ Figure 9. Industry convergence and competition between telecommunications, IT, and media, companies.



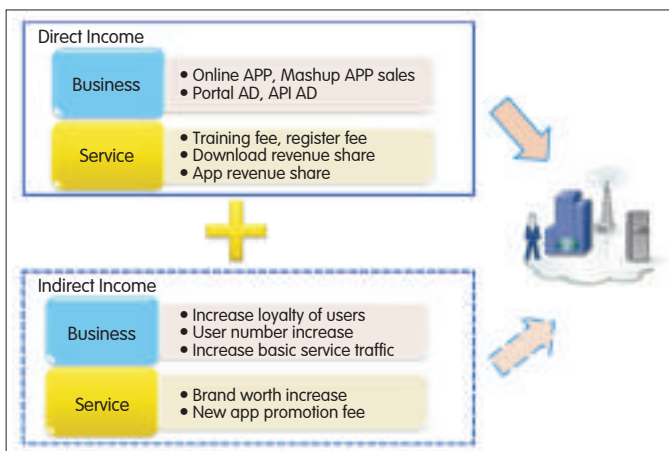
▲ Figure 10. SDP and application store is a "factory behind store" model.

service to anyone, irrespective of location. However, the following issues need to be addressed before this can become a reality:

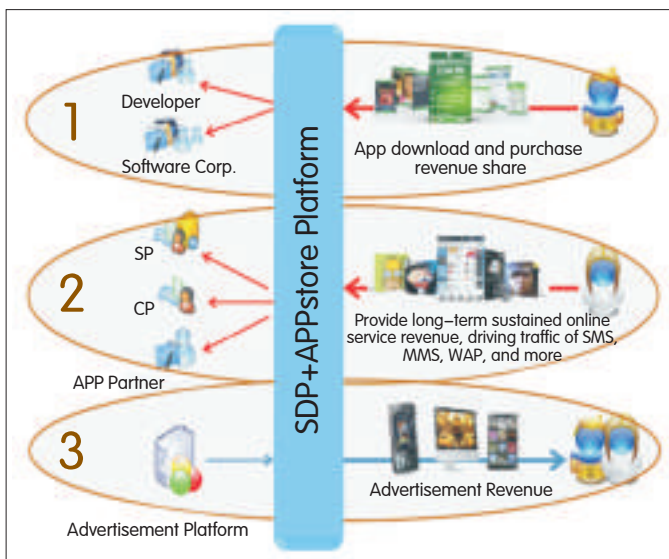
- virtualization of clients, desktops, applications, services, and databases for delivering customized UE for any service (convergence is the objective)
- mobility management in cloud, that is, in distributed shared network and resource environments
- APIs for developing and delivering services seamlessly over public, private, and hybrid mobile clouds (including support for single sign-on, unification of profiles, and service mash-ups)
- development of agile mobile cloud ecosystems
- visualization and dynamic provision of computing and communications resources, including automatic debugging and diagnosis
- cloud service logging and monitoring, including auditing and verification
- soft and hard privacy and security for cloud-based services
- privacy protection and on-demand security in open networked environments
- service continuity, automated software and hardware updates, and disaster recovery
- affordable and useful services, environmentally friendly evolution of networks and services
- regulatory compliance in a borderless world
- instant detection of violation of intellectual property rights
- protection of intellectual property rights
- policy management in a mobile cloud environment
- adaptive protocols for resources and service management in multidomain mobile cloud environments
- service- and content-specific addressability, networking extensions, service quality and experience agreement (SQEA)
- risk-tolerance, risk-sharing, and mean-time to failure and repair management for mobile clouds



▲ Figure 11. Developers want to develop an application once only for ubiquitous deployment. This requires unified network APIs such as Parlay X, and OMA RESTful interfaces.



▲ Figure 12. Business plus service constitutes a profit model.



▲ Figure 13. SDP with an intelligent application store is an innovative business model.

- mobile cloud service and infrastructure management
- Additional details about these and related topics can be found in [10].

Acknowledgements

This paper is based on my Distinguished Lecture on XaaS given at IEEE Region 1 Innovation Day (May 17, 2011). An earlier version of this paper was also presented at CommunicAsia 2011 during the mobile VAS strategy session on 22 June, 2011. I am grateful to the ZTE iVAS Product and Marketing Team for helping me put the slides together for the presentation. In particular, Meng Yu, Hu Jie, Chu JunSheng and Liang Liang have provided many contributions and drafts that have assisted me in my work with standards development organizations in the areas of virtualization, data center operation, and general clouds. I sincerely thank all of them.

References

- [1] IETF. *App area wiki* [Online]. Available: <http://trac.tools.ietf.org/area/app/trac/wiki/Clouds>
- [2] eWeek. *Cloud computing* [Online]. Available: <http://www.eWeek.com/c/b/Cloud-Computing>
- [3] NIST. *NIST Cloud Computing Program* [Online]. Available: <http://www.nist.gov/ftl/cloud/>
- [4] B. Khasnabish, "XaaS: The Next Frontier of Innovation in Communications," presented at IEEE Region 1 Innovation Day 2011, New York, May 2011. [Online]. Available: ewh.ieee.org/reg1/innovation_day/presentations/bhumip.pdf
- [5] D. Liu, B. Khasnabish, and H. Guanghua, "Cloud Edge Services," in *Proc. Broadband Forum 2011*, Berlin, May 2011, paper bbf2011.505.00.
- [6] B. Khasnabish, "Intelligent Application Stores: An Innovative Business Model," presented at CommunicAsia, Marina Bay Sands, Singapore, June 2011.
- [7] Jeffrey Peel. *Mobile Cloud Summit* [Online]. Available: <http://mobilecloudsummit.com/>
- [8] J. Wang, S. Ma, and L. Liang (Jan. 2011). *Virtual Desktop Infrastructure Problem Statement*. IETF. [Online]. Available: <http://www.ietf.org/draft-wang-appsawg-vdi-problem-statement-01.txt>
- [9] B. Khasnabish and D. Stiliadis (Editors) (Jul. 2011). *Cloud Services Virtual Desktop Requirements*. [Online] Available: http://www.atis.org/cloud/_Com/Docs/issue018.doc
- [10] B. Khasnabish et al. (Dec. 2011) *Cloud Reference Framework*. IETF. [Online] Available: <http://tools.ietf.org/draft-khasnabish-cloud-reference-framework-02.txt>
- [11] J. Chu, B. Khasnabish, Q. Yu, and Y. Meng (Jul. 2011). *Virtual Resource Management in Cloud*. IETF Operations & Management Area Working Group. [Online]. Available: <http://tools.ietf.org/draft-junsheng-opsawg-virtual-resource-management-00.txt>
- [12] S. Karavettil, B. Khasnabish, N. So, and W. Dong (Dec. 2011). *Security Framework for Virtualized Data Center Services*. IETF Operations & Management Area Working Group. [Online] Available: <http://tools.ietf.org/draft-karavettil-vdcs-security-framework-03.txt>
- [13] NGSON Working Group of the IEEE Standards Committee (May 2008). IEEE P1903™/D1 Draft White Paper for Next Generation Service Overlay Network. [Online]. Available: http://grouper.ieee.org/groups/ngson/P1903_2008_0026-White_Paper.pdf
- [14] T. Plevyak and V. Sahin, *Next Generation Telecommunications Networks, Services, and Management*. New York: John Wiley-IEEE Press, 2010.

Manuscript received: December 5, 2011

Biography

Bhumip Khasnabish (b.khasnabish@ieee.org), PhD, AMCPM, is a senior member of the IEEE and an emeritus distinguished lecturer of the IEEE Communications Society. He has initiated cloud and data center activities in the IETF and is co-chair of ATIS IPTV Interoperability Forum (IIF). He is currently a senior director in the Standards Development and Industry Relations Division, ZTE USA. His research interests include next-generation networking, platform and services that use virtualized computing and communication entities, and tighter cross-layer communications. He has worked in the Verizon/GTE next-generation laboratories, Waltham, MA, and in Bell-Northern Research (BNR) Ltd. in Ottawa, Canada. Dr. Khasnabish has published numerous articles, books, and book chapters and has been awarded several patents in his research areas.

Multiple-Constraint-Aware RWA Algorithms Based on a Comprehensive Evaluation Model: Use in Wavelength-Switched Optical Networks

Hui Yang¹, Yongli Zhao¹, Shanguo Huang¹,
Daijiang Wang², Xuping Cao², and Xuefeng Lin²

(1. State Key Laboratory of Information Photonics and Optical Communications, Beijing University of Posts and Telecommunications, Beijing 100876, China;
2. ZTE Corporation, Shenzhen 518057, China)

Abstract

Because of explosive growth in Internet traffic and high complexity of heterogeneous networks, improving the routing and wavelength assignment (RWA) algorithm in underlying optical networks has become very important. Where there are multiple links between different the node pairs, a traditional wavelength-assignment algorithm may be invalid for a wavelength-switched optical networks (WSON) that has directional blocking constraints. Also, impairments in network nodes and subsequent degradation of optical signals may cause modulation failure in the optical network. In this paper, we propose an RWA algorithm based on a novel evaluation model for a WSON that has multiple constraints. The algorithm includes comprehensive evaluation model (CEM) and directional blocking constraint RWA based on CEM (DB-RWA). Diverse constraints are abstracted into various constraint conditions in order to better assign routing and wavelength. We propose using the novel CEM to optimize routing according to an assessed value of constraints on transmission performance. This eliminates the effects of physical transmission impairments in a WSON. DB-RWA based on CEM abstracts directional blocking conditions in multiple links between network nodes into directional blocking constraints. It also satisfies rigorous network specifications and provides flexibility, scalability, and first-fit rate for the backbone, especially in multiple links between WSON nodes.

Keywords

RWA; WSON; multiple links between nodes pair; directional blocking constraint; comprehensive evaluation model

1 Introduction

The Internet has become a critical piece of infrastructure in modern societies, and explosive growth in the number of Internet users has given rise to a corresponding explosion in Internet traffic. Over time, data packets have become the main type of traffic being transmitted over networks. An optical network carries not only fixed-bandwidth voice services but also variable-bandwidth services, mobile services, and multimedia services. Optical networks must support grid computing, file downloading, video-on-demand, storage-area networks, and other new applications. Meanwhile, demand is growing for capacity, responsiveness, resilience, quality, and different types of services. Underlying optical networks are ultrahigh-capacity, large-scale platforms that support synchronous optical network and synchronous digital hierarchy (SONET/SDH), multiprotocol label-switching transport profile (MPLS-TP), and optical transport network (OTN) for transporting data at different granularities. In large-scale commercial applications, wavelength-switched optical networks (WSONs) must satisfy the needs of network service providers, who face strong pressure to increase availability, improve reliability, and reduce bandwidth cost.

Nodes in a WSON—unlike nodes in other types of generalized multiprotocol label-switching (GMPLS) networks—are highly asymmetric in their switching capabilities, and compatibility of signal types and network components needs to be considered. Label assignment can also be nonlocal [1]. In a WSON, wavelength continuity and resource availability constraints must be satisfied in order to determine optimal and cost-effective optical connections (paths) [1]. Such determining of paths is referred to as routing and wavelength assignment (RWA).

To design a new WSON for complex contexts, multiple constraint conditions need to be applied to the evaluation model and RWA algorithms. For redundancy and reliability in optical networks, most network operators place multiple optical fibers between the network nodes, especially in the

backbone network or main part of an access or metro network. Therefore, application scenarios based on multiple links between network nodes have become the focus of attention of network operators. Traditionally, RWA algorithms have been used for only one link between network nodes; however, such algorithms are invalid for routing between different links and nodes [2].

Because there are impairments of varying degrees in a large-scale optical network, degradation can cause unacceptable bit error rates or even a complete failure to detect and demodulate the received signal. Therefore, optical impairments need to be taken into account in an RWA algorithm so that signals with acceptable quality can be propagated in the WSON.

Many studies have been done on quality of transmission (QoT) compensation as well as impairment-aware routing and wavelength assignment (IA-RWA) [3]–[5] based on path computation element (PCE) strategies and extended resource reservation protocol (RSVP) [6]. Many traditional RWA algorithms have been studied only in one link field [7], [8]. When there are multiple links between the network nodes, few traditional RWA algorithms can successfully compute the optimal path, and few have been evaluated in terms of impairment assessment model [9].

In this paper, we describe a novel RWA algorithm based on a model for assessing multiple constraints in a WSON. The algorithm comprises a comprehensive evaluation model (CEM) and directional blocking RWA based on the CEM (DB-RWA). Diverse scenarios are abstracted into various constraint conditions so that routing and wavelength can be better assigned. We propose a novel CEM that optimizes routing based on a value derived from an assessment of constraints on transmission performance. The algorithm eliminates the effects of impairments in WSON transmission.

Directional blocking conditions are abstracted by DB-RWA based on CEM in multiple links between the network nodes into directional blocking constraints that satisfy the rigorous network specifications. DB-RWA based on CEM provides scalability and flexibility for the backbone, especially in multiple links between WSON nodes.

2 Comprehensive Evaluation Model

When an optical signal is being transmitted in a fiber link and is passing through an optical device or cell, physical impairments—such as reduced signal strength; triggering noise; or changing time domain, frequency domain, or polarization properties—are ineluctable. Especially in a transparent or translucent light network, which lacks photoelectric regenerators, the effects of impairments accumulate as the optical signal is transmitted. When an impairment threshold is exceeded, quality of transmission is seriously affected. Transmission impairments can be linear or nonlinear. The effects of linear impairments of every wavelength are independent, and the effects of nonlinear impairments are not independent. An IV module is used to estimate the transmission quality of the chosen wavelength

path so that the path meets QoT requirements [10]–[12].

Currently, the evaluation model most widely used is a multitarget constraint evaluation model. In this model, constraints are considered individually, and a light path is only eligible when it satisfies the thresholds for each target constraint. However, because this model ignores the interaction of factors, the estimation may be highly inaccurate.

In a comprehensive evaluation model, physical impairment is reflected in the error rate, which reflects a variety of impairments. This model uses a simulation and analytical fitting method to comprehensively evaluate physical impairments. It also uses bit error rate (BER) as a constraint when evaluating the QoT of a light path. Tolerance security reserve can be obtained from the BER.

A comprehensive evaluation model takes into account the interaction of physical impairments. It requires much calculation; the model is complex; and much information is acquired. However, the accuracy of the evaluation is greatly improved. A general way of implementing the model is through analytical and experimental simulation (fitting). By transforming the physical impairment into a BER, we can measure the quality of light transmission.

2.1 Sketch of Evaluation Model

BER is a key parameter for assessing systems that transmit digital data. BER is used to assess the full end-to-end performance of a system that includes transmitter, receiver, and the medium in-between. BER allows the performance of a whole system in operation to be tested, which differs from testing individual component parts and hoping that they will operate satisfactorily when in place. The BER is the rate at which errors occur in a transmission system. This can be directly translated into the number of errors that occur in a string of bits. According to the principle of Gaussian noise distribution, Q -factor corresponds to BER. By evaluating Q -factor, the quality of a transmission system can be estimated. Q -factor is given by

$$Q = g(\phi_{nl}, D_{res}, PMD) + \zeta(\phi_{nl}, D_{res}) OSNR \quad (1)$$

Where $g()$ is the accumulated cost of each kind of impairment in the transmission, and $\zeta()$ is the model effect caused by individual impairments such as dispersion, cross-phase modulation (XPM), and four-wave mixing (FWM). In normal circumstances, $\zeta() = 1$ when amplified spontaneous emission (ASE) noise plays a main role. As nonlinear effects increase, $\zeta()$ decreases below 1. This formula for evaluating transmission quality takes into account each kind of physical impairment, including residual dispersion, nonlinear phase shift, ASE noise, and polarization mode dispersion (PMD) [13]–[15]. The Q -factor cost of each physical impairment can be obtained by a semianalytical method in order to obtain the total performance index.

$OSNR_{ref}$ is the reference of the optical signal-to-noise ratio (obtained by experiment) when the BER requirement is met, that is, when $Q = Q_{ref}$. The reference $OSNR_{ref}$ is a function of physical impairments, including residual dispersion, nonlinear phase shift, PMD, and crosstalk. The Q function can be $\bullet N$

written as

$$Q = [OSNR - OSNR_{ref}(\phi_{nl}, D_{res}, PMD)]\zeta(\phi_{nl}, D_{res}) + Q_{ref} \quad (2)$$

We may assume that $OSNR_{BIB}$ is the OSNR when achieving Q_{ref} in the back-to-back configuration. The Q -factor cost, taking into account various transmission impairments, is

$$Pen_{Qref}(\phi_{nl}, D_{res}, PMD) = [OSNR_{Qref}(\phi_{nl}, D_{res}, PMD) - OSNR_{BIB}] \quad (3)$$

Then, the Q function is

$$Q = [OSNR - OSNR_{BIB} - Pen_{Qref}(\phi_{nl}, D_{res}, PMD)]\zeta(\phi_{nl}, D_{res}) + Q_{ref} \quad (4)$$

Because the combined effect of dispersion and nonlinear phase shift is not related to PMD and crosstalk, the Q function can be written as

$$Q = [OSNR - OSNR_{BIB} - Pen_{Qref}(\phi_{nl}, D_{res}) - Pen_{Qref}(PMD)]\zeta(\phi_{nl}, D_{res}) + Q_{ref} \quad (5)$$

Thus, by obtaining the combined effects of dispersion and nonlinear phase shift, Q -factor costs of PMD, and other impairments, we can work out the total Q function and BER of a transmission system. Q -factor costs can be obtained using a semianalytical method, that is, by collecting vast quantities of data from experiment (or simulation) about the relationship between a physical impairment and its Q -factor cost. The expression of the corresponding Q -factor cost can be obtained by polynomial regression. Finally, the regression formulas can be used to determine a performance index, such as Q -factor function or BER.

Pen_{Qref} is the OSNR cost when achieving Q_{ref} at the current impairment. OSNR cost assumes a BER. The smallest $OSNR_{BIB}$ can be obtained with the B2B configuration that has no noise, dispersion, or nonlinear effects. If we want the same BER when there is dispersion or nonlinear effects, a higher OSNR is needed. The OSNR cost is the difference between these two values.

If we only consider dispersion, the cost is called dispersion cost. Likewise, if we only consider nonlinearity, the cost is called nonlinear effect cost. There is a complicated interaction between nonlinear effects, such as SPM, XPM and FWM, and dispersion. Also, there is no need to consider nonlinear phase noise for a phase-modulation system or QAM system.

2.2 Computation of Correction Factor

Usually, the correction factor $\zeta(D_{res}, \phi_{nl})$ is a constant close to 1. Its value depends on span, optical power into the fiber, and residual dispersion. Span and optical power are the main factors affecting the correction factor, and residual dispersion has a minor effect on the correction factor. The correction factor can be expressed using Curve fitting when the influence of fiber span and optical power into fiber are taken into consideration:

$$\xi = \sum_{i=1}^4 \left(\sum_{k=1}^4 c_{ik} Nspan^{4-k} \right) Power^{4-i} \quad (6)$$

2.3 OSNR Cost of Residual Dispersion and Nonlinear Phase Shift

We can acquire the OSNR cost of residual dispersion and

nonlinear phase shift by analyzing $Pen_{Qref}(D_{res}, \phi_{nl})$ under a fixed reference BER (or Q value) in a simulation or experiment. Much experimental data is needed for function fitting.

Generally, the function can be obtained in two steps:

Step 1: When OSNR cost is less than 5 dB, fit each curve of residual dispersion and the cost to a binomial function:

$$Pen_{Qref}(D_{res}, \phi_{nl}) = a_{\phi} D_{res}^2 + b_{\phi} D_{res} + c_{\phi} \quad (7)$$

Step 2: The coefficients a_{ϕ} , b_{ϕ} , and c_{ϕ} should be fitted to a two, three, or four order polynomial based on ϕ_{nl} . The OSNR cost is

$$Pen_{Qref}(D_{res}, \phi_{nl}) = \sum_{i=0}^2 \left(\sum_{j=0}^i \alpha_{i,j} \phi_{nl}^j \right) D_{res} \quad (8)$$

2.4 Polarization Membrane Dispersion OSNR Cost

Polarization membrane dispersion in an optical fiber can be evaluated by the biggest group delay difference (DGD) probability statistical model. The independent cost of PMD can be determined by simulations in different DGD configurations.

3 DB-RWA based on CEM in Multiple Links Between Node Pairs

In the network topology, there are always more than one fiber link between the connected nodes. In a network where there are multiple links between adjacent nodes, finding a DB-RWA solution based on CEM is difficult. The network design must include route calculation, link assignment, and wavelength assignment. The design must also be capable of improving the algorithm complexity and time redundancy because of the larger network scale. The solution we propose can solve these problems. The procedures of the proposal are given in Fig. 1.

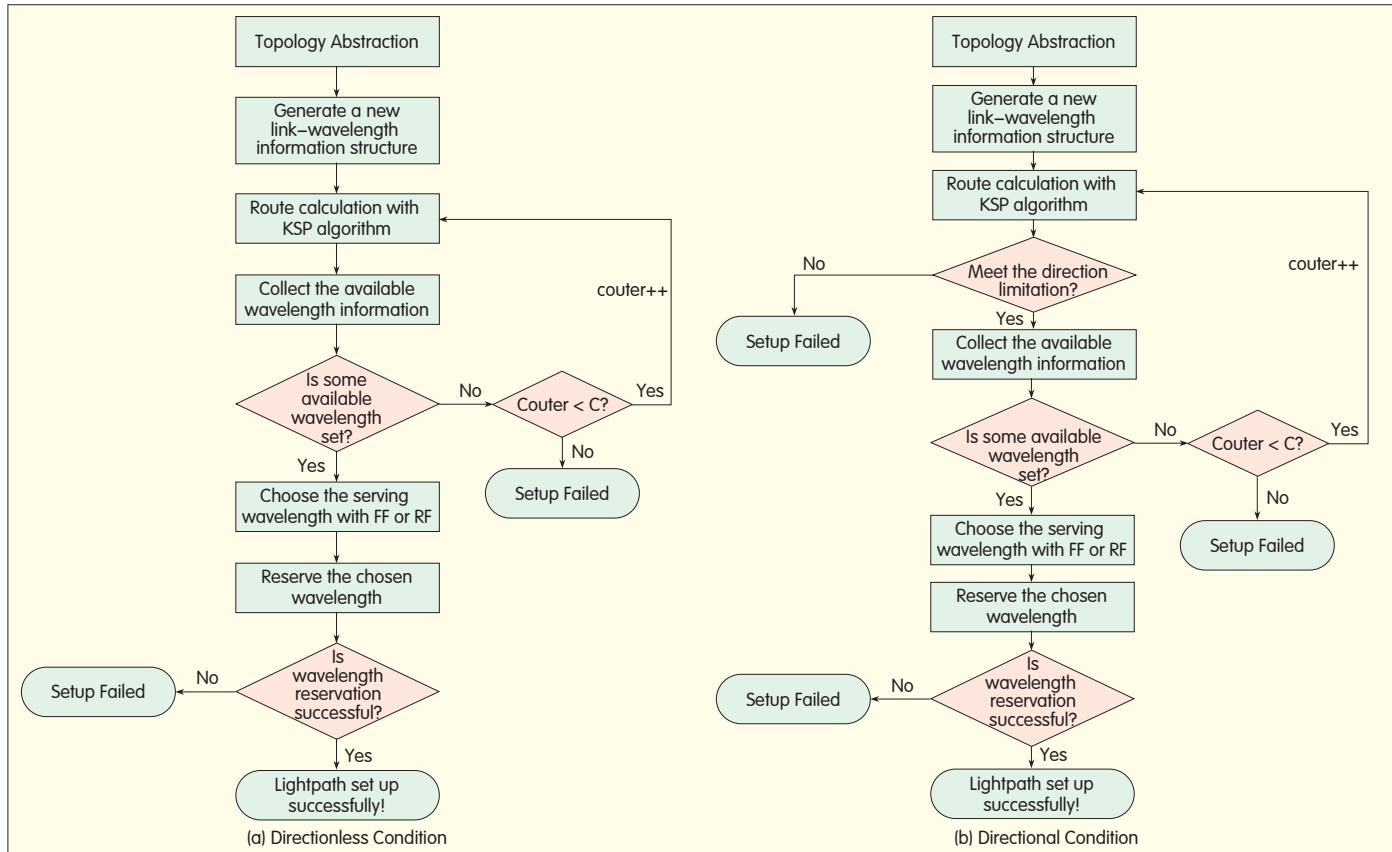
In a network environment where there are many fiber links between adjacent nodes, first we abstract a new network topology design according to the characteristics of the original network. The link information between the same hops is saved in the same structure so that it can be uniformly managed. Then, a KSP or other algorithm is used to calculate the path from source node to destination node. When the route is calculated, fiber and wavelength are assigned.

We abstract the multiple-link topology into a single-link topology. As a result, only the hops need to be calculated when calculating the route. There is no need to assign the specific link between adjacent nodes. This is done during backward wavelength assignment.

The most important part of the design is reflected in the wavelength allocation scheme (Table 1). The improved information structure ensures topology abstraction is achieved. A normal routing algorithm, such as D or KSP, can be used.

In Table 1,

$$\begin{aligned} & \bullet b_i = \sum_{j=1}^N a_{i,j} \quad 1 < i \leq M \\ & \bullet c_i = \begin{cases} 0 & b_i > 0 \\ 1 & b_i = 0 \end{cases} \quad 1 < i \leq M \end{aligned}$$



▲ Figure 1. The procedures for DB-RWA in multiple links between the node pairs.

▼ Table 1. Link and wavelength information

	Wavelength 1	Wavelength 2	...	Wavelength i	...	Wavelength $M-1$	Wavelength M
Fiber 1	$a_{1,1}$	$a_{1,2}$...	$a_{1,i}$...	$a_{1,M-1}$	$a_{1,M}$
Fiber 2	$a_{2,1}$	$a_{2,2}$...	$a_{2,i}$...	$a_{2,M-1}$	$a_{2,M}$
...
Fiber j	$a_{j,1}$	$a_{j,2}$...	$a_{j,i}$...	$a_{j,M-1}$	$a_{j,M}$
...
Fiber $N-1$	$a_{N-1,1}$	$a_{N-1,2}$...	$a_{N-1,i}$...	$a_{N-1,M-1}$	$a_{N-1,M}$
Fiber N	$a_{N,1}$	$a_{N,2}$...	$a_{N,i}$...	$a_{N,M-1}$	$a_{N,M}$
Number of Available Wavelengths	b_1	b_2	...	b_i	...	b_{M-1}	b_M
Overall Availability Wavelengths	c_1	c_2	...	c_i	...	c_{M-1}	c_M

is the number of the fiber links between adjacent nodes

- M is the number of wavelengths in every fiber
- i is the i th wavelength, $i = 1, 2, \dots, M$
- j is the j th fiber, $j = 1, 2, \dots, N$
- $a_{i,j}$ is the occupancy of the i th wavelength in the j th fiber, 0 = occupied, 1 = available

0 = occupied, 1 = available

- b_i is the number of available fibers with the i th wavelength
- c_i is the occupancy of the i th wavelength. If the i th wavelength of any fiber is available, $c_i = 1$. If the i th wavelength of every fiber is occupied, $c_i = 0$.

We implemented and evaluated the proposed approach in the eighteen-node topology (Fig. 2). The testbed has the same topology as the network topology, in which there are 10 fiber links per hop, and each fiber link contains five wavelengths. In terms of traffic characteristics, uniformly distributed light path requests arrive at the network following a Poisson process. The holding time of the light path is exponentially distributed using unit mean.

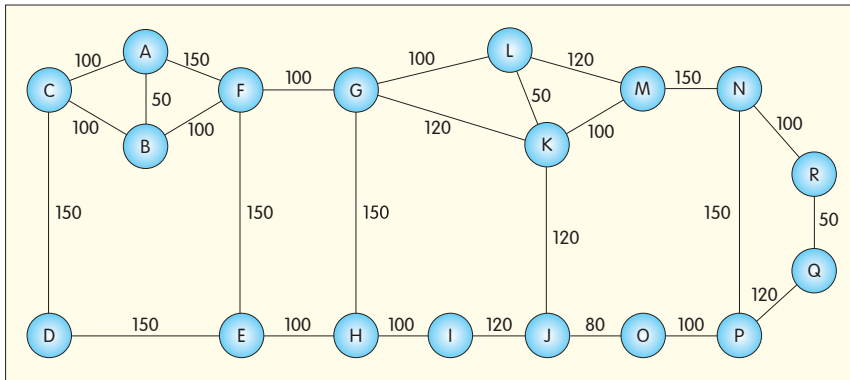
For the directionless condition, if the traffic moves from node A to K, the path derived using D algorithm is A-F-G-K. If the paths are calculated using KSP algorithm, the first best path is A-F-G-K; the second best path is A-B-F-G-K; and the third best path is A-F-G-L-K. For the directional condition, we assume that link A-F and

link B-F can only exchange with link F-E. The three best paths cannot meet the directional limitation, but the path A-F-E-H-G-K can be used. As a result, we can try to find the RWA solution in the directional condition.

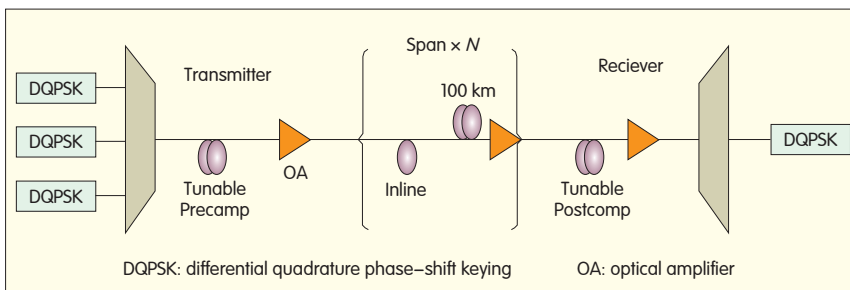
4 Simulation and Results

4.1 CEM Experimental Simulation System

Because an analytical solution to OSNR cost of impairment



▲ Figure 2. Network topology.



▲ Figure 3. Structure of the simulation system.

cannot be obtained directly, a simulation or experimental fitting can be used to work out a second cost curve of impairment OSNR and obtain an approximate analytical solution.

In this simulation method, the structure of the simulation system in Fig. 3 can be used.

At the transmitting terminal, the required number of wavelengths can be dispersed to emulate the physical impairment in the context of a single channel and multiple channels. After the optical multiplexer, the optical signal enters a dispersion compensating fiber (DCF) with predispersion compensation. Predispersion compensation depends on the value of dispersion parameters, span residual dispersion, and number of spans. Postdispersion compensation depends on the residual dispersion configuration of a span. The receiver performs decoding and judging based on the demux and demodulator and arrives at the BER.

In the simulation of OSNR cost curves, only one kind of impairment should generally be considered, and other impairments should be ignored. Other system parameters should be fixed. In simulation, parameters for the transmission fiber span, transmitting signal, in-span DCF, pre-DCF, and post-DCF are fixed. The fixed parameters of the transmission fiber span include fiber type, optical attenuation coefficient, optical fiber dispersion coefficient, span length, and nonlinear coupling coefficient. The fixed parameters of the transmitting signal are modulation format, signal rate, signal transmission power, symbol line code, duty cycle of optical pulse, rolling pressure coefficient, channel interval, and center wavelength.

In-span DCF contains dispersion coefficient, attenuation, and nonlinear coupling coefficient. The length of the compensation fiber depends on each segment's residual dispersion value. Pre-DCF and post-DCF maintain the dispersion coefficient, nonlinear coupling coefficient, and fiber length (which is determined by compensation value).

When calculating the impairment OSNR cost curve, we can change the number of spans and the scheme for the span dispersion compensation in order to obtain more comprehensive data.

4.2 DB-RWA-Based CEM Simulation and Results

We have implemented and evaluated the proposed approach in the eighteen-node topology (Fig. 2). The testbed describes the same topology as the network topology in Fig. 2, in which 10 fiber links per hop are assumed. Each fiber link contains five wavelengths. In terms of traffic characteristics, uniformly distributed light path requests arrive at the network following a Poisson process. The holding time of light path is exponentially distributed using unit mean.

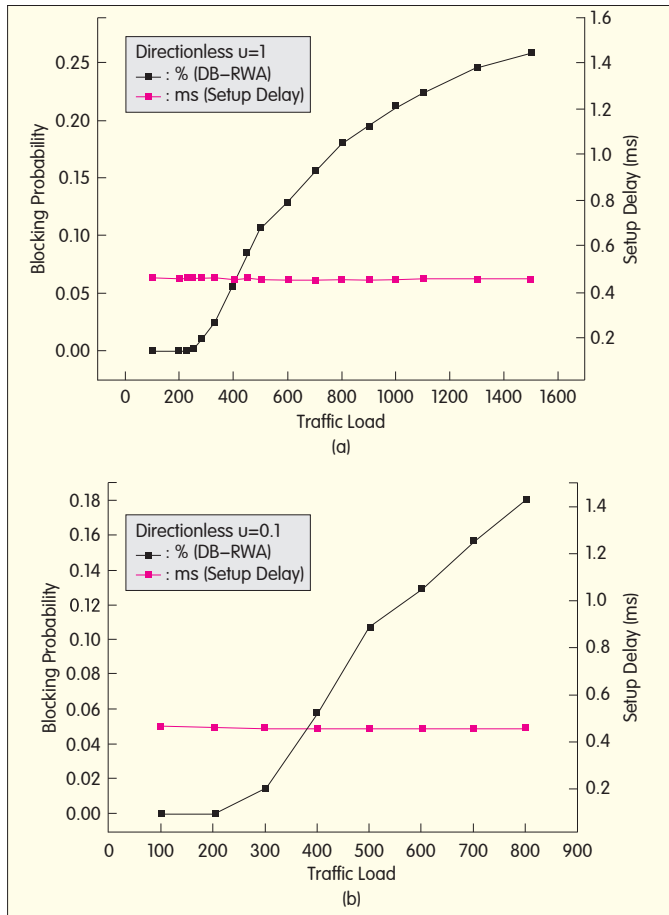
In the directionless condition, the simulation environment is independent of the direction limitation. The statistics are obtained for 100 to 1500 Erlangs. Table 2 shows the blocking rates and setup delays.

Fig. 4(a) is based on the data in Table 2.

We assume the leaving rate $\mu = 0.1$ and the arriving rate ranges from 10 to 80 services per second. The statistics are

▼ Table 2. Blocking rate and setup delay when leaving rate is 1.

Leaving Rate	Arriving Rate	Blocking Probability	Setup Delay (ms)
1	100	0	0.465361
1	200	0	0.458513
1	230	0	0.465361
1	250	0.001	0.465361
1	280	0.01	0.465361
1	330	0.025	0.465361
1	400	0.058	0.457298
1	450	0.085	0.465361
1	500	0.107	0.4566
1	600	0.129	0.456607
1	700	0.156	0.454074
1	800	0.18	0.457297
1	900	0.195	0.454469
1	1000	0.212	0.45702
1	1100	0.224	0.459608
1	1300	0.245	0.457635
1	1500	0.259	0.459166



▲ Figure 4. Blocking probability and setup delay when leaving rate is (a) 1 and (b) 0.1.

▼ Table 3. The blocking rate and the setup delay when leaving rate is 0.1.

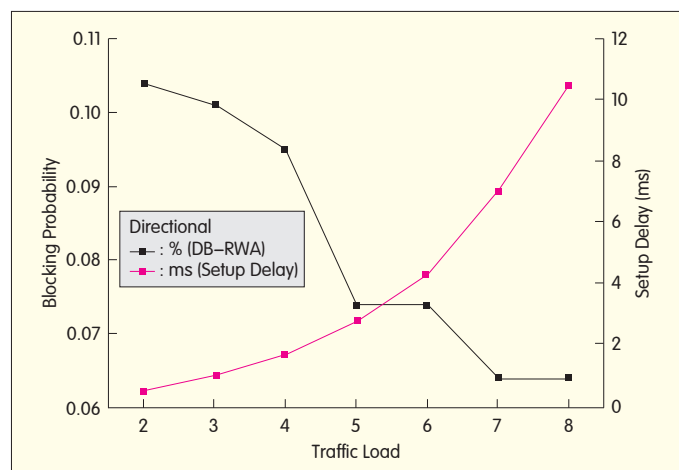
Leaving Rate	Arriving Rate	Blocking Probability	Setup Delay (ms)
0.1	10	0	0.465361
0.1	20	0	0.458513
0.1	30	0.015	0.456782
0.1	40	0.058	0.457298
0.1	50	0.107	0.4566
0.1	60	0.129	0.456607
0.1	70	0.156	0.454074
0.1	80	0.18	0.457297

obtained for 100 to 800 Erlangs. The blocking rate and the setup delay are shown in Table 3.

Fig. 4(b) is based on the data in Table 3. As the traffic load increases, blocking probability increases. Fig. 4(b) also confirms that the simulation is correct and reasonable. The setup delay is around 0.457 ms with small fluctuation. The setup delay is calculated from the beginning of route calculation to the end of wavelength assignment. Because the K of the KSP algorithm remains unchanged, the setup delay barely changes in different arriving-rate scenarios.

▼ Table 4. Blocking rate and setup delay in directional condition

K	Blocking Probability	Setup Delay (ms)
2	0.104	0.462131
3	0.101	0.957029
4	0.095	1.64138
5	0.074	2.75116
6	0.074	4.28191
7	0.064	6.98775
8	0.064	10.4983



▲ Figure 5. The setup delays with K values.

In the directional condition, where the network is limited by direction, we assume the arriving rate remains at 40 services per second and the leaving rate remains 0.1. KSP algorithm followed by the K -value is equal to 2, 3, ..., 8. Table 4 and Fig. 5 show the blocking probabilities and the setup delays.

Fig. 5 shows the setup delays with K values. When K increases, the setup delay, which is determined by the complexity of the KSP algorithm, gradually becomes longer. According to the data in Table 4, K increases, the probability of blocking reduction decreases. When the number of alternative paths increases, there is more chance a route will be chosen that has a lower chance of blocking.

5 Conclusion

In this paper, we have presented a novel CEM and DB-RWA algorithm based on CEM for use in a WSON with multiple constraints. Taking into account the interaction between physical impairments, a comprehensive evaluation model eliminates the effects of physical transmission impairments in a WSON. CEM improves the evaluation accuracy in the mathematical method and reasonably obtains and calculates large amount of information. The implementation method and quality of light transmission are analytical and transform the physical impairment factor into a BER price, especially in the transparent light network that lacks photoelectric regenerators. DB-RWA algorithm based

Multiple-Constraint-Aware RWA Algorithms Based on a Comprehensive Evaluation Model: Use in Wavelength-Switched Optical Networks

Hui Yang, Yongli Zhao, Shanguo Huang, Daijiang Wang, Xuping Cao, and Xuefeng Lin

on CEM in multiple constraint conditions in WSON not only solves the problem of RWA in multiple links between network adjacent nodes but also substantially decreases the setup delay and cost of computation. With increasing scope in the multiple links between adjacent nodes in the network, time performance can be optimized. The simulations in both directional and directionless condition demonstrate that the network is optimized to for shorter routing time as the number of network nodes and links in adjacent nodes increases. An optimal path can be chosen for ultrahigh capacity with lower blocking probability.

Acknowledgment

This work was supported in part by 973 Program (2010CB328204), NSFC project (60932004) and RFDP Project (20090005110013).

References

- [1] *Framework for GMPLS and Path Computation Element (PCE) Control of Wavelength Switched Optical Networks (WSONs)*, IEEE RFC 6163, Apr. 2011.
- [2] Xiaowen Chu, Bo Li, I. Chlamtac, "Wavelength converter placement under different RWA algorithms in wavelength-routed all-optical networks," *Communications, IEEE Trans. Commun.*, vol. 51, no. 4, pp. 607–617, Apr. 2003.
- [3] S. Azodolmolky, Y. Pointurier, M. Angelou, D. Careglio, J. Sole–Pareta, I. Tomkos, "A Novel Impairment Aware RWA Algorithm With Consideration of QoT Estimation Inaccuracy," in *IEEE/OSA J. Opt. Commun. Netw.*, vol. 3, no. 4, pp.290–299, Apr. 2011.
- [4] D. Adami, S. Giordano, M. Pagano, L. Zuliani, "Online light path provisioning and critical services: New IA–RWA algorithms to assure QoT and survivability," in *Proc. 12th Int. High Performance Switching and Routing Conf.*, Cartegna, Spain, Jul. 2011., pp. 101–106.
- [5] S. Azodolmolky, Y. Pointurier, M. Klinkowski, E. Marin, D. Careglio, J. Sole–Pareta, M. Angelou, I. Tomkos, "On the Offline Physical Layer Impairment Aware RWA algorithms in transparent optical networks: State-of-the-art and beyond," in *Proc. 13th Opt. Netw. Design and Modeling (ONDM'09)*, Braunschweig, Germany Feb. 2009.
- [6] Ying Wang, Jie Zhang, Yongli Zhao, XuPing Cao, Hai Huang, WanyiGu, YuefengJi, "Double Cooperating PCEs for IA–RWA computation with QoT compensation in transparent optical networks," in *Proc.36th European Conf. Opt. Commun., (ECOC '10)*, Sep. 2010, pp. 1–3.
- [7] K. Manousakis, K. Christodouloupoulos, E. Varvarigos, "Impairment-Aware Offline RWA for Transparent Optical Networks," in *Proc. INFOCOM 2009*, Rio de Janiero, Apr. 2009.
- [8] D. Adami, S. Giordano, M. Pagano, L. Zuliani, "Online light path provisioning and critical services: New IA–RWA algorithms to assure QoT and survivability," in *Proc. 12th Int. Conf. High Performance Switching and Routing (HPSR '11)*, Cartagena,

Spain, pp.101–106.

- [9] Yongtao Gong, Peiyuan Lee, WanyiGu, "A novel adaptive RWA algorithm in wavelength-routed network," in *Proc. Global Telecommunications Conf. (GLOBECOM '03)*, San Fransisco, CA, vol. 5, pp. 2580–2584.
- [10] J. Antona, S. Bigo, "Physical design and performance estimation of heterogeneous optical transmission systems," in *Comptes Rendus Physique*, vol. 9, no. 9, pp. 963–984, 2008.
- [11] A. Morea, N. Brogard et al., "QoT function and A* routing: an optimized combination for connection search in translucent networks," in *J. Opt. Netw.*, vol. 7, no. 1, pp. 42–61, 2008.
- [12] F. Leplindard, A. Morea, T. Zami, N. Brogard, "Interest of an adaptive margin for the quality of transmission estimation for light path establishment," in *Proc. Conf. on Opt. Fiber Commun. (OFC '09)*, San Diego, CA, paper OW16, 2009.
- [13] H. Keang–Po, "Error probability of DPSK signals with cross-phase modulation induced nonlinear phase noise," in *IEEE J. Selected Topics in Quantum Electronics*, vol. 10, no. 2, pp. 421–427, 2004.
- [14] Alberto Bononi et.al, "Cross-phase modulation induced by OOK channels on higher-rate DQPSK and coherent QPSK channels," in *J. Lightw. Tech.*, vol.27, no. 18, pp. 3974–3983, 2009.
- [15] Wenlu Chen, Shan Zhong, Zhonghua Zhu, Wei Chen, Chen, Y.–J.R., "Adding OSNR monitoring functionality on AWG based power monitoring circuits," in *Opt. Fiber Commun. Conf. (OFC '02)*, Anaheim, CA, pp. 668–670.

Manuscript received: January 11, 2012

B iographies

Hui Yang (yanghui@bupt.edu.cn) is a PhD candidate in communication and information systems at Beijing University of Posts and Telecommunications (BUPT). His research interests include network architecture, dynamic optical network, flexible bandwidth optical network, software driven networks, and cross-stratum optimization. In 2011, he authored an academic paper about network architecture that was accepted by the Technical Program Committee of the Optical Fiber Communications/ National Fiber Optic Engineering Conference (OFC/NFOEC).

Yongli Zhao (yonglizhao@bupt.edu.cn) is a lecturer at the Institute of Information Photonics and Optical Communications at BUPT. He received his BSc degree in communication engineering and PhD degree in electromagnetic field and microwave technology from BUPT in 2005 and 2010. He has published more than 80 articles. His research interests include wavelength switched optical networks, spectrum-efficient optical transport networks, and packet transport networks.

Shanguo Huang (shghuang@bupt.edu.cn) is an associate professor and doctoral supervisor at BUPT. He has presided over and participated in more than 10 national and provincial research projects, including the National Natural Science Fund, the Project of "863", and the Key Plan and Military Projects of the Ministry of Education. He has also participated in projects of important research institutions and enterprises. He has authored more than 50 articles for international conferences and periodicals, 30 of which are indexed in SCI and EI. He has also authored three international guest reports, 18 patents for invention, three IETF international standard drafts, and two monographs. His main research interests include data optical network and ASON technology, and transmission network planning and optimization.

Daijiang Wang received his master's degree in Machinery Manufacturing and Automation from Shanghai University in 2001. He was a system engineer and pre-research project manager for ZXUCP A200, and now is the planning manager for ZXUCP A200 products. He led several R&D projects on RWA algorithm, PCE, and unified control plane.

Xuping Cao (cao.xuping@zte.com.cn) received his PhD from the Institute of Information Photonics and Optical Communications, BUPT. His research interests include next-generation optical networks. From 2004 to 2006, he worked in the optical network product line at Huawei. Since 2010, he has worked in the Advanced Optical Network Research Department at ZTE Corporation, where he researches MPLS/GMPLS network control plane technology. He has published more than 10 articles (indexed in SCI and EI), 18 patents, and three IETF international standard drafts.

Xuefeng Lin (lin.xuefeng@zte.com.cn) received his PhD degree in computer science from NorthEast University, China. He is currently a system engineer of Bearer Network Pre–Research Department, ZTE Corporation. His research interests include control plane of optical transport network, and the integration between data equipment and optical equipment.

Introduction to ZTE Communications

ZTE Communications is a quarterly peer-reviewed technical magazine ISSN (1673–5188) and CODEN (ZCTOAK). It is edited, published and distributed by ZTE Corporation. The magazine focuses on hot topics and cutting edge technologies in the telecom industry. It has been listed in the Ulrich's Periodicals Directory, Index of Copernicus (IC), and Cambridge Scientific Abstracts (CSA). *ZTE Communications* is distributed to telecom operators, science and technology research institutes, and colleges and universities in more than 140 countries.

New Members of ZTE Communications Editorial Board

(in alphabetical order)



Houlin Zhao was elected deputy secretary-general of ITU-T at the Plenipotentiary Conference in Antalya, Turkey, in November 2006. He was re-elected for a second four-year term in 2010. He graduated from Nanjing University of Posts and Telecommunications and holds an MSc in Telematics from the University of Essex.

From 1986 to 1992, he was a senior staff member in the CCITT. From 1993 to 1998, he was a senior staff member in TSB. From 1999 to 2006, he was the director of the ITU telecommunication standard bureau. Among his responsibilities as counselor for ITU-T study groups, he coordinated international technical bodies, including ISO and IEC. Prior to joining ITU, Mr Zhao was an engineer in the Design Institute of the Ministry of Posts and Telecommunications, China. He contributed important articles to a number of prestigious Chinese technical publications. In 1985 he was awarded a prize for his achievements in science and technology in the Ministry of Posts and Telecommunications.



Huifang Sun received his BSc degree from Harbin Military Engineering Institute. He received his PhD degree from the University of Ottawa, Canada. In 1990, he was an associate professor at Fairleigh Dickinson University. In 1990, he also joined Sarnoff Corporation. In 1995, he joined Mitsubishi Electric Research Laboratories and was promoted to vice president, deputy director, and fellow (2003). He has co-authored two books and published more than 140 journal and conference papers. He holds more than 60 US patents. In 1994, Huifang Sun received a Technical Achievement award for the optimization and specification of the Grand Alliance HDTV video compression algorithm. In 1992, he won the Best Paper award from IEEE Transactions on Consumer Electronics. In 1996, he won the Best Paper award at ICCE; and in 2003, he won the Best Paper award from IEEE Transactions on CSVT. He was the associate editor of IEEE Transaction on

Circuits and Systems for Video Technology and was the chair of the Visual Processing Technical Committee of IEEE's Circuits and System Society. He is also an IEEE Fellow.



Ke-Li Wu (M'90-SM'96-F'11) received his BS and MEng degrees from Nanjing University of Science and Technology in 1982 and 1985. He received his PhD degree from Laval University, Quebec, in 1989. From 1989 to 1993, he was a research engineer at the Communications Research Laboratory, McMaster University. In March 1993, he joined the Corporate R&D Division, COM DEV International. Since October 1999, he has been the director of the radio frequency radiation research Laboratory (R3L) at the Chinese University of Hong Kong.

He has authored or coauthored numerous publications. His research interests include PEEC and DPEC electromagnetic modeling of high speed circuits, RF and microwave passive circuits and systems, synthesis theory and practices of microwave filters, antennas for wireless terminals, LTCC-based multichip modules (MCMs), and RF identification (RFID) technologies.

Professor Wu is a Fellow of IEEE and a member of the IEEE MTT-8 subcommittee. He was an associate editor of IEEE Transactions on MTT from 2006 to 2009.



Lirong Shi has been the executive director of the board of ZTE Communications since February 2001. He was elected CEO of ZTE Corporation in March 2010, and committed himself to accelerating ZTE's global expansion. From 1989 to 1997, he was the engineer and production manager of ZTE semiconductors and was the deputy general manager of Zongxing Telecom Equipment Ltd.

From 1997 to 2006, he was the senior vice president of ZTE marketing. From 2006 to March 2010, he was the executive vice president of ZTE, responsible for the sales, marketing, and customer service activities of more than 20,000 salespeople in more than 140 countries.

Shi Lirong holds a bachelor's degree in radio electronics and information technology from Tsinghua University and a master's degree in communications and electronics engineering from Shanghai Jiao Tong University,

New Members of ZTE Communications Editorial Board

(in alphabetical order)



Shidian Cheng is a professor at the State Key Laboratory of Networking and Switching Technology at Beijing University of Posts and Telecommunications (BUPT). She graduated from BUPT in 1963 continued there as an assistant professor. From 1984 to 1987 and in 1994 she was a visiting scholar at Alcatel Bell, Belgium. In 1987 she was the vice dean of the Department of Computer Science and Technology, BUPT. From 1992 to 1999 she was the director of the State Key Laboratory of Networking and Switching Technology of BUPT. During the same period, she was also the head of the Expert Group on Networking and Switching in 863 program of China. From 1999 to February 2006, she was the vice director of Academic Committee of BUPT.

She has published more than 200 academic papers and four books. She also holds dozens of patents on ATM and IP technology. Her research interests include IP network performance, QoS and new applications, broadband wireless networks, NGN, and NGI.



Wen Gao received his PhD degree in electronics engineering from the University of Tokyo in 1991. From 1991 to 1995, he was chairman of the Department of Computer Science at Harbin Institute of Technology. From 1996 to 2005, he was a professor at the Institute of Computing Technology (ICT), Chinese Academy of Sciences (CAS). During his career at CAS, he was the managing director of the ICT from 1998 to 1999, the executive vice president of Graduate School of Chinese Academy of Sciences from 2000 to 2004, and the vice president of University of Science and Technology China from 2000 to 2003. Dr. Gao currently researches video coding and processing, facial recognition, image retrieval, and multimodal interfaces. He is a fellow of the IEEE and a member of the Chinese Academy of Engineering.



Wenjun (Kevin) Zeng is director of the Mobile Networking and Multimedia Communications Labs in the Computer Science Department of the University of Missouri, Columbia, MO. He received his BE degree in electrical engineering from Tsinghua university, his MS degree from the University of Notre Dame, and his PhD degree from Princeton University. His research interest include mobile computing, social media analysis, semantic search, distributed source/video coding, 3-D analysis and coding, multimedia networking, and content and network security. He is the editor "Multimedia Security Technologies for Digital Rights Management" (Elsevier, 2006), and has been granted 15 US patents.

Prior to joining the University of Missouri in 2003, he worked for PacketVideo Corp., Sharp Labs America, Bell Labs, and Panasonic Technology. He is an associate editor of the IEEE Transactions on Information Forensics and Security, IEEE Transactions on Circuits and Systems for Video Technology, and IEEE Multimedia Magazine. He is also on the Steering Committee of IEEE Transactions on Multimedia. He is a fellow of the IEEE.



Zhenge (George) Sun received his masters and doctoral degrees from North Polytechnics University, Xi'an, China. He then continued as a postdoctoral researcher at the Chinese Academy of Sciences.

He is now vice president of ZTE Corporation. He is in charge of the strategy planning for ZTE Corporation. Prior to that he was the CEO of ZTE(USA). He is in charge of the standardization activities as well as marketing in North America and Western Europe.

He was previously the senior director of the Corporate Technology Center, ZTE Corporation. He was responsible for the company's strategy planning, technical marketing, strategic cooperation in developed markets, and basic research on Internet and platform. He was also the deputy general manager of the Mobile Products Division and developed the technical marketing of UMTS products.



Zhengkun Mi received his BSc degree from Fudan University in 1967 and his masters degree from Nanjing University of Posts and Telecommunications (NUPT) in 1981. He is a professor at the College of Communication and Information Engineering, NUPT. He held a visiting professorship at the University of Surrey, UK for six months and a visiting scholarship at the University of Arizona for twelve months. His research interests include next-generation networks, ubiquitous networks, and Internet of things, with an emphasis on heterogeneous network convergence for QoS and QoE, ubiquitous service provisioning, and joint resource management. He is a member of the Chinese expert delegation to the ITU. His work has contributed to one ITU-T SG11 recommendation and one Chinese Communication Standards Association (CCSA) standard, both on intelligent networking. He has published more than 50 academic papers and is the author of six monographs on telecommunication switching, signaling, and services. He is a fellow of the Communication Association of China (CAC)



**Picture your ideal
IPTV solution.
Then come and
talk to us.**

At ZTE, we've already seen phenomenal success in IPTV with solutions that have propelled us to number 1 in Asia. Now we're ready to bring IPTV everywhere.

Our unique triple-screen topology platform - covering TV, PC and mobile and based on mature designs - allows for lightning fast, highly customized multimedia delivery, enabling operators to link hundreds of channels and services to a single system.

Of course, we also let you customize everything down to the minutest detail, so you can be sure of receiving a solution that's a perfect fit for your market.

All across the world, we're ready. So if you're looking to give your subscribers the entertainment that'll set you apart, give ZTE a call.

www.zte.com.cn

ZTE中兴